SPE SOLIDS PROCESS ENGINEERING & PARTICLE TECHNOLOGY TUHH

SPE-Schriftenreihe 10

Herausgegeben von Prof. Dr.-Ing. habil. Dr. h.c. Stefan Heinrich

Anna Riebensahm

Effect of feed composition and drying conditions on surface properties of multicomponent food powders produced by spray drying

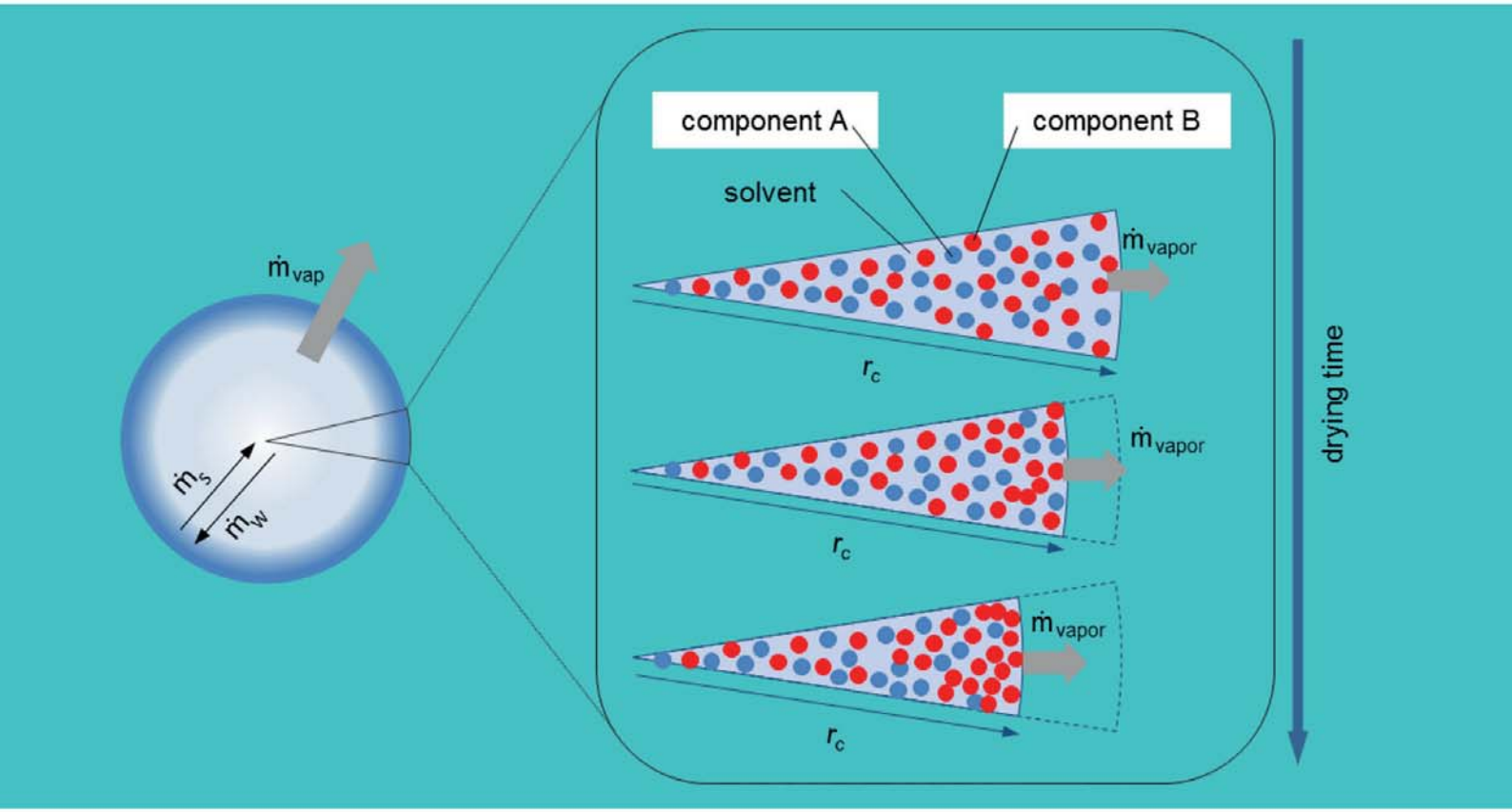

Cuvillier Verlag Göttingen
Internationaler wissenschaftlicher Fachverlag

Effect of feed composition and drying conditions on surface properties of multicomponent food powders produced by spray drying

Effect of feed composition and drying conditions on surface properties of multicomponent food powders produced by spray drying

Dem Promotionsausschuss der
Technischen Universität Hamburg-Harburg
zur Erlangung des akademischen Grades
Doktor-Ingenieurin (Dr.-Ing.)
vorgelegte Dissertation

von
Anna Riebensahm

aus
Warschau

2017

Bibliografische Information der Deutschen Nationalbibliothek
Die Deutsche Nationalbibliothek verzeichnet diese Publikation in der Deutschen Nationalbibliografie; detaillierte bibliografische Daten sind im Internet über http://dnb.d-nb.de abrufbar.
1. Aufl. - Göttingen: Cuvillier, 2017
Zugl.: (TU) Hamburg-Harburg, Univ., Diss., 2017

Gutachter:

1. Prof. Dr.-Ing. S. Heinrich
2. Prof. Dr.-Ing. M. Kaltschmitt
3. Prof. Dr.-Ing. S. Palzer

Tag der mündlichen Prüfung: 14 Juni 2017.

Nonnenstieg 8, 37075 Göttingen
Telefon: 0551-54724-0
Telefax: 0551-54724-21
www.cuvillier.de

1. Auflage, 2017
Gedruckt auf umweltfreundlichem, säurefreiem Papier aus nachhaltiger Forstwirtschaft.

ISBN 978-3-7369-9581-9
eISBN 978-3-7369-8581-0

ACKNOWLEDGEMENTS

A number of people have contributed to the successful accomplishment of this thesis. At this point I wish to express my sincere gratitude towards all of them.

Firstly, I would like to thank my advisor Prof. Dr.-Ing. Stefan Heinrich for the granted trust and the opportunity to conduct my Ph.D research at his institute. His commitment, expertise and the freedom, he granted me, in conducting my research, created an environment, in which I could explore and realize my ideas, including necessary measurements outside of the institute.

Moreover, I would like to acknowledge the entity Nestec S.A., which provided funds for conducting the research. Especially, I would like to thank Prof. Dr.-Ing. Stefan Palzer, Dr. Alessandro Gianfrancesco and Dr.-Ing. Lennart Fries. Despite the geographical distance, Prof. Stefan Palzer took every opportunity to involve in a discussion with me. His knowledge and engagement taught me to look at my research from various perspectives and to try out new approaches. Alessandro Gianfrancesco was always ready to share with me his practical experience and to discuss the results. Lennart Fries took every opportunity to provide feedback regarding modeling as well as experimental work and encouraged me to try out new approaches.

Furthermore, I would like to thank Dr. Nico Scharnagl from the Helmholtz Zentrum Geesthacht for his expertise in the x-ray photoelectron spectroscopy and the help in the analysis of the surface composition.

Likewise, I would like to acknowledge my colleagues from the Institute of Solids Process Engineering and Particle Technology, who were always ready to listen and to involve in a discussion as well as to suggest practical solutions. Especially, I appreciate the great support of Dr.-Ing. Maksym Dosta in the modeling part of this work and his constant optimism. The commitment, experience and creativity of Bernhard Schult, Heiko Rohde and Frank Rimoschat allowed me to introduce modifications in the technical equipment in a short time I am very grateful for their help.

Last but not least, I would like to thank my family for their patience and continued moral support during the five years of work on this thesis.

List of Figures

List of Tables

Nomenclature

Roman characters

c_p	specific heat capacity of a drop	$J \cdot kg^{-1} \cdot K^{-1}$
a	diameter of the circular contact area between particles	m
c	form factor	m
d	particle diameter	m
D	diffusion coefficient	$m^2 \cdot s^{-1}$
f	solid based mass fraction of component B	$kg \cdot kg^{-1}_{\text{total solid}}$
F_{vdW}	van der Waals force	N
F_t	force with which two particles are contacted	N
h	diameter of a sinter bridge	m
H	Hamaker constant	J
h_s	distance between two particles	m
H_V	enthalpy of vaporization flow	$J \cdot s^{-1}$
hω	Lifshitz-van der Waals constant	J
i	index	-
I	atom % on a surface	Atom %
j	flux	$kg \cdot m^{-2} \cdot s^{-1}$
k	constant in Gordon-Taylor equation	-
k_a	thermal conductivity of air	$W \cdot m^{-1} \cdot K^{-1}$
k_B	Boltzmann's constant	$J \cdot K^{-1}$
k_{surf}	surface enrichment ratio	-
l	solvent penetration distance	m
M	molecular mass	$g \cdot mol^{-1}$
$\dot{m}_V$	mass flow	$kg \cdot s^{-1}$
m_b	mass of bulk powder	kg
N_A	Avogadro's number	mol^{-1}
Nu	Nusselt number	-

Pr	Prandtl number	-
$\dot{Q}$	heat flow	$J \cdot s^{-1}$
$\bar{r}$	mean pore diameter	m
r_c	radius of liquid drop core	m
R	gas constant	$J \cdot mol^{-1} \cdot K^{-1}$
Re	Reynolds number	-
r_h	hydrodynamic radius of a molecule	m
r_L	outer radius of a drop	m
s	ratio of diffusive fluxes of solutes	-
Sc	Schmidt number	-
Sh	Sherwood number	-
T	temperature	°C
t	time	s
T_{air}	temperature of drying gas	°C
t_c	contact time between particles	s
T_g	glass transition temperature	°C
TS	total solids	$kg_{solid} \cdot kg_{total\ mass}^{-1}$
T_{wb}	adiabatic cooling temperature	°C
u	gas velocity	$m \cdot s^{-1}$
$\dot{V}$	volumetric flow	$m^3 \cdot s^{-1}$
$\dot{V}_c$	volume of a cylinder	m^{-3}
X	moisture	$kg_{water} \cdot kg_{dry\ mass}^{-1}$
x	mass fraction	$kg \cdot kg^{-1}$
Y	absolute air humidity	$kg_{water} \cdot kg_{dry\ air}^{-1}$

Greek characters

α	heat transfer coefficient	$W \cdot m^{-2} \cdot K^{-1}$
β	mass transfer coefficient	$m \cdot s^{-1}$

γ	surface tension	$mN \cdot m^{-2}$
η	viscosity	$mPa \cdot s$
θ	contact angle	°
θ_{cr}	time to crystallization	s
θ_g	time to crystallization at glass transition temperature	s
ρ	density	$kg \cdot m^{-3}$
ρ_b	density of bulk powders	$kg \cdot m^{-3}$
σ_1	consolidation stress	Pa
σ_c	unconfined yield strength	Pa
φ	relative air humidity	%
ψ	surface coverage	%

Superscripts and subscripts

0	initial
A	solute A
b	bulk
B	solute B
crit	critical
d	drop
eq	equilibrium
L	liquid
L	lactose
p	particle
P	protein
S	solid
sat	saturated air
surf	surface
V	vapour

W	water
wtb	wet bulb

Abbreviations

ds	dry solids
Eq.	equation
SEM	scanning electron microscopy
St. Dev.	standard deviation of a sample
tm	total mass
vol.	volume
wb	wet solid based
WPI	whey protein isolate
XPS	x-ray photon electron spectroscopy

Abstract

Many food powders are multicomponent systems, composed of substances with different physico-chemical properties. Concentration gradients, which develop in a drop of spray dried multicomponent food material due to water evaporation and differences in molecular weight or hydrophilic properties of the components, can lead to a preferential accumulation of one of the components on powder surface. This issue is highly relevant to spray drying of any multicomponent material, as properties of powders, such as flowability, reconstitution behaviour or particle adhesion, depend on the properties of the surface of a powder. These properties are related to the chemical composition of the surface of particles. Accumulation of specific components on the powder surface was observed during spray drying of many multicomponent food materials.

This work focuses on components migration during formation of a multicomponent particle from a drop in spray drying process. The main concern is the influence of drying temperature and of the initial composition of a drop on the surface composition of the resulting particle. Another concern is the impact of the chemical composition of powder surface on powder properties. The methodology of this research combines a theoretical approach of modelling of a particle formation in spray drying with experimental analysis of properties of powders produced by spray drying.

The formulated drying model of a single drop describes a system containing a solvent and two solutes. Differences in mass flow rates between the two solutes, which are caused by differences in their diffusion coefficients, result in an enrichment of the surface in one of the components. The model was applied to simulate drying of an aqueous drop containing lactose, as a main solute, and β-lactoglobulin, as the additive component. Drops with the initial size of 100 μm were modelled. Drying temperatures were chosen between 65°C and 80°C, which correspond to the air exit temperature in a spray dryer.

The experimental study investigated the effect of the whey protein isolate and drying temperature on wetting and flowability of lactose powders. The powders were obtained by spray drying of lactose solutions with and without addition of whey protein isolate, WPI, at gas inlet temperatures between 180°C and 200°C. The total solid content of the feed was 30 wt. %.

Enrichment of the surface in the slowly diffusing component by 10 % to 150 % was predicted for systems with different initial total solid fractions, solid based mass fraction of the slowly diffusing component and different drying temperatures.

Simulation results showed that the initial total amount of solute in a feed solution has a dominating effect on the surface enrichment, compared with the influence of the solute

ratio in the feed or the drying temperature. For a spray drying process this signifies that it is important to act on the evaporation degree of the feed material before spray drying.
The experimental results confirmed these result qualitatively. An analysis of the surface composition of the powders, which contain 1 wt. % and 10 wt. % WPI in the bulk, by x-ray photon electron microscopy revealed, that the coverage of powder surface by protein is almost the same in both powders. Addition of the whey protein isolate extended powder wetting times by more than three-fold in comparison with the wetting time of lactose powders dried at the lower temperature. Wettability and flowability of the lactose powders dried at different temperatures were strongly affected by the drying temperature. However, the effects were minor in all powders with addition of the protein. Changes in wettability and flowability of the powder are attributed not only to the increased surface coverage with the protein, but also to the change in the morphology of the powders and their supramolecular structure. Despite different bulk compositions, these powders have similar wetting times. However, the experimental results underline that also powder morphology, especially the surface topology as well as the degree of crystallinity and powder moisture, have an impact on powder surface properties.

1 Introduction

Spray drying is a drying technique used in a vast variety of industries [(Masters, 1985), (Mujumdar, 1995)] in which in one process step a particulate, dried material is obtained from a liquid feed. Rapid solvent evaporation assures that the thermal stress in the particles is low in comparison with other drying methods, like drum or belt drying. Therefore, despite a poor energetic efficiency in comparison to other drying methods, spray drying finds often application in the food industry in production of dairy products, coffee as well as fruit and vegetable juices.

The obtained powder can either be applied as a final product or be further processed. In some specific applications, as in case of skim milk in confectionery products, such dried food powders are applied directly in a powdered form. However, often products are used in a liquid state by mixing a powder with water.

Among important properties of powdered products are flowability, reconstitution behaviour, dust formation and powder bulk density. Powder flowability is important for precise powder dosage in packaging and in beverage systems. Good reconstitution behaviour is a prerequisite for easy application in a liquid form as well as digestion of powder. Due to dust explosion hazard, minimizing dust formation of powders assures safe powder handling. Higher powder bulk density minimizes a volume of a silo and a constant powder bulk density is necessary, if a volumetric dosage system is applied.

The above mentioned properties of powders depend on the properties of particles, such as moisture, particle size distribution and particle morphology. These properties of particles, which in the literature are also called primary properties of a powder (Kim et al., 2009b), are determined by properties of the liquid feed and by spray drying conditions. Alternatively, properties of a given powder can be optimized by such processes like agglomeration or granulation.

Many food products, which are dried by spray drying, are mixtures of multiple components. Spatial distribution of these components within a particle can also determine product properties, as in case of oxygen sensitive components or additives with unpleasant odour, which should be located in the centre of a particle. Location of specific components on particle surface can enhance or inhibit wetting of powders as well as have a negative effect on powder flowability.

In order to tailor properties of multicomponent powders to product requirements, it is important to understand the underlying processes, which lead to distribution of components within a particle. A relevant question is, if a surface composition can be controlled by drying conditions or feed composition. Another important question is, in what extend

the surface composition influences the properties of a spray dried particulate product. In answering these questions the link between the process and the properties of resulting powder remains in focus.

In this work a theoretical model is formulated, which describes drying and component transport within a drying drop. The model is applied to simulate profiles of two solutes, which differ in their molecular size, in a drop during drying and to predict the composition on the surface of a formed particle. The considered material is a dairy model-system, which contains two solutes – lactose and whey protein isolate, WPI – dissolved in water. Further insights on the relationship between the mass fraction of the solutes in the total solids and the drying rate are delivered by experimental investigation of the surface composition, powder wetting and flowability of powders produced by spray drying of the model-system.

After presentation of the fundamentals of the process and powder science, which are believed to be relevant for the scope of this work, a drying model of a single drop with two solutes is introduced. It is followed by presentation of used materials and experimental methods applied in characterization of powders. The next chapter reports the results of simulations and the following one presents the experimentally observed effects of the investigated parameters on the properties of the powders. The last chapter covers a synthetic discussion of the obtained results and conclusions with practical recommendations for a spray drying process.

1.1 General description of a spray drying process

Spray drying is a process in which pumpable feed, like solutions, suspensions and pastes are atomized into drops and dried into particulate form. A schematic of a typical spray dryer is shown in Figure 1.1. The feed is pumped into a drying chamber and at the inlet atomized by a nozzle or a rotary atomizer into minute drops, which contact the hot drying medium. The typical drop size in spray drying is between 10 and 250 μm (Mujumdar, 1995). A large contact surface between a feed material and a drying gas enables rapid solvent removal. At the outlet of the dryer a particulate product is obtained. During drying due to moisture evaporation the temperature of the drying medium decreases and its moisture content increases. In order to obtain desired properties of the product, minimize material losses, improve process efficiency and fulfil safety standards various designs of drying chambers and atomizing equipment were developed. The details of different spray dryer layouts are given, for example, by Masters (1985). Spray drying is applied in chemical, pharmaceutical and food industry. In the food industry it is used to production of diary powders, coffee and vegetable and fruit powders.

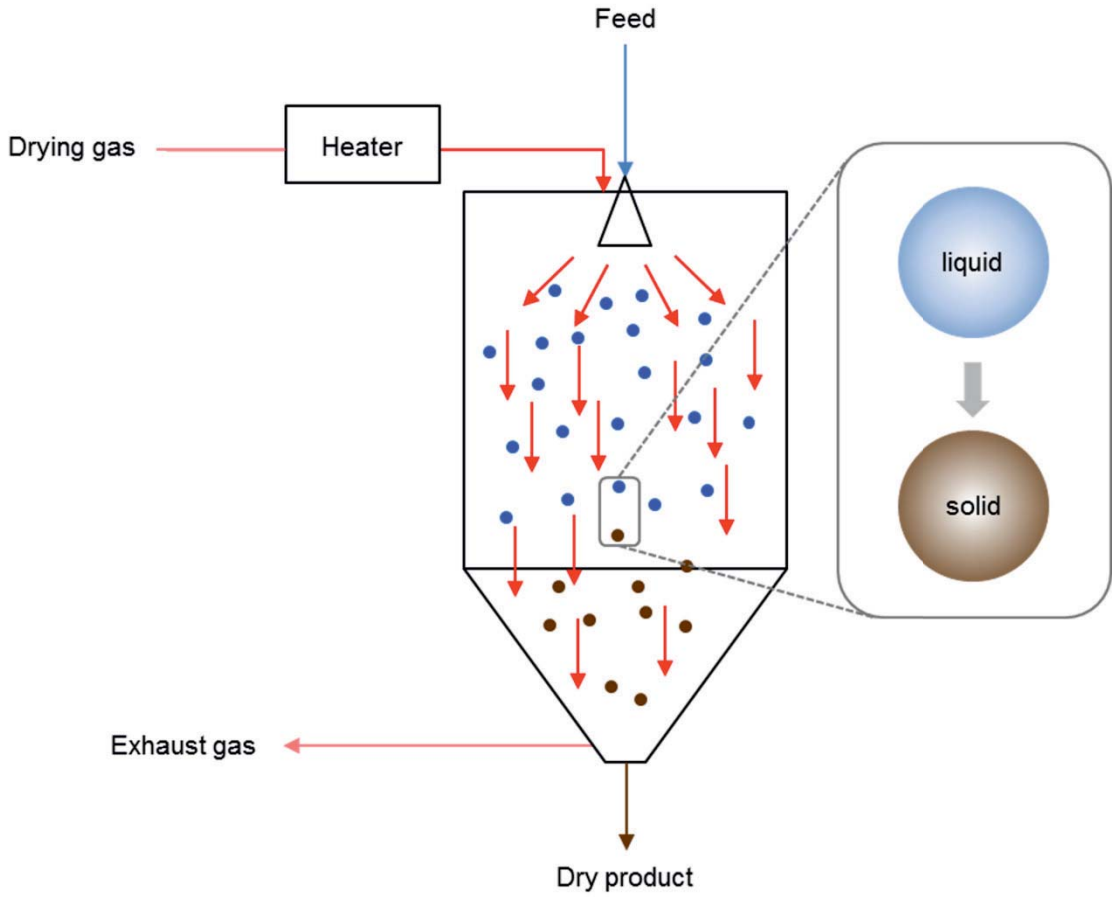

Figure 1.1 Schematic of a typical spray dryer.

1.1.1 Solid formation in spray drying

The knowledge of the physical fundamentals of solids formation in spray drying originates from observations of drying of single drops on hanging wire [(Furuta et al., 2007), (Chen and Lin, 2005), (Fu et al., 2011)], in magnetic field (Griffith et al., 2008) and acoustic levitator [(Schiffter and Lee, 2007), (Groenewold et al., 2002)], in towers (Vehring et al., 2007) and by taking powder samples along a spray drying tower (Zbicinski et al., 2002). The mechanism of solid formation depends on the nature of the material as well as the drying conditions. In the following as first the most basic scenario of particle formation is presented, afterwards few alternative scenarios, which lead to modified particle morphology, are named.

A drop produced by one of the atomization methods contacts drying medium in the spray drying tower. It is characteristic for spray drying feeds that the solvent content is high. In laboratory experiments initial water contents are between 70 and 90 wt. % [(Millqvist-Fureby et al., 1999), (Wang, 2010)], in industrial processes it reaches 50 wt. %.

Due to high amount of solvent in a drop and high temperature of the drying medium the partial pressure of the solvent on the surface of the drop is higher than the partial pressure of the solvent in the drying gas. The difference in the partial pressures of the solvent in

both phases is a driving force for solvent removal from the surface of a drop. As long as there is sufficient solvent on the surface the evaporation rate is constant, which corresponds to a linear decrease in moisture shown in Figure. 1.2a. During this period a drop remains in a liquid state, or respectively as a suspension. The drop radius shrinks and solute or solid concentration, in case of suspensions, in the drop increases. At this stage, due to the heat removed by evaporation, a temperature of the drop reaches the adiabatic cooling temperature, T_{wtb}, (Figure 1.2b). This period of uninhibited solvent removal from a surface of a drop is called the first stage of drying.

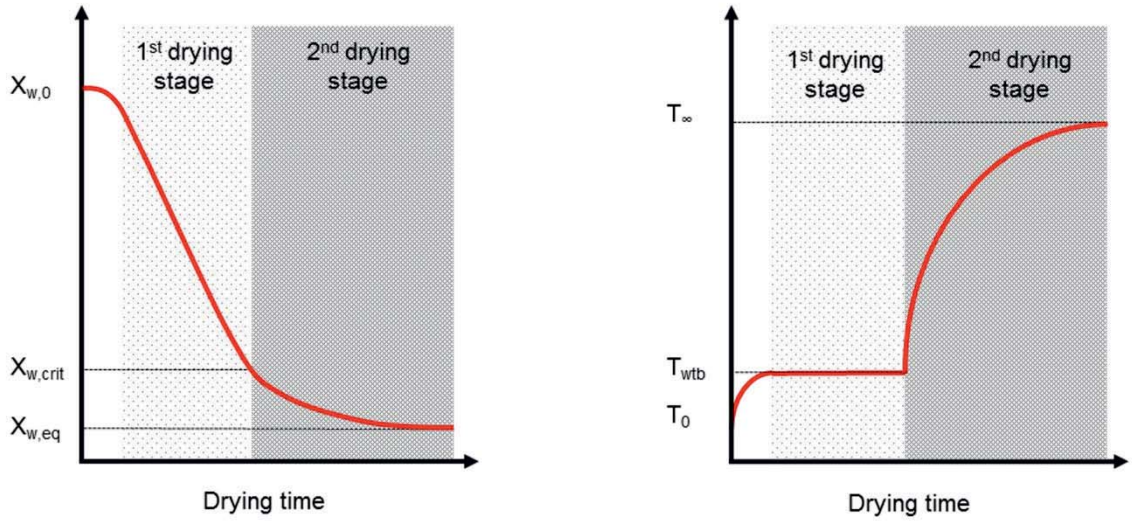

Figure 1.2 Typical change in a) drop or particle moisture content and b) temperature during drying.

As the solvent is removed, the solute accumulates in the vicinity of the surface. The concentration gradient between the surface and the core of a drop is levelled out by advective flux of solutes away from the surface towards the centre of a drop. If the mass transport is fast, the concentration of the solute or solids particles remains uniformly distributed in a volume of the drop. As drying progress, the increasing solute concentration results in a lower mobility of water molecules in the drop. This leads to a decreased solvent transport towards the surface and to a lower solvent evaporation rate. Particle moisture content from which the evaporation rate starts to decrease is described as the critical moisture content, $X_{W,crit}$. The decreasing solvent evaporation rate (Figure 1.2a) decreases the rate of heat removal from the drop. Therefore, in the second stage of drying the temperature of a drop increases (Figure 1.2b), approaching the drying gas temperature. Once the majority of the solvent is removed, a solid particle appears. The morphological changes, which correspond to this drying history, are pictured in Figure 1.3.

If solvent removal from the surface is faster than the mass transport of the solute away from the surface, the solute accumulates on the surface forming a porous shell or skin. This solid layer results in mass transport resistance to solvent transport, which leads to decreased drying rate and transition to second drying period at higher total water contents

in a drop. Once a solid layer, skin or shell, forms on the surface, a particle cannot uniformly shrink further (Tsotsas, 2012). As the process is very rapid, even crystalizing materials form amorphous particles (Vehring, 2008).

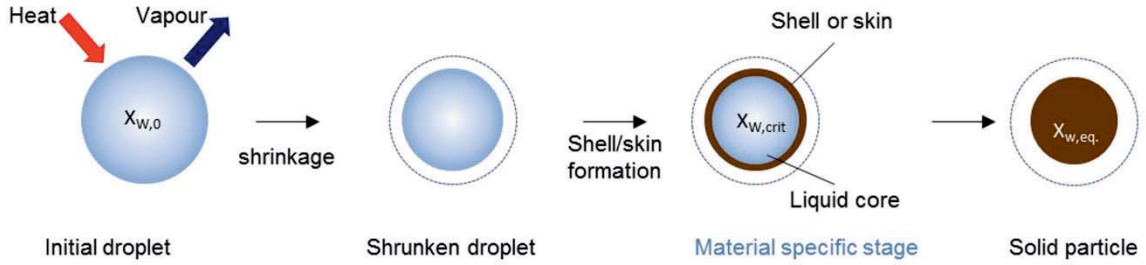

Figure 1.3 Development of particle morphology during particle formation.

The amount of moisture in the material at the end of drying results from an equilibrium between the partial pressure of water in the two phases, i.e. between the relative humidity of the drying gas and the water activity of dried material. The dependence between the equilibrium moisture content ($X_{W,eq}$) and the water activity of a given material during drying is described by moisture desorption isotherm. An example of a moisture desorption isotherm of skimmed milk powder at 25°C, which was determined and fitted by Vuataz et al. (2002) to Brunauer-Emmett-Teller model is shown in Figure 1.4.

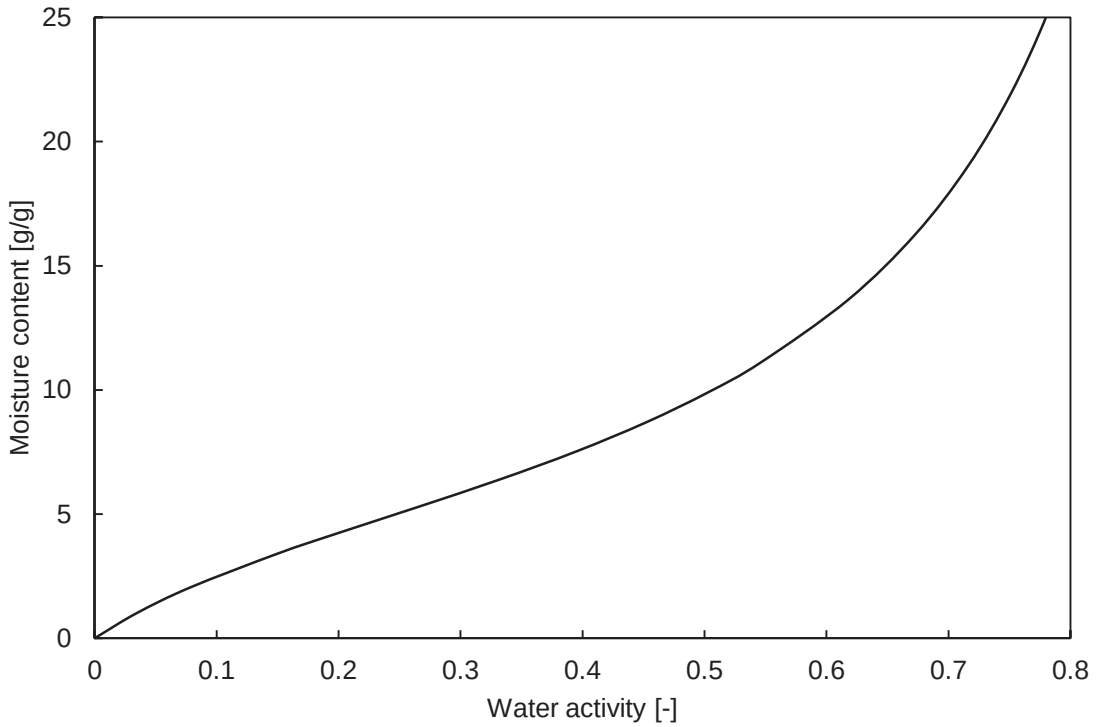

Figure 1.4 Desorption isotherm of skimmed milk powder at 25°C determined by Vuataz et al. (2002) and fitted to Brunauer-Emmett-Teller model.

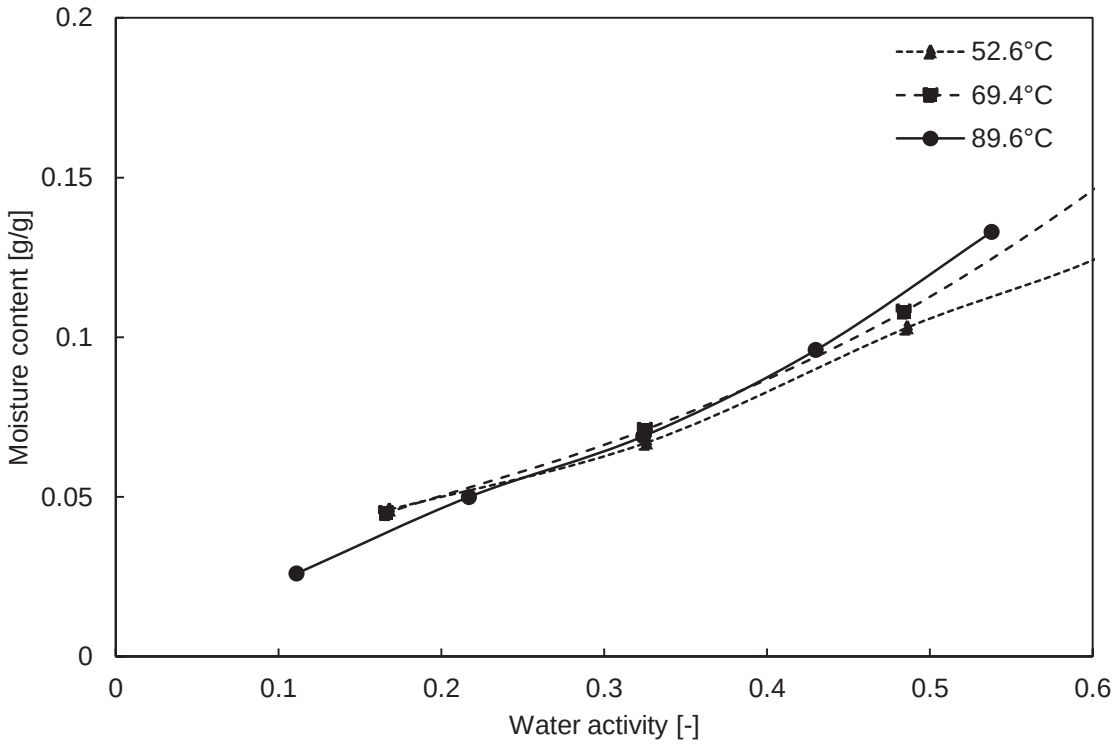

Figure 1.5 Moisture desorption isotherm of skimmed milk powder measured by Lin et al. (2005).

For many materials the equilibrium moisture content decreases with the increasing temperature (Tsotsas et al., 2000). Lin et al. (2005), however, have observed that the desorption isotherms of skimmed milk powder at temperatures above 50°C are characterized by an inversion point, so that at relative humidity above 20 % the equilibrium moisture in the material increases with the temperature. The desorption isotherms of skimmed milk powder measured by Lin et al. (2005) are shown in Figure 1.5.

1.1.2 Development of particle morphology

Depending on material properties and drying history the solidification of the outer layer of a drop can lead to formation of hollow, shuttered or wrinkled particles (Handscomb et al., 2009b). In a spray dryer there is some distribution in drying histories due to temperature, velocity and residence time distributions [(Mezhericher et al., 2012), (Schmitz-Schug et al., 2016)]. This can result in some distribution in morphology of spray dried particles.

1.2 The meaning of powder properties

Good quality of any powder product is determined by adjustment of the powder properties to the application. During powder production (Bhandari et al., 1997), conveying, packaging and mixing good product flowability is desired (Fitzpatrick et al., 2004). However, during powder tableting or pelleting a certain level of adhesion of particles to each other under a load is expected (Palzer, 2011). In powder agglomeration the adhesive behaviour of a powder is imposed by, for example, addition of a plasticizer, which locally

decreases the glass transition temperature of a particle (Palzer, 2009). For powders, which are used by dissolving in a solvent, like milk powder or coffee, good reconstitution properties are important. In case of some particles a controlled dissolution upon exposure to specific conditions is required. Mechanical properties of particles play a role in a release of certain flavour components (Gouin, 2004).

Among these, powder flowability, and caking as the opposite, as well as wetting are influenced by the properties of the surface as explained below. However, other characteristics like particle size and shape or submolecular structure of the material also impact flowability and wetting.

1.2.1 Wetting and instant properties of powders

Wetting is one of the steps of powder reconstitution and often the rate limiting step (Hogekamp and Schubert, 2003). The capillary forces play a dominating role during wetting. The Washburn equation (Eq. 1.1) can be used to describe the rate of capillary rise in a powder pore network (Forny et al., 2011). In Eq. 1.1 $\bar{r}$ is the mean pore diameter of the pores in the bulk material, l is the solvent penetration distance, γ the surface tension of the liquid, η its dynamic viscosity, c, the form factor and θ the Young's contact angle. Therefore, the rate of wetting of a powder bulk is favoured for large capillaries, which correspond to large particles, and materials on which the contact angles are small.

$$\frac{l^2}{t} = \frac{\gamma \cdot c \cdot \bar{r} \cdot \cos\theta}{2\eta} \tag{1.1}$$

Contact angle delivers information about the strength of the interaction between a solid and the solvent. On an ideal, rigid, homogeneous surface a contact angle of a solvent is given by Young's equation (Eq. 1.2), which describes the interfacial energy balance [(Good, 1992), (Decker et al., 1999)]. For a given solvent the contact angle depends on the chemical composition of the solid. In Figure 1.6 a shape and a contact angle of a water drop on a hydrophobic and hydrophilic surface is shown. On a hydrophilic surface the contact angle of water drop is smaller, because the interaction with the liquid is stronger than on a hydrophobic surface.

Real surfaces are characterized by some roughness, which amplify the effects (Palzer, 2001). An apparent contact angle between such a surface and a contour of a sessile drop placed on the surface is not equal to the Young's contact angle (Lazghab et al., 2005). Nevertheless, it is used as an assessment of the strength of interaction between the solvent and the solids [(Puri et al., 2010), (Ji et al., 2016), (Susana et al., 2012), (Lerk et al., 1976)].

$$\gamma_{SL} - \gamma_{SV} - \gamma_{LV}\cos\theta = 0 \qquad (1.2)$$

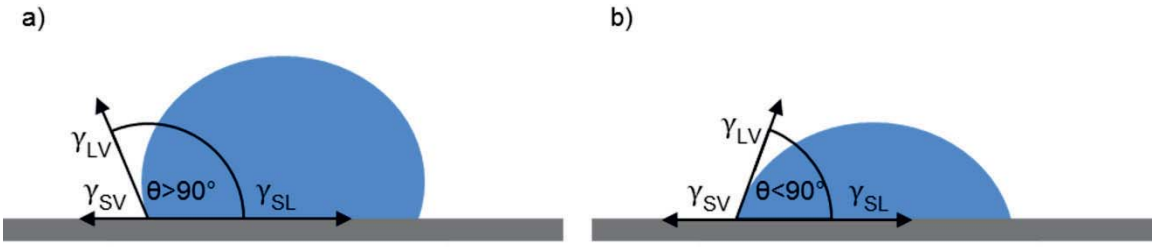

Figure 1.6 Young's contact angle of a test hydrophilic solvent drop on a) hydrophobic and b) hydrophilic surface, where γ_{SL} is the surface tension between the solid and liquid, γ_{SV} is the surface tension between the solid and vapour, γ_{LV} is the surface tension between the liquid and vapour.

Further powder properties which influence the rate of solvent penetration are: powder dissolution and particle swelling, which can lead to an increase in liquid viscosity or affect the pore size. The further steps of powder reconstitution are sinking, dispersion and dissolution (Hogekamp and Schubert, 2003). Sinkability is driven by a difference between the apparent density of the powder and solvent density. The sunken powder should disperse in order to provide large contact surface to accelerate dissolution. Analogically to the powder wetting, powder dispersion is influenced by the type of the solid-solvent interaction.

1.2.2 Flow properties of powders

Powder flow is a plastic deformation of the powder bulk due to movement of the individual particles against each other (Schulze, 2008). The degree of movement of the particles in a bulk depends on the strength of adhesive forces and friction between particles (Schulze, 2008).

Lifshitz: $$F_{vdW} = \frac{h\omega}{32 \cdot \pi \cdot h_s^3} \cdot a^2 \qquad (1.3)$$

Hamaker, for h_s<150 nm $$F_{vdW} = \frac{H}{24 \cdot h_s^3} \cdot a^2 \qquad (1.4)$$

The dominating adhesive force especially for the small and dry particles is the van der Waals force due to plastic and visco-elastic deformations of particles, which for two particles separated by a distance h_s can be described by Eq. 1.3 or Eq. 1.4 (Dopfer et al., 2013), in which a is the diameter of the circular contact area between the particles and $h\omega$ is the Lifshitz-van der Waals constant and H the Hamaker constant. The magnitude of the van der Waals force depends on the size of the contact area and on the chemical composition of the surface, since the constants are related to the surface energy of the material of which the particles consist (Lifshitz, 1956, Hamaker, 1937).

Further adhesion mechanism relevant to powder flowability is formation of sinter bridges between particles (Hartmann and Palzer, 2011). Formation of the sinter bridges can be described with Frenkel's equation (Eq. 1.5) or equation given by Rumpf (Eq. 1.6.), (Hartmann and Palzer, 2011).

$$\left(\frac{h}{d}\right)^2 = \frac{1}{6} \cdot \frac{\gamma}{d} \cdot \frac{t_c}{\eta} \tag{1.5}$$

$$\left(\frac{h}{d}\right)^2 = \left(\frac{4}{5} \cdot \frac{\gamma}{d} + \frac{2 \cdot F_t}{5 \cdot \pi \cdot d^2}\right) \cdot \frac{t_c}{\eta} \tag{1.6}$$

In both equations h is the diameter of a sinter bridge, d is the particle diameter, t_c the contact time between the particles and F_t in Eq. 1.6 is the force with which the particles are contacted with each other. It can be seen that the size of a sinter bridge increases with time, the contact force and surface tension of the material as well as with decreasing material viscosity.

The change in viscosity of the surface or the whole particle concerns especially the amorphous materials. On contrary to crystalline structures, in which the molecules are arranged in a thermodynamically stable lattice, amorphous materials are formed by rapid removal of a solvent from the matrix and cooling, which results in unordered supramolecular structure called glass [(White and Cakebread, 1966), (Alexander and Judson King, 1985), (Vehring, 2008)]. In many particulate food materials the amorphous or semi-amorphous structure is advantageous (Palzer et al., 2012). Due to viscosity of about $10^{12} – 10^{13}$ Pa·s (Schmelzer and Gutzow, 2011) of such materials the mechanical properties are like those of solids. However, due to moisture sorption properties the structure enables fast dissolution of the materials (Palzer et al., 2012).

$$T_g = \frac{(1 - X) \cdot T_{g,S} + k \cdot X \cdot T_{g,W}}{(1 - X) + k \cdot X} \tag{1.7}$$

The viscosity of amorphous materials depends strongly on the temperature and the solvent content, which affects molecular mobility (Roos and Karel, 1990). The relationship between the temperature, at which the viscosity of the materials suddenly drops by three orders of magnitude, i.e. the glass transition temperature T_g, and moisture content X of the materials is described by the Gordon-Taylor-equation (Gordon and Taylor, 1952) (Eq. 1.7), where $T_{g,S}$ and $T_{g,W}$ are the glass transition temperatures of the substance and water respectively and k is a constant characteristic for the pair substance-water.

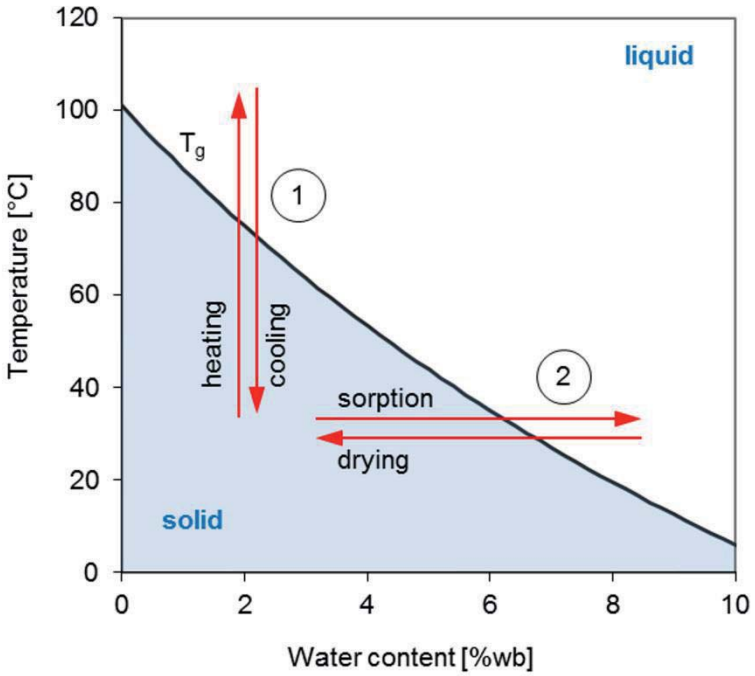

Figure 1.7 Typical dependency of glass transition temperature on powder moisture.

A typical glass transition curve can be seen in Figure 1.7. Above the glass transition temperature the material is in a liquid form and below it is solid. A transition from a solid to a liquid form can take place due to either exposure to increased temperature (path 1) or sorption of moisture (path 2). During spray drying the material follows path 2 in the first stage of drying. In the second stage of drying, if the temperature of the material increases, the material can liquefy and become sticky (path 1). When a powder is exposed to moisture, for example in the air, it can absorb the moisture and change from solid to a viscous rubber (path 2). Exposure to temperatures above the glass transition temperature at a given powder moisture results in a decreased viscosity of the surface, which can lead to formation of viscous bridges between particles [(Roos and Karel, 1991), (Lloyd et al., 1996), (Bhandari et al., 1997), (Downton, 1982)].

$$\log\left(\frac{\theta_{cr}}{\theta_g}\right) = \frac{-17.44\ (T - T_g)}{51.6 + (T - T_g)} \tag{1.8}$$

The empirical Williams-Landel-Ferry (WLF) (Williams et al., 1955) equation describes the temperature dependency of mechanical relaxation time of amorphous polymers. Roos and Karel (Roos and Karel, 1990) showed that above the glass transition temperature the time to crystallization θ_{cr} follows the WLF equation (Eq. 1.8), in which θ_g is time to crystallization at glass transition temperature.

1.2.3 Conclusion

As can be seen from equations 1.3 – 1.8, the surface energy and supramolecular structure of a particle influence wetting and flowability of powders. The surface energy of particles depends on its chemical composition. Therefore, in multicomponent powders accumulation of specific components on the surface of particles can lead to modified powder properties.

1.3 Overview of previous research

The literature on spray drying covers a wide range of topics. Their aim can widely be described as improvement of process efficiency and control of properties of a product. The reported research covers studies of drying gas flow in a tower, atomization, interaction between gas and liquid phases, methods of measurement and modelling of drying kinetics as well as morphology and physico-chemical properties of the dried product. Due to this wide range of the topics, this literature overview focuses on these researches, which concerned drying of multicomponent materials and modelling of single drop drying. Special attention is given to multicomponent systems.

1.3.1 Component reorganization during spray drying

Many types of food, like dairy products or coffee are mixtures of components, which contain next to carbohydrates, fats and proteins, smaller molecules like vitamins and ions. For specific applications, like encapsulation of aromas or active ingredients in particles, wall material is added to a solution and spray dried. During spray drying of such multicomponent solutions, migration of solute components and selective accumulation of specific solutes on the particle surface might take place (Kim et al., 2003).

Distribution of components in spray dried particles was investigated by application of such analytical methods as confocal laser scanning microscopy with dying of the lipid fraction (Kim et al., 2002), free fat extraction [(Kim et al., 2005b), (Kim et al., 2005a), (Murrieta-Pazos et al., 2012)], x-ray photon electron microscopy (Fäldt et al., 1993) and fluorescence method (Landström et al., 1999).

Migration of the components in such a multicomponent system determines the quality of encapsulation. However, the accumulation of specific component on the surface has also an effect on physico-chemical powder properties. Although the properties of the powder can be modified by further processing steps, the surface composition is determined during drying (Kim et al., 2009a).

The composition of the surface is related to powder properties. Presence of fat on the surface of dairy powder particle increases powder cohesion [(Kim et al., 2005a), (Nijdam

and Langrish, 2006)] and decreases wetting of diary powders [(Gaiani et al., 2010), (Kim et al., 2002)]. Accumulation of protein reduced stickiness of carbohydrate powders in the spray dryer chamber [(Wang, 2010), (Adhikari et al., 2009a)]. However, addition of surfactant can result in replacement of the protein from the surface (Adhikari et al., 2009b) and recurring decrease in powder recovery. Increase in amount of lactose on the surface of diary powder improves powder wettability [(Gaiani et al., 2006), (Gaiani et al., 2010)]. Accumulation of a component on the particle surface can be deteriorating to product quality, like in case of accumulation of trypsin, an enzyme, on a surface of spray dried powder results in a loss of enzyme's activity (Millqvist-Fureby et al., 1999). Tailored accumulation of sodium caseinate and lecithin on powder surface can assure a controlled drug release and taste masking (Hoang Thi et al., 2013).

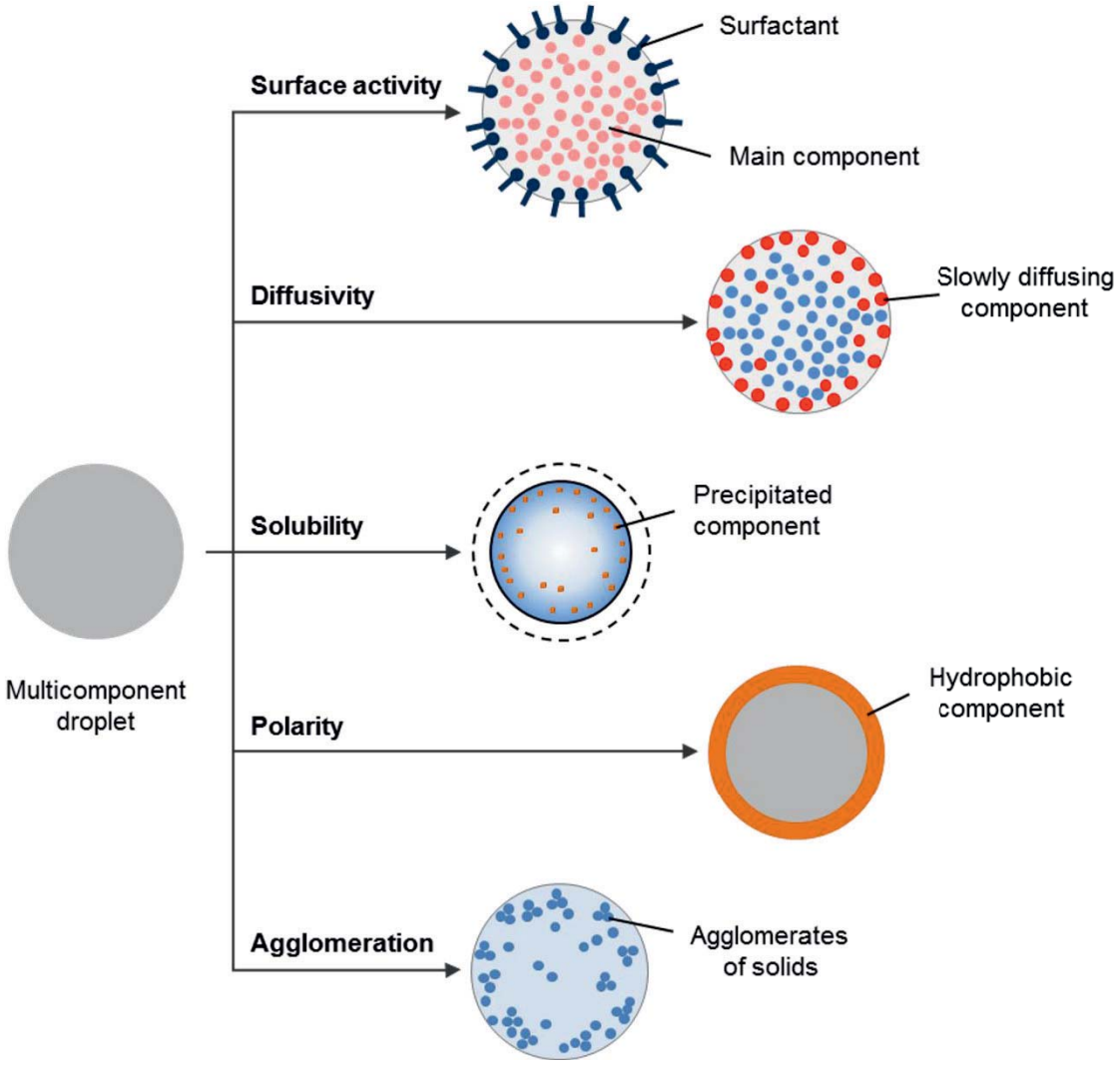

Figure 1.8 Driving forces of component redistribution during drying of a drop.

Different phenomena can be named in relation to component reorganization in a drying drop as schematically shown in Figure 1.8, whereas it is also possible that different effects occur simultaneously. As the potential driving forces for component reorganization authors named the surface activity of protein (Fäldt and Bergenståhl, 1994), differences

in component diffusivities (Meerdink and van't Riet, 2004) and solubilities (Chen et al., 2011).

When at least one of the components is amphiphilic, like surfactants or proteins, the accumulation of this component on the drop-gas interface can be driven by its surface activity. If solutes are characterized by large difference in the molecular size, the slow diffusion of the larger component can lead to its accumulation in the vicinity on the drop surface. This difference in diffusion coefficients can also be important when a drying drop is an emulsion or a suspension, which contains drops of immiscible phase, like fat, or particles, respectively. Some authors (Jayasundera et al., 2011) named the differences in component solubility as another reason of component separation in a drying drop. When the concentration of one of them reaches the solubility limit, the component precipitates forming primary particles. These might again diffuse slower than the dissolved component.

Another process which can be named in relation to component reorganization is based on the model developed by Bück et al. (2012), who considered agglomeration process between primary nano-particles during drying of a single drop. If a suspension contains two different types of primary particles, the different agglomeration rates between the particles of the same and between the particles of different types could influence the distribution of components in a final particle.

1.3.2 Modelling of single drop drying

The objective of modelling of spray drying process on different scales is to mathematically describe a relationship between drying conditions and the properties of the obtained products. In order to predict the effect of a change in process conditions or equipment geometry on the final product a drying process is analysed with the help of computational fluid dynamic tools (CFD). The analysis of the air (Wawrzyniak et al., 2012) and solids flow (Mezhericher et al., 2010a) in a spray dryer allows understanding of the drop trajectories and drying behaviour of the dispersed phase, in order to localize the deposition and agglomeration zones. For more elaborated applications, the knowledge of the properties of materials is necessary to predict the result of particle collisions and the resulting final particle size distribution [(Pawar et al., 2014), (Blei, 2006)]. By coupling the particle drying kinetics with a CFD model of the equipment the sticky zones can be identified in order to localize position where fine particles should be recirculated to the system in order to agglomerate those (Gianfrancesco et al., 2010).

Models, which describe a single drop drying and particle formation, can be applied to study the effect of the drying conditions on the drying kinetics. Three types of modelling

approaches are in use: the drying curve and the reaction engineering approach (REA), which are lumped parameter models, as well as deterministic models.

In the drying curve approach a solvent evaporation is divided into two phases. In the first drying period solvent evaporation takes place at its maximal rate, which is determined by the drying air conditions. Transition to the falling rate drying period, i.e. second drying period, takes place when solute content reaches critical moisture content, at which the drying rate decreases due to mass transfer resistance in a material. This approach has been applied by Langrish and Kockel (2001) in a simulation of drying of a single drop of milk, which was applied into a CFD simulation of a spray dryer.

In reaction engineering approach, solvent evaporation is modelled as energy activated reaction, in which every material is characterized by activation energy, which changes with solvent content. The advantage of these types of models is that they do not require solution of partial differential equations and much computational powder. Therefore, they can be coupled with a CFD simulation (Langrish and Kockel, 2001).

The deterministic models include description of heat and mass transport and can include in different extent the physical and chemical processes taking place in drying materials and the development of the mechanical properties of forming particles. Sano and Keey (1982) developed a drying model of a milk drop, which includes formation of a hollow particle, if the pressure within a particle is sufficiently high. The effect of the drying condition on the porosity of a particle, which forms during drying of a suspension of crystalline primary particles, was modelled by coupling a population balance of the primary particles with drying of a suspension drop (Seydel, 2006). The model of Handscomb et al. [(Handscomb et al., 2009a), (Handscomb et al., 2009b)] considers the growth of primary crystal particles due to crystallization and the effect of the material properties on the final morphology of a particle. Bück et al. (Bück et al., 2012) considered the effect of the interaction between the primary particles on the resulting particle morphology. A wide overview of the current state of development in this field is presented by Mezhericher et al. (Mezhericher et al., 2010b).

Few authors investigated component segregation in a drying drop. A moisture-fraction distribution at different times of drying is reported by Sano and Keey (Sano and Keey, 1982). Handscomb [(Handscomb et al., 2009a), (Handscomb et al., 2009b)] presents solids mass fraction and particle porosity along the radius of a forming particle. Seydel (Seydel, 2006) analysed the particle number density along the drop radius and Bück et al. (Bück et al., 2012) the normalized number concentration along the drop radius.

Among systems containing more than one solute Hecht and King (Hecht and King, 2000) calculated the radial concentration of moisture and a gas tracer in a drying particle at dif-

ferent drying times. The model predicted a concentration peak of the tracer within a forming particle due to decreasing molecular mobility in the vicinity of drops surface. Meerdink and van't Riet (Meerdink and van't Riet, 2004) formulated a drying model of a ternary system, which predicted segregation of saccharose and sodium caseinate during drying in agar slabs. Wang at al. (2013) proposed a distributed parameter model which enabled prediction of the amount of surface active component on the surface of spray dried particles. Gac and Gradoń (2013) formulated a model, which describes migration of two solutes characterized by different solubilities and diffusion coefficients. Chen et al. (2011) considered component segregation in a multicomponent system during initial stages of drop drying and estimated a surface enrichment of the milk powders with a fat component. This approach was further developed into a continuum diffusion model coupled with a molecular level geometrical interpretation [(Chen et al., 2013), (Xiao and Chen, 2014), (Xiao et al., 2015)]. This model enables prediction of selective solute accumulation on the surface layer of nanometre thickness of a particle containing two solutes with different molecular size. However, it requires assumptions on the hypothetical packing of the molecules in a surface-layer of a forming particle.

1.3.3 Conclusion

As can be seen from this overview, in experimental studies the difference between the composition of powder surface and powder bulk has been given a significant attention. Only few authors so far have focused on a theoretical prediction of surface enrichment. Currently, a continuum model is missing, which would enable investigation of the effects of drying rate and feed properties on the composition of the surface of a spray dried particle.

2 Single drop drying model with two solutes

In this chapter a novel drying model of a single drop, which contains two solutes with different diffusivities is formulated. Equations, which describe mass and heat transfer in a drop are presented. Drop composition is spatially distributed, so that the mass fraction profiles within the drop during the drying process can be tracked.

2.1 General model of particle formation

Reorganization of solutes during formation of a particle in spray drying can be driven by different factors (section 1.3.1). The objective of the model is to investigate the reorganization of solutes within a drop in case of a system in which the solutes are characterized by different molecular sizes and consequently different diffusion coefficients. A distributed parameter model is formulated, which enables tracking of components within a drop. The model is based on certain assumptions, which for better understanding of their relevance are discussed in the final section of the chapter (2.2.6).

The macroscopic process of a drop drying is shown schematically in Figure 2.1. Initially, a drop of an aqueous solution formed in a spray dryer is ideally mixed. When a drop of the feed solution contacts hot air in a spray dryer, the solvent begins to evaporate from the drop surface and the drop radius begins to shrink. The local concentration of a solvent decreases close to the particle surface and that of a nonvolatile solute increases (Räderer, 2001). A concentration gradient is formed, which is the driving force for the mass transport of water towards the surface and the mass transport of solutes away from it.

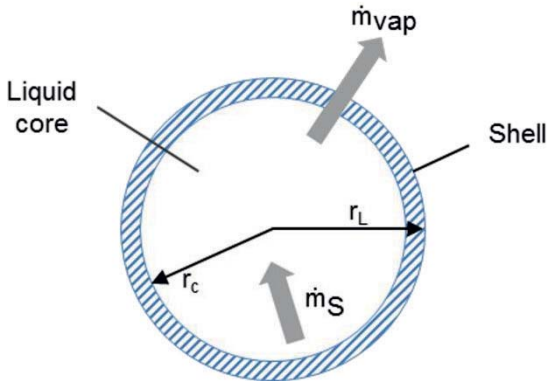

Figure 2.1 Schematic of a particle formation during drop drying.

2.1.1 Solvent evaporation

The driving force of solvent evaporation from a surface of a drop is a difference in the absolute humidity of drop surface and the drying gas. The vapour mass flow ($\dot{m}_V$) from particle surface, which depends on vapour density (ρ_V), mass transfer coefficient (β), ab-

solute humidity on drop surface (Y_{sat}) and absolute humidity of drying gas (Y), was calculated as:

$$\dot{m}_V = \rho_V(T)\beta(Y_{sat} - Y)4\pi r_L^2. \quad (2.1)$$

The mass transfer coefficient β is obtained from the definition of Sherwood number.

$$\beta = \frac{Sh\ D_V}{2r_L} \quad (2.2)$$

There are various correlations developed for the Sherwood number. In spray drying the Ranz-Marshall correlation (Ranz et al., 1952) is commonly used,

$$Sh = Sh_0 + 0.6Re^{0.5}Sc^{0.33} \quad (2.3)$$

with Reynolds (*Re*) and Schmidt (*Sc*) number given by equations 2.4. and 2.5, respectively.

$$Re = \frac{u\ 2r_L\ \rho_{air}}{\eta_{air}} \quad (2.4)$$

$$Sc = \frac{\eta_{air}}{\rho_{air}\ D_V} \quad (2.5)$$

2.1.2 Mass fraction profiles of components

Water mass transfer in an aqueous drop along the drop radius *r* is described by diffusion according to Fick's law (Eq. 2.6), where x_W is the mass fractions of water.

$$\frac{\partial x_W}{\partial t} = -\frac{\rho_W \cdot D_W(x_W)}{r^2}\frac{\partial}{\partial r}\left(r^2\frac{\partial x_W}{\partial r}\right) \quad (2.6)$$

In concentrated solutions, and such are usually encountered in spray drying, the diffusion coefficient of water depends on the concentration of the solutes. A diffusion coefficient of a solvent in a matrix of a solute at changing concentrations can be described by empirical correlations (Räderer, 2001). In such correlations diffusion of the solvent is treated independently of the diffusion of the solutes.

The water transported from the centre of a drop towards the surface is replaced by the solute, which is transported in the opposite direction (Eq. 2.7 and 2.8). The total volumetric flux of solute caused by diffusion is proportional to that of water and described with Eq. 2.9, in which x_S is the mass fractions of solute and ρ_W and ρ_S are water and solute densities.

$$\left|\dot{V}_W\right| = \left|\dot{V}_S\right| \tag{2.7}$$

$$\left|\frac{j_W}{\rho_W}\right| = \left|\frac{j_S}{\rho_S}\right| \tag{2.8}$$

$$\frac{\partial x_S}{\partial t} = \frac{\rho_S}{\rho_W}\frac{D_W(x_W)}{r^2}\frac{\partial}{\partial r}\left(r^2\frac{\partial x_W}{\partial r}\right) \tag{2.9}$$

The diffusion coefficient of water in the matrix of the solute depends on the moisture content and can be described by a correlation given by Adhikari et al. (Adhikari et al., 2003).

$$D_W = D_{W,0}\cdot\exp\left(\frac{-16}{1+16\cdot X_W}\right) \cdot\exp\left(\left(-\frac{100+195\cdot X_W}{1+10\cdot X_W}\right)\cdot\frac{1}{R}\left(\frac{1}{T_d}-\frac{1}{303}\right)\right) \tag{2.10}$$

The resulting diffusive mass flow, $\dot{m}_S$, in a drop is described by Eq. 2.11.

$$\dot{m}_S = -\frac{\rho_A}{\rho_W}\frac{D_W(x_W)}{r^2}\frac{\partial}{\partial r}\left(r^2\frac{\partial x_W}{\partial r}\right)4\pi r^2 dr \tag{2.11}$$

2.1.3 Formation of a solid shell

As a result of the difference in the water evaporation rate from the surface of a drop and the velocity of the solute diffusion away from the surface, the solute accumulates at the surface forming a shell. Authors, who modelled a formation of a solid shell or skin during drying of a drop, considered crystallization and agglomeration of crystals as a shell growth mechanism. Seydel (Seydel, 2006) assumed in his model a critical particle packing in a shell of 55 vol. %. In that model the further number density of particles increases only due to drop volume decrease. Handscomb et al. (2009a) in a drying model of colloidal silica drop allowed a porosity of 35 vol. % in a shell. In the extended model Handscomb et al. (2009b) formulated a shell formation condition as a moment when the solids reach a critical volume and the shell a specific thickness at which its strength is sufficient to withhold capillary pressure.

In the current model formation of an amorphous solid is assumed. On contrary to crystallization and crystal growth, the transition from a rubbery to glassy state is related to the increase in viscosity of a solution, which depends on the solute concentration in the solu-

tion. Therefore, in the model no kinetics of the solid formation was introduced and it is assumed that a shell forms when the local mass fraction of the solute in the vicinity of the surface reaches a predefined value, related to the glass transition. This amount of solute is characteristic to a given material and depends on its physico-chemical properties.

2.1.4 Drop shrinkage and shell growth

Due to water evaporation at the surface of a particle, the radius of the drop shrinks proportionally to the mass of evaporated water according to Eq. 2.12.

$$\frac{\partial r_L}{\partial t} = \frac{\rho_V}{\rho_W} \cdot \beta \cdot (Y_{sat} - Y) \tag{2.12}$$

As a result of the difference in the water evaporation rate from the surface and the velocity of the solute diffusion away from the surface, the solute accumulates at the surface forming a shell. The velocity of the shrinkage of the liquid core due to the growth of the particle shell is obtained from the change of the shell volume and is described with Eq. 2.13. In this equation the first term on the right side describes the velocity of the shell growth due to the evaporation of the water, the middle term describes the reduction of the shell thickness due to the removal of the solid from the shell zone by diffusion (Eq. 2.11) and the last term originates from the change of the outer radius, r_L.

$$\frac{\partial r_c}{\partial t} = -\frac{\dot{m}_V(1 - x_W)}{4\pi r_c^2 \rho_S x_W} + \frac{\dot{m}_S}{4\pi r_c^2 \rho_S} + \left(\frac{r_L}{r_c}\right)^2 \frac{dr_L}{dt} \tag{2.13}$$

2.2 Drop with two solutes

If a drop contains two solutes the difference in their properties might lead to solutes interactions. For example, the solutes can differ in their molecular sizes, which results in different diffusion coefficients of these solutes. In Figure 2.2 development of a concentration gradient during drying of a ternary drop is presented schematically.

The drop contains a solvent, which is presented as a continuous phase, and solutes A and B. The solute A is the main solute component characterized by a smaller molecular weight and thus higher diffusion coefficient (D_A). Solute B can be an additive macromolecular component, which is present in a smaller amount. It is characterized by a lower diffusion coefficient (D_B). It is assumed that initially all components in a drop are ideally mixed.

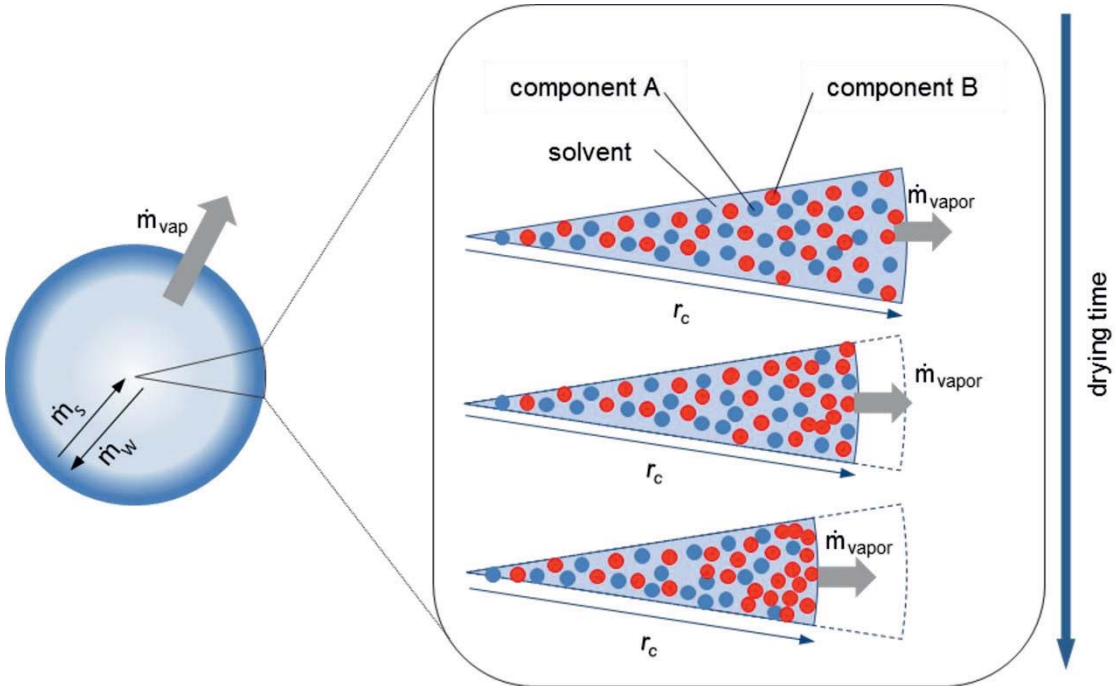

Figure 2.2 Schematic illustration of a concentration gradient in a drying drop, due to water evaporation and accumulation of the slowly diffusing component (B) in the vicinity of the surface (s – solids, w – water).

2.2.1 Solutes interaction

In a ternary or multicomponent system the diffusive flows of the components can affect each other (Cussler, 1984). However, the literature data on the multicomponent diffusion coefficients, which describes the magnitude of this effect for different substances, is rare. Further on, Meerdink and van't Riet (2004) showed that in a ternary water-sucrose-protein system the Maxwell-Stefan diffusion coefficient of the sucrose and protein is one to two orders of magnitude smaller than the diffusion of the solutes in water. Therefore, in order to simplify the calculation, the diffusion of the solutes in this model is treated independently.

In order to introduce the effect of different diffusion coefficients in the diffusive mass transport of solutes in a drop, the interaction between the solute components was described by the ratio *s* of the diffusive flux of the solutes (Eq. 2.14). The flux of solutes depends on the binary diffusion coefficient of the solute in the solvent and the mass fraction gradient of the component.

$$s = \frac{j_A}{j_B} = \left| \frac{D_A \frac{\partial x_A}{\partial r}}{D_B \frac{\partial x_B}{\partial r}} \right| \tag{2.14}$$

Eq. 2.8 is then modified to Eq. 2.15, in which the volume flow of the solvent is equal to the sum of volume flows of the two solutes.

$$\left|\frac{j_W}{\rho_W}\right| = \left|\frac{j_A}{\rho_A} + \frac{j_B}{\rho_B}\right| \tag{2.15}$$

In this modified model the diffusive flux of solvent within a drop remains as described by Eq. 2.1 and the change in the mass fraction of the solutes A and B along the drop radius is proportional to the diffusive flow of water within the drop, as expressed with the Eqns. 2.16 and 2.17 respectively.

$$\frac{\partial x_A}{\partial t} = -s \cdot \frac{\rho_A \cdot \rho_B}{\rho_W \cdot (s \cdot \rho_B + \rho_A)} D_W(x_W) \frac{1}{r^2} \frac{\partial}{\partial r}\left(r^2 \frac{\partial x_W}{\partial r}\right) \tag{2.16}$$

$$\frac{\partial x_B}{\partial t} = -\frac{\rho_A \cdot \rho_B}{\rho_W \cdot (s \cdot \rho_B + \rho_A)} D_W \frac{1}{r^2} \frac{\partial}{\partial r}\left(r^2 \frac{\partial x_W}{\partial r}\right) \tag{2.17}$$

The modified diffusive mass flow of solutes in a drop, $\dot{m}_s$, can then be described by Eq. 2.18.

$$\dot{m}_s = -(1+s)\rho_W \frac{\rho_A \cdot \rho_B}{(\rho_A + s \cdot \rho_B)} \frac{D_W}{r^2} \frac{\partial}{\partial r}\left(r^2 \frac{\partial x_W}{\partial r}\right) 4\pi r^2 \tag{2.18}$$

2.2.2 Diffusion coefficients

To calculate the flux ratios *s* in Eq. 2.14 the diffusion coefficients of solute components are needed. It was mentioned in section 2.1.2 that the diffusion coefficient of water in the solid matrix is described by an empirical correlation. As proposed by Kim et al. (2003), the diffusion coefficients of solutes can be expressed according to the Stokes-Einstein equation, which describes the change in the diffusion coefficient in the relation to the matrix viscosity.

$$D = \frac{k_B T}{6\pi\mu r_{h,i}} \tag{2.19}$$

As in any point of a drying drop both solutes experience the same viscosity of the solution, therefore the diffusion coefficients of the solutes can be expressed as reversely proportional to the hydraulic radiuses of the molecules (Eq. 2.20),

$$\frac{D_A}{D_B} = \frac{r_{h,B}}{r_{h,A}}. \tag{2.20}$$

2.2.3 Driving force of drying

The absolute humidity at the drop surface, Y_{surf}, is related to the vapour pressure on the drop surface. It is lower than the saturated vapour pressure of the pure water at a given temperature due to the presence of solutes. The decrease in the saturated vapour pressure due to the influence of the dissolved solids can be described with a sorption isotherm. This is especially important at low water contents, when the water is strongly bound to the surface. At high water contents many food sorption isotherms are linear or not reliable due to progressing crystallization. Therefore, in this model a typical food isotherm (Al-Muhtaseb et al., 2002) was approximated. At high water contents the absolute humidity at the surface is equal the one of pure water (Eq. 2.21) and when the water content reaches the critical value $x_{W,isotherm}$ the absolute humidity at the surface decreases proportionally to the water content at the surface, $x_{W,surf}$:

$$x_{W,surf} > x_{W,isotherm} \qquad Y_{surf} = Y_{sat}, \tag{2.21}$$

$$x_{W,surf} \leq x_{W,isotherm} \qquad Y_{surf} = \frac{Y_{sat}}{x_{W,isotherm}} \cdot x_{W,surf}. \tag{2.22}$$

2.2.4 Boundary conditions

In the initial time point the radius of the liquid core equals the radius of the drop:

$$r_c(t = 0) = r_L(t = 0) = R_0. \tag{2.23}$$

The boundary conditions for the diffusion equations (Eqns. 2.6, 2.16 and 2.17) in the centre of the drops impose, that the mass fraction of water remains constant in the centre of the drop, i. e.

$$\left.\frac{\partial x_W}{\partial r}\right|_{r=0} = 0. \tag{2.24}$$

As it was mentioned previously, the water concentration in the solid shell is equal to zero.

$$x_W|_{r_C \leq r \leq r_L} = 0 \tag{2.25}$$

2.2.5 Temperature history

Change in drop temperature is the result of heating of the drop by the drying air (Eq. 2.26) and cooling due to the heat of evaporation $\dot{H}_V$ (Eq. 2.29). The heat delivered to a drop is given as

$$\dot{Q}_d = \alpha(T_{air} - T_d)4\pi r_L^2. \tag{2.26}$$

The convective heat transfer coefficient α was calculated according to Eq. 2.27, in which the Nusselt number was obtained from the Ranz-Marshall correlation (Ranz et al., 1952) (Eq. 2.28) and k_a is the thermal conductivity of air. The Reynolds number is defined by Eq. 2.4 and Prandtl number (*Pr*) is calculated according to a correlation given by Glück (1991), (section 8.1).

$$\alpha = \frac{k_a Nu}{2r_L} \tag{2.27}$$

$$Nu = Nu_0 + 0.6Re^{0.5}Pr^{0.33} \tag{2.28}$$

The flow of heat of evaporation was obtained from Eq. 2.29, in which for latent heat of evaporation the correlation given by Glück (1991) was applied (section 8.1).

$$\dot{H}_V = h_V \dot{m}_V \tag{2.29}$$

The resulting change in drop temperature was calculated according to Eq. 2.30, in which the mass of a drop, m_d, is described by Eq. 2.31.

$$\frac{dT_d}{dt} = \frac{\dot{Q}_d - \dot{H}_V}{m_d c_{p,d}} - \frac{T_d \dot{m}_V}{m_d} - \frac{T_d \frac{dc_{p,d}}{dt}}{c_{p,d}} \tag{2.30}$$

$$m_d = m_W + m_A + m_B \tag{2.31}$$

Specific heat capacity of the drop, $c_{p,d}$, was calculated as the mass based average of the specific heat capacities of the components (Eq. 2.32), where m_A, m_B and m_W are the masses of components A and B as well as of water. The temperature dependencies of the specific heat capacities of the components were described by correlations given by Choi and Okos (1986), given in section 8.1

$$c_{p,d} = \frac{c_{p,W} m_W + c_{p,A} m_A + c_{p,B} m_B}{m_d}. \tag{2.32}$$

2.2.6 Model assumptions

The presented above equations are based on the following assumptions:

- ideal symmetry of a drop,

- ideal drop shrinkage and no porosity of the forming shell,
- no interaction between the solutes components and linear dependency of diffusion coefficients of solutes on the viscosity of the matrix according to Stokes-Einstein equation,
- no internal convection in a drop,
- no mass transport resistance in the shell.

The assumption of the symmetry of a drying drop aims at simplifying the equations. It has been used in other models, which were mentioned in section 1.3.2. In reality most of the spray dried particles are not ideally symmetrical, as can be seen in the scanning electron images of the dried powders presented in chapter 5 or in many examples presented by other authors [(Walton and Mumford, 1999), (Alexander and Judson King, 1985)].

No details of particle morphological structure, such as formation of shell porosity or internal gas bubbles, are modelled and the change in drop volume is proportional to the volume of evaporated water. As pointed out by Räderer (2001), this assumption allows description of the mass transport in a drop by diffusion only. Such approach was motivated by a fact, that it is the chemical composition of a drop surface which is in the focus.

It was mentioned in section 2.2.1 that no interactions between solute components are assumed. In reality the gradients of the component can be mutually dependent, especially at low solvent concentrations. Such dependency was observed by Schabel et al. (2007) in a ternary polymer-film system and by Müller et al. (2010) in a polymer system, in which at low solvent concentrations diffusion coefficient of a plasticizer depends on its own concentration. The level of the detail of the model could be further improved by implementing directly in the flux ratio s (Eq. 2.14) the diffusion coefficients in dependence of the concentration of both solute components. However, this requires further measurements in the whole possible range of concentrations of the other two components.

Convection within a drop could lead to remixing of the components. Räderer (2001) argues that with a rapidly increasing viscosity of drop surface during drying the internal circulation can be neglected.

Due to drying the water front moves away from drop surface towards its centre. The evaporated water needs to be transported away from the wet part of the drop through pores of the shell. This mass transport of water vapour through the dry part of the drop is not considered in the model.

2.2.7 Numerical solution

In order to solve the system of the partial differential equations described above, the finite difference method was applied. The distance to the particle centre was used as the property coordinate. The whole simulation domain [0, R_0] was discretized into a set of classes with an equidistant grid. To model a drop with a radius of 50 μm, 1200 classes were used. The discretization was done only once at the initial time point. During simulation the grid remains constant. It should be noted, that such a grid leads to cells with unequal volumes. The resulting system of ordinary differential equations was solved with Euler method with a constant time step of 10^{-6} second. In each time step the following operations were performed for all classes:

Step 1: calculate diffusion rates and mass flows between cells.
Step 2: calculate evaporation mass flow from the drop surface.
Step 3: according to vapour flow, remove water from the boundary cells.
Step 4: shift the solute from outer layers into empty space caused due to evaporation.
Step 5: based on water and solute content in all cells, approximate drop diameter.
The described model and calculation algorithm were implemented into Matlab software package. The implemented equations in discretized form are presented in section 8.2.

3 Materials and experimental methods

If, as postulated in chapter 1, accumulation of molecules on the particle surface is a dynamic process, modification of surface solidification time in a multicomponent drop could lead to different surface compositions of a powder with a given bulk composition. The aim of the experimental work was to see, if any differences in wetting or flowability of powders can be related to differences in composition of powder surface. In the experiments the time of surface solidification was controlled by the drying rate, which was realized by applying different drying temperatures and, thus, allowing different times for components accumulation on drops surface. The materials used as a test systems and the methods of powder preparation, as well as methods applied to characterize the obtained powders are presented in the following sections. If not otherwise specified, the measurements were conducted at the Institute of Solids Process Engineering of Hamburg University of Technology.

3.1 Materials

As a model main component lactose was used, due to its importance in the dairy products, and pharmaceutical applications (Fox, 2003). As the additive a whey protein isolate was used.

3.1.1 Lactose

Crystalline lactose food grade was obtained from Bayerische Milchindustrie GmbH and used for preparation of solutions. According to supplier's specification a typical chemical composition of this product is: lactose min 99.0 wt. %, proteins max. 0.3 wt. %, minerals max. 0.3 wt. %, moisture 0.5 wt. %.

3.1.2 Whey protein isolate

The whey protein isolate (WPI) food grade was obtained from Davisco Foods International, Inc.. According to supplier's specification a typical chemical composition of this product is: protein 97.6 wt. %, fat below 0.5 wt. %, ash 2.0 wt. %, lactose 0.4 wt. %, moisture 4.6 wt. %.

Whey protein isolate is not a uniform product but a mixture of various globular proteins, mainly beta-lactoglobulin, alpha-lactalbumin and bovine serum albumin (de Wit, 1998). The density of the globular proteins, like whey proteins, is 1.34 kg/m^3. WPI is characterized by poor wettability. The initial apparent water contact angle on a surface of non-compacted WPI powder is 130° and decreases to 100° after 300 s (Ji et al., 2016).

3.1.3 Feed composition and preparation

Feed solutions were prepared by placing crystalline lactose and, when required, whey protein isolate powders in a stainless steel container and mixing it with distilled water at room temperature. Before adding water powders were mixed with a spoon in order to improve dispersion of protein powder. Suspension was stirred with a Rushton stirrer and heated on a heating plate to 60°C in order to dissolve lactose. For each drying charge 3 kg of feed solution was prepared. Composition of the feed solutions are summarized in the Table 3.1.

Table 3.1 Compositions of the feed solutions. Mass fraction of the solutes in the feed are given on the solid basis.

Material	Total solids [% g/100g$_{solution}$]	Lactose [% g/g$_{total\ solids}$]	Whey protein [% g/g$_{total\ solids}$]
Lactose	30	100	-
Lactose + 1 % wt. WPI	30	99	1
Lactose + 10% wt. WPI	30	90	10

3.2 Spray drying installation

Powders were prepared in a spray dryer Niro Minor, Type ‚Hi-Tec' with closed circuit, shown in Figure 3.1. A flow chart of the spray dryer installation is presented in Figure 3.2. Drying was conducted in a top spray with co-current air and product flow. Solutions were fed with a peristaltic pump (Medorex type TU/200, Medorex, Germany) and sprayed by a two fluid nozzle with an orifice diameter of 800 µm (type SS-35100, Spraying Systems, Germany).

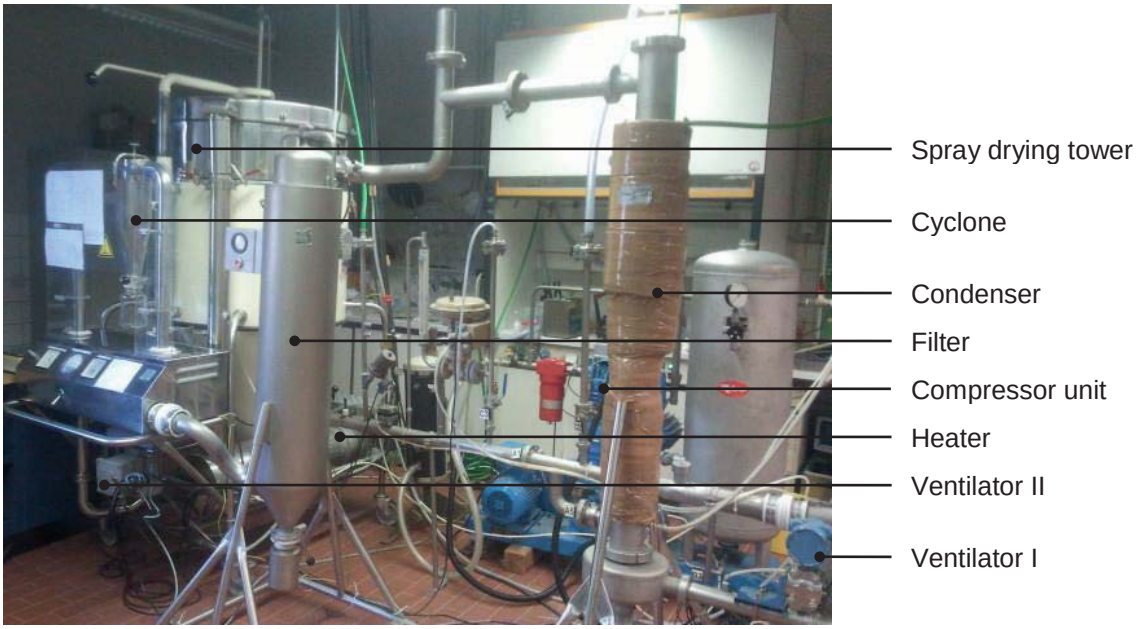

Figure 3.1 Niro Minor Type ‚Hi-Tec', installation used in spray drying experiments.

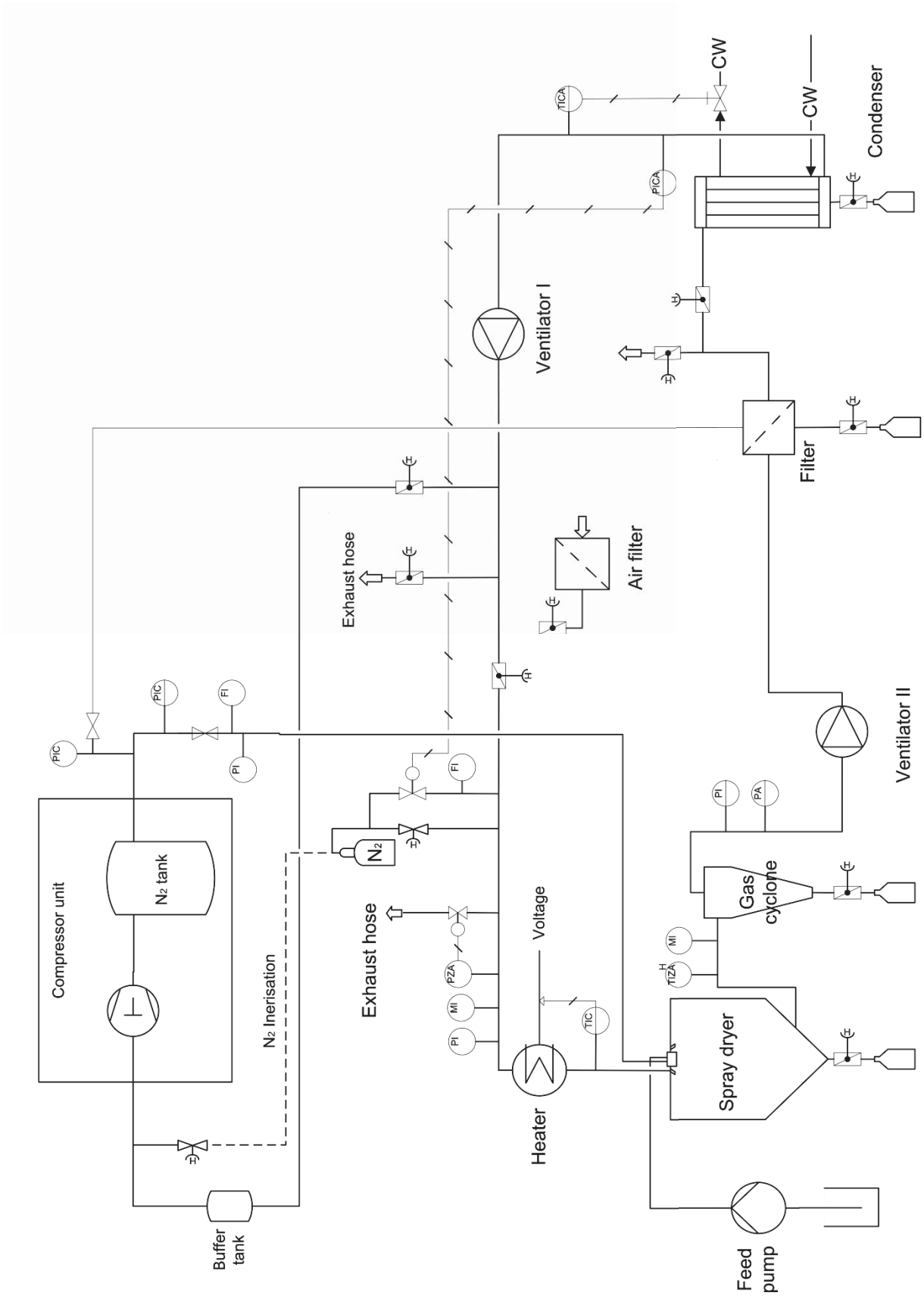

Figure 3.2 Flow chart of the used spray dryer installation.

All drying experiments were conducted in a nitrogen atmosphere. Oxygen concentration was monitored throughout the experiment by an oxygen sensor and maintained below

3 %. Hot nitrogen contacted the sprayed feed at the top of the dryer. Dry powder was collected in an insulated glass container at the bottom of the dryer. Fine particles, which were carried away from the drying chamber with the gas stream, were separated in a cyclone. The remaining, not separated fines fraction was separated in a cartridge filter.

In order to recycle the drying nitrogen, moisture was removed in a condenser. The cooled-off dehumidified drying gas was then again heated and introduced into the dryer. Compressed nitrogen for the spray nozzle gas and cleaning of the cartridge filter was obtained from the compressor loop. The inlet and outlet gas temperature in the installation were measured by a Pt100. Moisture of the drying gas was measured before the heater and at the outlet of the spray drier by a capacitive humidity sensors (Galltec Mess- und Regeltechnik GmbH).

3.3 Drying conditions

Powders were dried at two drying gas inlet temperatures: 180°C and 200°C, with the aim of obtaining two different drying rates. The flow rate of the feed was kept constant in all experiments at 4 ± 0.1 kg/h. The outlet gas temperature resulted from the given feed flow rate and the drying gas inlet temperature. In the further text for the sake of simplicity, the drying conditions at the 180°C of drying gas inlet temperature are referred to as drying at the lower temperature and drying conditions at the 200°C of drying gas inlet temperature are referred to as drying at the higher temperature.

For spray drying the spray dryer installation and the compressor were inertised with nitrogen. The feed was atomized by a two fluid nozzle, with the gas over-pressure of 1.2 bars. Before the feed was introduced to the dryer, hot water was sprayed into the installation at the same volume flow rate as later the feed, in order to keep the temperature of the dryer outlet at similar conditions as during drying and to prevent powder overheating due to contact with hot equipment walls. The change from water to the feed caused increase in the dryer exhaust gas temperature.

The feed solution was sprayed within 30 to 40 minutes. In this time the outlet temperature changed by less than 3°C. Two batches of each composition were produced at each temperature. Due to low recovery of lactose powder at 200°C of drying gas inlet temperature, three drying runs were conducted in order to obtain sufficient amount of powder for all analyses. The additional batch of the lactose has the batch number 13. The specific conditions of each experiment are summarized in the Table 3.2.

Table 3.2 Summary of the details of drying conditions in every spray drying run.

T_{inlet} [°C]	Batch No.	Composition (ratio of lactose to WPI)	φ_{in} [%]	$T(\varphi_{in})$ [°C]	T_{out} [°C]	φ_{out} [%]
180	1	Lactose	67.6	24.3	87.2	20.3
	2	Lactose	67.3	25.2	85.6	20.8
	3	Lactose + WPI (99:1)	66.0	25.4	85.9	20.9
	4	Lactose + WPI (99:1)	66.7	25	93.9	18.1
	5	Lactose + WPI (99:10)	65.3	25.4	92.1	18.7
	6	Lactose + WPI (99:10)	69.0	26.1	89.8	19.7
200	7	Lactose	63.7	25.3	105.7	17.2
	8	Lactose	69.1	26.3	104.3	17.5
	9	Lactose + WPI (99:1)	69.7	25.2	105.8	16.2
	10	Lactose + WPI (99:1)	70.3	25.5	104.8	16.3
	11	Lactose + WPI (99:10)	68.4	25.5	105.0	16.0
	12	Lactose + WPI (99:10)	69.9	26.4	105.4	15.7
	13	Lactose	66.5	29.0	107.4	16.4

T_{inlet}: Inlet temperature of drying gas
T_{out}: Outlet temperature of drying gas
φ_{in}: Relative humidity of drying gas at the inlet
$T(\varphi_{in})$: Temperature of the gas at the relative humidity measurement at the inlet
φ_{out}: Relative humidity of drying gas at the outlet [%]

3.4 Measurement methods for evaluation of primary powder properties

3.4.1 Powder moisture and powder conditioning

Moisture of the obtained powders was measured gravimetrically with a moisture analyser (Precisa Gravimetrics AG, Switzerland). 1 g of powder was placed on an aluminium plate and heated by a halogen lamp to 105°C. The loss of mass was recorded until the mass loss was less than 1 wt. % within 120 s or maximum of 10 minutes.

The spray dried powder differed in the moisture content. In order to remove the influence of moisture content in the measurement of powder wetting and flowability, powders were conditioned by storing in a climatic chamber at 20 % r.h. and 30 % r.h. at 20°C.

For powder wetting test 30 g of each powder was stored in an opened container at 30 % r.h. for two weeks. In flowability measurement powders stored at 20 % r.h. for one month were used. Between 0.15 – 0.3 kg of each powder was placed in an opened container into the climatic chamber. The content of each container was regularly shaken in order to minimize the special distribution of moisture content in the container.

3.4.2 Particle size distribution

Particle size influences the magnitude of interaction forces between particles and has an impact on flowability and wetting of powders. Particle size distribution of the obtained powders was measured by dynamic image analysis (Camsizer XT, Retsch Technology Germany).

Due to the particle size and cohesive nature of the powder, particle size was measured in the air dispersion mode, with air pressure at 50 mbars. The dispersed, flowing particles were illuminated with a pulsating light and the shades of the particles were recorded by cameras.

The velocity of the fine particles is influenced by the particle's size. Before the actual measurement, the velocities of the particles in the optic measurement system had to be adjusted. For this purpose the location of the particles in two subsequent frames, which were taken at defined time interval, was tracked. Different velocity was ascribed to each particle size, as overlapping of the projected areas of the particles can lead to measurement error and has to be avoided.

Particle size distribution of each powder was measured in triplicate as the minimal chord length. The presented results are averaged values. The minimal chord length is the length of the shortest chord of the measured set of the maximum chords and gives a result similar to the results of a sieve analysis.

3.4.3 Powder morphology

Scanning electron microscope (Zeiss Supra VP 55, Carl Zeiss, Germany) was used at the Electron Microscopy Unit of the Hamburg University of Technology to investigate morphology of the powder particles. Samples were mounted on adhesive carbon tabs and sputtered with a 6 nm layer of gold in order to prevent charge accumulation. The applied accelerating voltage was 3 kV, aperture 30 µm and the working distance was between 5 and 10 mm.

3.4.4 Glass transition temperature

Glass transition temperatures of the powders were measured by a differential scanning calorimetry (Q100 TA Instruments, US) at the Nestlé Product Technology Centre in

Konolfingen, Switzerland. The scanning protocol included two scans. The first scan was conducted at 10°C/min from 25°C to 120°C. Next, the sample was cooled at the same rate to 25°C. The second scan was conducted at 5K/min to 120°C and the glass transition temperatures were measured as the onset temperature at the second scan.

3.4.5 Bulk density

Density of bulk powders, ρ_b, was determined as mass of bulk powder m_b, which was filled by a spoon into a cylinder with a volume V_c as given by Eq. 3.1. The radius of the cylinder was 12.75 mm and the height 27.00 mm. For each powder the measurement was done in a triplicate.

$$\rho_b = \frac{m_b}{V_c} \tag{3.1}$$

3.4.6 Apparent particle density

Apparent particle density, which was defined as the density of the particles including closed pores, is important for powder sinking below solvent surface (Freudig et al., 1999). It was measured with a helium pycnometry according to DIN 66137-2. 1 g of powder was filled into a 5 cm^3 container, weighted and placed in the measurement chamber. The sample was flushed five times with helium. The container was pressurized to 20 psi. A valve, which connects the measurement and reference chamber, was opened until the pressure in the system reached the constant value. The measurement was repeated five-fold.

Density of crystalline lactose, which was used for preparation of feed solutions, and of whey protein isolate powder as delivered was measured in order to compare it with densities of spray dried powders.

3.4.7 Surface composition of powders

Atomic surface composition of powders dried at 180°C was measured by x-ray photon electron spectroscope (Kratos Axis Ultra DLD) at the Magnesium Innovation Centre at Helmholz Zentrum Geesthacht. The size of the analysed surface was 300 µm x 700 µm, the emission current 10 mA and the anodes voltage 15 kV. For the overview spectrum four scans were conducted. The protein and lactose fractions on the surface were calculated based on the method proposed by Fäldt et al. (1993).

The method assumes that the signal obtained from the tested sample for each investigated atom is a linear combination of the signals from the components in the sample, as described by Eq. 3.2. In which I^i is the measured atom % of a specific atom i = C, O, N on

the surface of a sample or reference powder. As reference powder spray dried lactose powder (Batch 2) and untreated WPI powder were applied.

$$I^{i}_{sample} = \psi_{\gamma P}\, I^{iP} + \psi_{L}\, I^{iL} \qquad (3.2)$$

To determine the surface coverage of the composite powders a matrix which describes the set of linear equation is solved to find fractions ψ_P and ψ_L.

Two samples of powders dried at the same drying rate, which corresponded to the dryer gas inlet temperature of 180°C (section 3.3) were analysed. The specific samples are listed in Table 3.3.

Table 3.3 Powders used in the analysis of the surface composition by XPS.

Batch No.	Composition	T_{inlet} [°C]
3	Lactose + WPI (99:1)	180
5	Lactose + WPI (90:10)	180

The theoretical atomic composition of lactose ($C_{12}H_{22}O_{11}$) and whey protein isolate were calculated from the chemical formula of the compounds. In the calculation the chemical formula of lactose was used, since due to fast water removal the structure of lactose in the powder should be amorphous. For the calculation of the chemical formula of WPI the typical composition of whey protein isolate given by de Wit (de Wit, 1998) was used. The amino acid sequences of the proteins which occur in the WPI were taken from the Protein Data Bank. The following sequences of the proteins were used: bovine beta lactoglobulin in unliganded form (3NPO); alpha-lactalbumin (1HFZ); immunoglobulin (1IGT); bovine serum albumin (4F5S). The sequence of proteose pepton component 3 was taken from the National Center for Biotechnology Information.

Nikolova et al. (2015) investigated the accuracy of XPS method by comparing surface composition of freeze dried diary powders measured by XPS with the composition measured by the Kjeldahl method. The results showed a good accuracy in case of binary systems containing lactose and protein, especially at low protein contents. When experimentally measured composition of the reference components was used in the matrix, the mean relative error was 8%. For all testes samples the error was below 25 %.

3.4.8 Measurement of atomic composition of powder bulk

Bulk composition of the powders was measured by elemental analysis (Vario Macro, Elementar Analysensysteme GmbH, Germany). Powders were burned at excess of oxygen and the combustion products separated. The mass of the components was obtained from the changes in electric signal of the thermal conductivity detector.

The organic nitrogen it the powder samples was determined by Kjeldahl method (Büchi K436 equipped with a distillation unit B-323 and a titration unit Schott T100). Concentrated sulphuric acid was used to convert organic nitrogen contained in the samples into ammonium sulphate. After addition of sodium hydroxide and steam distillation the obtained ammonia was titrated in sulphuric acid by sodium hydroxide.

Before the analyses all samples were dried overnight in an oven. These measurements were conducted by the Analytical Laboratory of Hamburg University of Technology.

3.5 Powder wetting

In order to evaluate wetting properties of the powders a static wetting method and a contact angle method were applied. The contact angle was measured on tablets of compressed powder and thin layers obtained by spin coating. In order to remove the influence of powder moisture on powder wetting, powder moisture was brought to a constant value by exposing 30 g of each of the powders to an atmosphere of 30 % r. h. and 20°C for two weeks.

3.5.1 Static wetting

The static wetting method was conducted according to a procedure suggested by Gaiani et al. (2010) with some modifications. 1 g of powder was poured into a beaker with a volume of 100 mL, which was filled with 20 mL of distilled water at constant room temperature, and the time until the whole powder was submerged below water surface was recorded. The measurements were done in triplicates. One set of measurements was made with powders as obtained from spray drying, without moisture control. In the second set with controlled powder moisture, powders were poured through a funnel into the beaker.

3.5.2 Apparent contact angle

Another method, which was used to compare water affinity to the powders is a measurement of a contact angle of the solvent on the powders by a sessile drop shape method. As substrates discs of compacted powders obtained by spray drying (sections 3.3) were used. The discs surfaces were prepared by filling powder into a matrix and compacting it by applying a normal stress of 1.3 MPa. The obtained powder-discs were 10 mm in diameter and 4 mm in height. Powders used in the measurement had adjusted moisture content, as described above. Tablet discs were not saturated with the lactose solution as suggested by some authors (Buckton, 1993), as this could lead to powder dissolution and surface deformation.

Despite the applied pressure the obtained powder-discs were porous and their surface had some roughness. The contact angle measured on such powder-discs is a combination of

drop spreading on the surface and sinking into the pores of the bed due to capillary action. Further on, some dissolution of lactose and protein as well as swelling of protein, which disturb the measurement, can be expected (Forny et al., 2011). Thus, a measured apparent contact angle is different from a real contact angle (Lazghab et al., 2005), from which a surface energy according to Young's equation (Eq. 1.2) can be obtained. Charles-Williams et al. (2013) showed that also penetration of water drops into a powder bed depends on surface properties of the powder. Therefore, the measured apparent contact angle can be used to rank powder affinity to water (Ahfat et al., 2000).

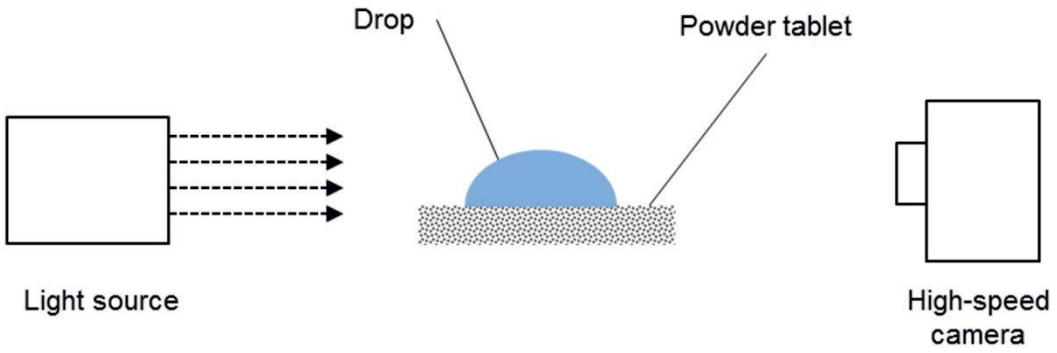

Figure 3.3 Experimental set up for contact angle measurement.

In measurement of Young's contact angle, the three phase contact line does not move (Decker et al., 1999). Since this condition is not fulfilled, the contact angle is measured over time. The obtained curves are ranked in the order of increasing apparent contact angle at a given time.

Schematic of the experimental set up is shown in Figure 3.3. A cold, scattered light source and a high speed camera (Model NX4-S2 Imaging Solutions GmbH) were mounted in one axis with the investigated substrate, which was placed in between. The camera was equipped with a microscope objective "Optem Zoom 125" with a zoom objective „Polaris II". A drop of distilled water with a volume of 2 µl was placed with a pipette on the substrate surface. The image of the drop was recorded 30 seconds with a frequency of 200 Hz by the camera.

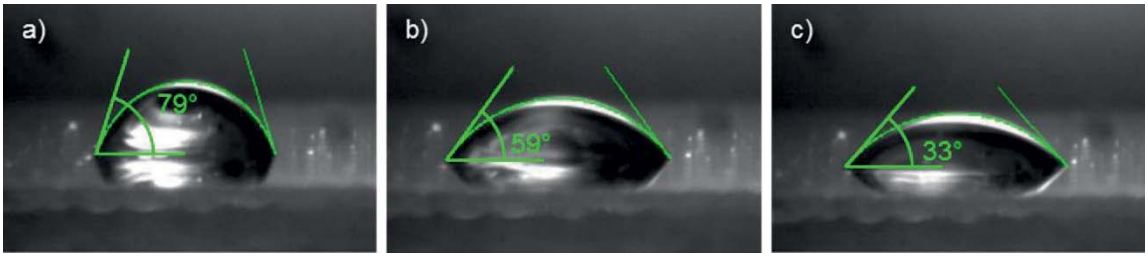

Figure 3.4 Example of evaluation of a water drop shape on a layer of protein conducted with a plug-in "drop analysis LBADSA" of ImageJ software, a) initial, b) 5s, c) 30s.

The images were analysed with the image processing programme ImageJ. The contact angle was obtained using the ImageJ plug-in "drop analysis LBADSA" (Stalder et al., 2010). An image was opened and a base line was found. By placing an arch along the liquid-air interphase, i.e. drop contour, a contact angle between the base line and the drop was found (Figure 3.4). On each sample three drops were measured.

3.5.3 Measurement of contact angle on thin film layers

The contact angle, which was measured on the surface of compacted powder, results from the surface roughness as well as from the surface composition of the particles. The order of the apparent contact angles on the surface of compacted powders was compared with the apparent contact angle on thin film layers obtained by spin coating with the same composition.

To produce thin film layers by spin coating feed solutions with 18 wt. % of total solids content were prepared. The corresponding compositions of the feed solutions are summarized in Table 3.4. Solutions were heated up to 50°C and stirred until all solids dissolved. As a background for the thin layers glass slides were used. The glass slides were rinsed of with nitrogen gas and cleaned by soaking for 20 hours in isopropanol to remove any contamination.

Table 3.4 Composition of feed solutions used in preparation of thin layers and the solids ratio in the thin layers.

Sample No.	Lactose [wt. %]	WPI [wt. %]	Lactose:WPI
1	18.00	-	100:0
2	17.82	0.18	99:1
3	16.20	1.80	90:10
4	-	18.00	0:100

For spin coating the Spin Coater SPIN150, available at the Institute of Advanced Ceramics of Hamburg University of Technology, was used. The glass slide was placed on the vacuum substrate holder. For each layer three drops of a solution were placed on the glass slide and spin coated for 60 seconds. The spinning rate was 100 rpm. This procedure was repeated three times. The obtained layers were then dried for 20 hours at 30 % r.h. over saturated salt solution in a desiccator. It was not possible to measure the surface roughness of the obtained solid layers by optical means such as microscopy, because they were transparent. However, by visual observation no differences in the surface morphology could be seen.

3.6 Powder flowability

Flowability of the powder was tested on untempered powders as obtained from spray drying process by a uniaxial compression test in order to estimate the flowability under high consolidation stresses, which can be relevant in such processes as compacting. In a ring shear cell tester flowability under lower consolidation stresses, which do not lead to powder compaction, was measured.

Flowability of the powders was analysed by determining flow functions for each powder and comparing it between the powders and with the classification given by Jenike (Schulze, 2008). The flow function is the ratio of the consolidation stress (σ_1) to the unconfined yield strength (σ_c), Eq. 3.3. The unconfined yield strength was measured on fresh powders by uniaxial compression test and on powders with tempered moisture contend in a ring shear test.

$$ff_c = \frac{\sigma_1}{\sigma_c} \tag{3.3}$$

3.6.1 Uniaxial compression test

The uniaxial compression test was used to evaluate the effect of powder composition on its flowability. Powders obtained from spray drying were filled into a cylinder with 3 mm diameter and compacted under different normal forces between 100 N and 200 N, which resulted in consolidation stress of 7.96 to 15.92 MPa. A pellet was removed from a mould and a breakage force of the pellet was measured by moving a probe cylinder with a constant velocity of 0.20 mm/s and recording the force until 50 % of the strain was reached. For compaction and breakage force measurement the Texture Analyzer TA.XTPlus (Stable Microsystem) was used.

3.6.2 Ring shear cell test

In order to apply lower normal stress mechanical properties of the spray dried powders were measured by a ring shear tester. In this test powder moisture was brought to a constant value by storing the powders at 20 % of relative humidity for four weeks.

Mechanical properties were measured with a ring shear tester (RST-XS.s, Dr.-Ing. Dietmar Schulze Schüttgutmesstechnik). Powder was filled into the ring of the shear tester, the exceeding powder smoothened with a spatula and the ring with the powder was weighted. The ring was placed on the ring holder and the lid and beams were placed. Normal loads in the range between 2 and 6 kPa were applied and the powder was sheared at three normal loads to determine the yield locus of the powders and flow function.

4 Modelling and simulation

The model of a single drop drying, which was presented in chapter 2 was validated. Next the model was applied to simulate drying in a drop system containing lactose and, as a large molecule, protein. From a simulation the history of component mass fraction in a drop until the moment of rigid shell formation was obtained. Furthermore, accumulation of the slowly diffusing component on the surface in dependence of the initial total solids content, ratio of solutes and drying temperature could be simulated.

4.1 Model validation

Drying of a drop with initial solid content of 40 wt. % was simulated in order to compare the model performance with experimental results of Adhikari et al. (2004), who investigated drying of various carbohydrates. Initial drop diameter was taken as 2.3 mm. The drying air temperature was 65°C, the air velocity 1 m/s and relative gas humidity 2.5 %.

In Figure 4.1 the change in drop moisture content and temperature with the drying time is plotted. Experimental results of Adhikari et al. (2004) are plotted as points. The change in drop moisture corresponds well to the experimental data. Drop temperature predicted by simulation is initially higher than the measured temperature and from 230 s it is lower than the experimental results. The maximal deviation from the experimental data is 16 %, therefore, the model performance is considered satisfactory.

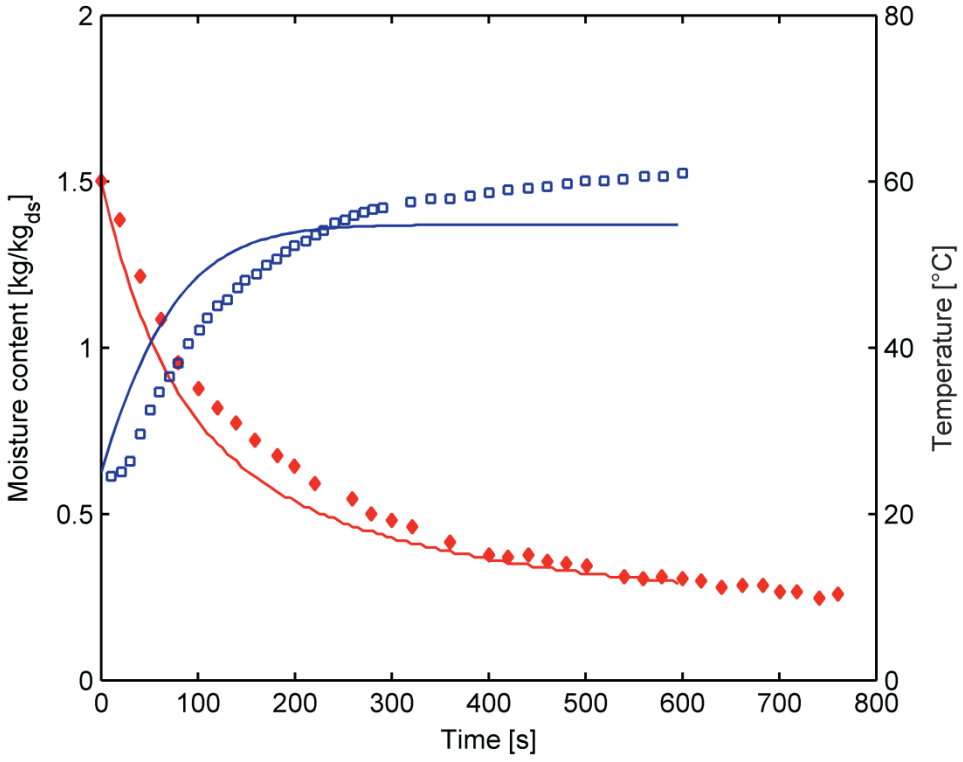

Figure 4.1 Comparison of the simulation results with experiment of Adhikari et al. (2004) (marked in points).

4.2 Drying of lactose drops with protein addition

Drying of an aqueous drop containing lactose as a main solute (component A) and β-lactoglobulin as the additive component (component B) was simulated. Similar system with sucrose instead of lactose was studied by Adhikari et al. [(Adhikari et al., 2009a), (Adhikari et al., 2009b)] in relation to the reduction of stickiness by addition of the whey protein isolate to a solution of sucrose. However, it could also be used to simulate, for example, a dairy matrix.

4.2.1 Simulation parameters

Drops with the initial diameter of 100 μm, which is typical to spray drying process, were modelled in order to predict the effect of the initial total solids content and the ratio of the solute components on the surface composition of a forming particle. The total solids content, TS, is the mass fraction of all solids in a solution related to its total mass. Drying temperatures between 65°C and 80°C were chosen, which correspond to the air exit temperature in a spray dryer. The absolute humidity of the drying air was 0.05 $kg/kg_{dry\ air}$.

It was assumed that when the solid content reaches 97 wt. % in a 5 μm thick outer layer of the drop, the material is mechanically stable enough to form a shell. This moment is defined as the shell formation time, from which on the surface composition remains constant. This mass fraction is close to the fraction of lactose at which a non-sticky solid shell is achieved in the range of the considered drying temperatures (Haque and Roos, 2005). The initial solid content in a drop was varied between 10 wt. % and 70 wt. %.

The diffusion coefficient of water in the solute matrix was described by a correlation given by Adhikari et al. (2003), (Eq. 2.10). The hydrodynamic radius of a β–lactoglobulin molecule was calculated, as suggested by Young and Carroad (1980), by assuming that the volume of the molecule is proportional to its molecular mass (*M*) and that the molecule is ideally spherical:

$$r_B = \sqrt[3]{\frac{3}{4\pi}\frac{M}{\rho_B N_A}}. \tag{4.1}$$

Accumulation of the slowly diffusing component on the surface was expressed as a surface enrichment ratio, k_{surf} (Eq. 4.2), which is defined as the solid based mass fraction of the component B on the surface, $f_{B,surf}$, to the solid based mass fraction of this component in the bulk of the particle, as in Eq. 4.3.

$$k_{surf} = \frac{f_{B,surf}}{f} \tag{4.2}$$

$$f = \frac{x_B}{TS} \tag{4.3}$$

Table 4.1 Summary of the data applied in the model.

Parameter	Value	Reference
Hydrodynamic radius of lactose, r_A	$0.43 \cdot 10^{-9}$ m	(Ribeiro et al., 2006)
Hydrodynamic radius of β–lactoglobulin, r_B	$1.8 \cdot 10^{-9}$ m	Eq. 4.1
Molecular mass of β–lactoglobulin	18000 g/mol	(Loch et al., 2011)
Density of water	998 kg/m^3	(Lide, 2008)
Density of lactose (amorphous)	1520 kg/m^3	(Chen and Mujumdar, 2008)
Density of β–lactoglobulin	1350 kg/m^3	(Fischer et al., 2004)

The solid based mass fraction of component B in the bulk, f, was varied between 0.1 and 0.5. The surface of the forming particle was defined as an outer layer of the particle with a thickness of 0.18 μm, which is equal to a length of 100 protein molecules. Further simulation parameters are listed in Table 4.1.

4.2.2 Component profiles during drop drying

In Figure 4.2 a decrease in drop mass and increase in the temperature of drops dried at 65°C and 80°C are plotted until the moment of shell formation. The mass of the drop dried at 80°C decreases faster than the mass of the drop dried at 65°C. However, at the moment of shell formation the mass of this drop is higher than of the drop dried at 65°C. This is because water removal from the surface is very fast and too little water is transported in this time to the surface of the drop. The drop dried at 65°C reaches the temperature of the drying gas at the moment of shell formation. The temperature of the drop dried at 80°C, at the moment of the shell formation, reaches 61°C. The lower temperature of this drop is due to fast shell formation and higher vapour mass flow from the drop.

In Figure 4.3 and 4.4 the mass fractions profiles of the components along the radius until the moment of shell formation are plotted during drying of drops at 65°C and 80°C respectively. The initial total solids content of the feed was 30 wt. % and the solid based mass fraction of the slowly diffusing component in drop bulk, f, is 0.1.

A mass fraction of water decreases towards the surface of the drop as water is removed. Correspondingly, the mass fraction of solutes increases. In the region in which water is completely removed from the drop (drying time of 0.30 s and 0.02 s in Figures 4.3 and 4.4 respectively) the shape of the mass fraction profiles of the solutes changes. The ratio

between the solute components remains constant and the mass fraction of component A decreases, whereas that of component B increases. Therefore, in the profile of component A a peak in the mass fraction develops.

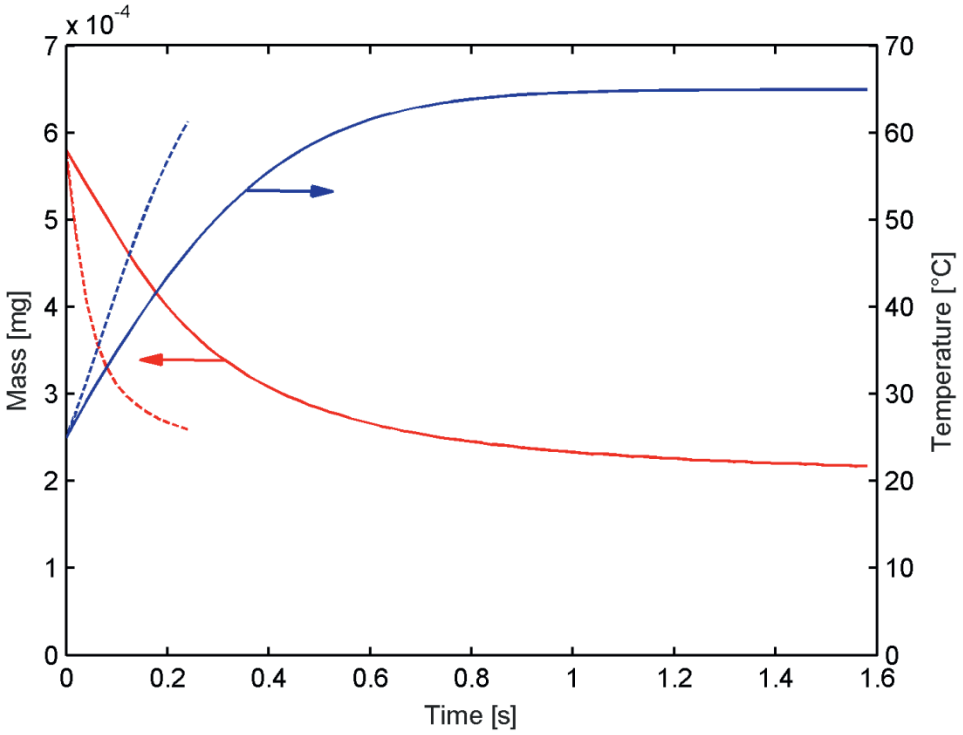

Figure 4.2 Change in drop mass and temperature over drying time. Solid line: T_{air} = 65°C, dashed line: T_{air} = 80°C, r_0 = 50 µm, TS_0 = 30 wt. %, u = 1 m/s, Y_g = 0.05 kg/$kg_{dry\ air}$, f = 0.1.

With the progress of drying, the mass fraction of water in the bulk of the drop dried at 65°C decreases and the mass fraction of component A increases. At the moment when the shell is formed, i.e. 1.58 s, the mass fraction of component A everywhere in the drop is at least the double of its initial mass fraction.

In the drop dried at 80°C, due to the fast water removal from the drop, water mass fraction almost instantly (profile at drying time 0.02 s in Figure 4.4) decreases in the vicinity of the surface, whereas it remains at the level of the initial mass fraction in the bulk of the drop. The water mass gradient covers only a small part of the radius. This results in an increase in mass fraction of solutes only in a narrow range of the drop.

At the later stage of drying (drying time 0.16 s) the water mass fraction gradient in the drop becomes smoother, covering a wider range of drop diameter. The mobility of solutes increases and component A diffuses towards the drop centre. Corresponding to the peak in the mass fraction profile of component A, a minimum in the profile of component B develops. At the moment of the shell formation, the mass fraction profiles in the drop dried at 80°C are steeper than in the drop dried at 65°C. This can be attributed to the faster water removal from the drop and faster decreasing mobility of the solutes.

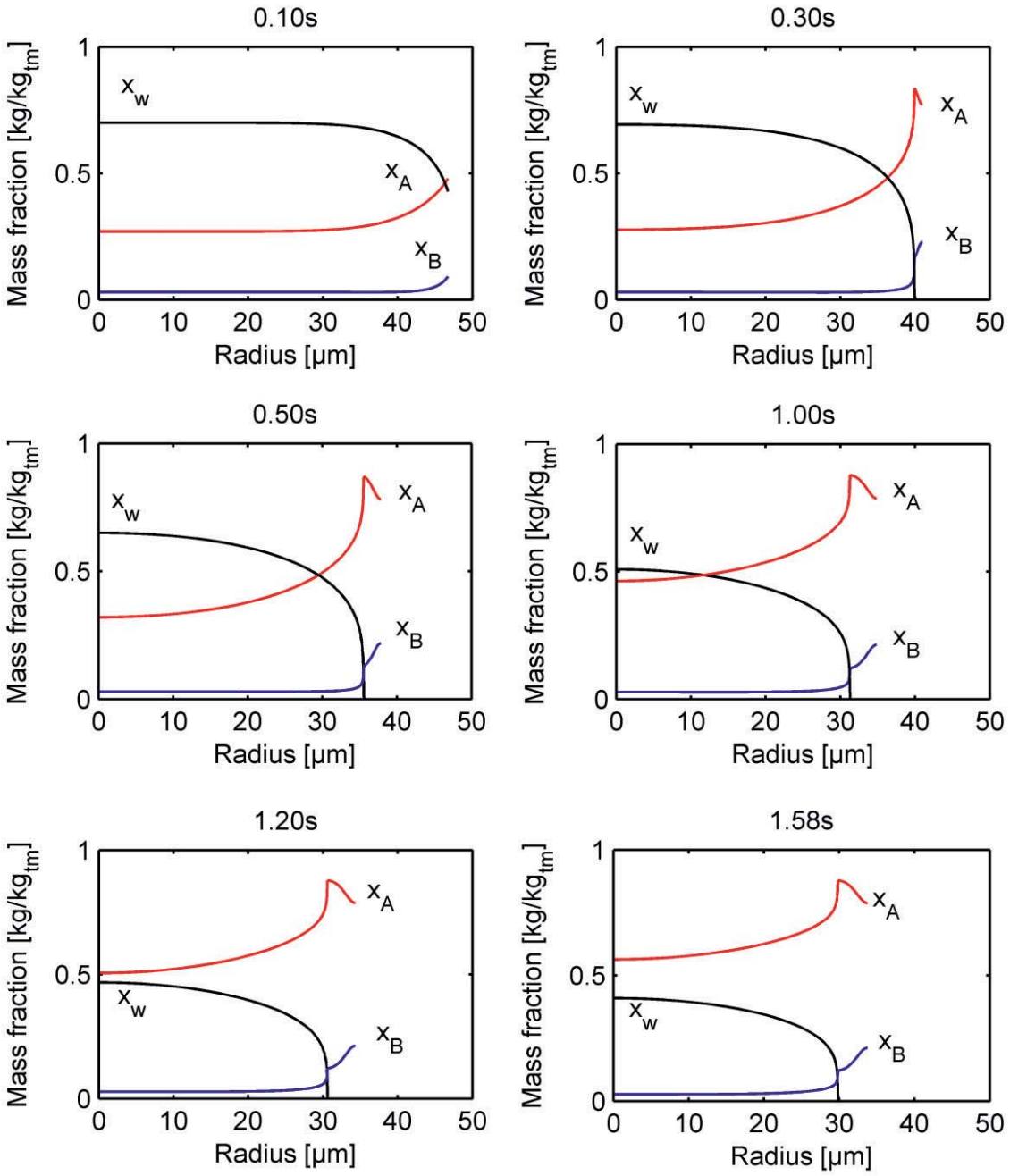

Figure 4.3 Development of a mass fraction profiles of water (x_W), fast diffusing component A (x_A) and slowly diffusing component B (x_B) during drying of a drop at 65°C until the moment of shell formation t_{shell} = 1.58 s. Fraction of slowly diffusing component was f = 0.1.

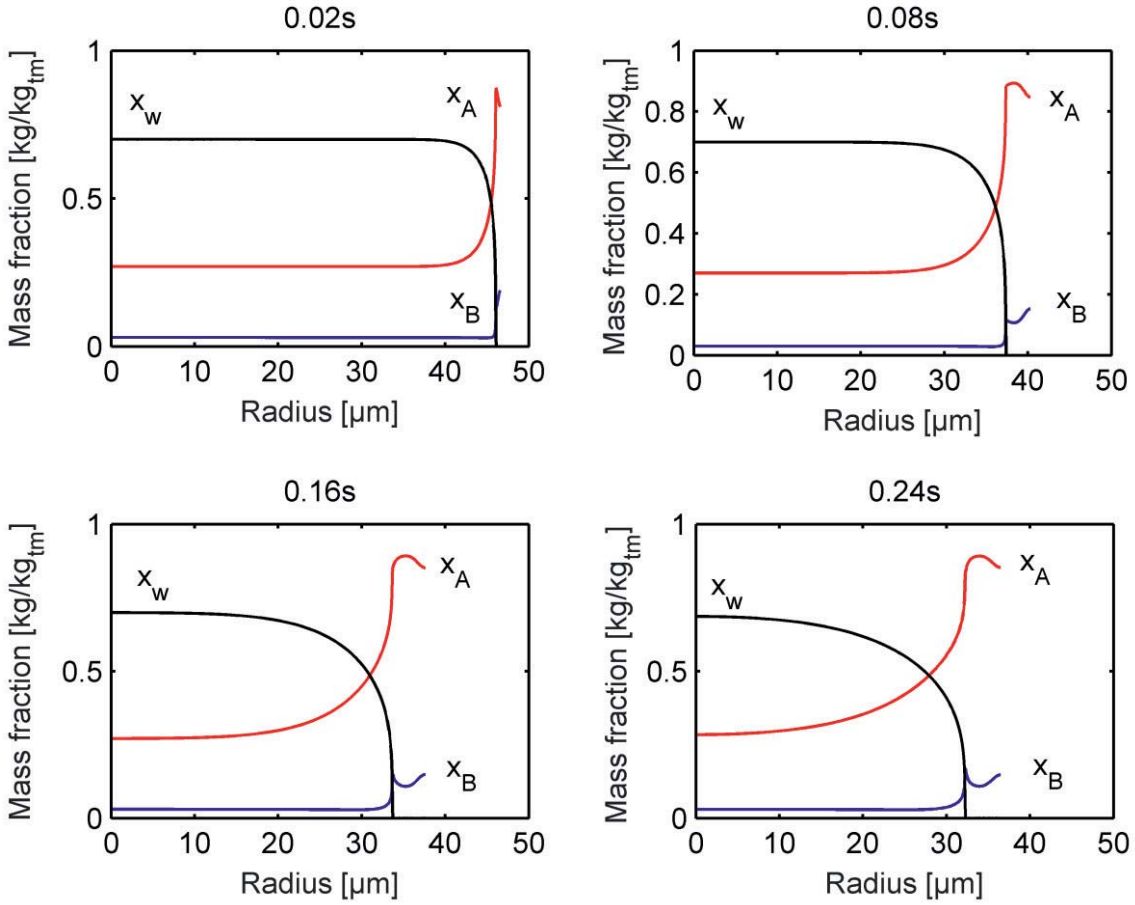

Figure 4.4 Development of a mass fraction profiles of water (x_W), fast diffusing component A (x_A) and slowly diffusing component B (x_B) during drying of a drop at 80°C until the moment of shell formation t_{shell} = 0.24 s. Fraction of slowly diffusing component was f = 0.1.

4.2.3 Composition on particle surface

In Figure 4.5 the effect of the initial total solid fraction on the enrichment of a 0.18 µm surface layer is shown for different solid based mass fractions of the slowly diffusing component B in the bulk. An enrichment of the surface layer in component B by 10 % to 150 % at the considered drying conditions is predicted. The highest enrichment can be seen for the lowest initial total solids contents and low bulk fraction of component B. With increasing initial total solids fraction, the surface enrichment decreases and the surface composition approaches the bulk composition. This is due to a decreasing time of shell formation. With increasing bulk fraction of component B, the surface enrichment also decreases, due to the decreasing mass fraction gradient of component B.

Surface compositions, which correspond to the above discussed surface enrichments, are shown in Figures 4.8 and 4.9 as mass fractions of component B on the surface of forming particles. For the spray dried lactose particles with addition of 10 wt. % of the whey protein isolate in bulk solid and initial total solids content of 10 wt. %, the surface coverage with the additive was about 45 wt. % (Wang, 2010). This amount corresponds to a 4.5-fold surface enrichment. Our model predicts at similar drying conditions 31 wt. % of the

slowly diffusing component on the surface of the particle. This value is in a good agreement with this experimental results. The differences can be explained by the fact that in the model, the particle surface is defined as an outer hole sphere of the drying drop of 0.18 μm depth, whereas the analytical method applied by Wang and Langrish (2010) had a sensitivity of few nanometres, where the accumulation of the slowly diffusing component can be even more pronounced. Moreover, other effects that were not included in the model, like the surface activity of the additive, might contribute to the increased concentration on the surface. It is also important to note, that drops which are falling down in a tower are rotating and exposed to shear forces from the gas phase (Frohn and Roth, 2000), which acts on the surface. This leads to some drop internal turbulences, at least at the initial stage of drying, when viscosity is low. Thus a partial redistribution of the components by convection can be expected.

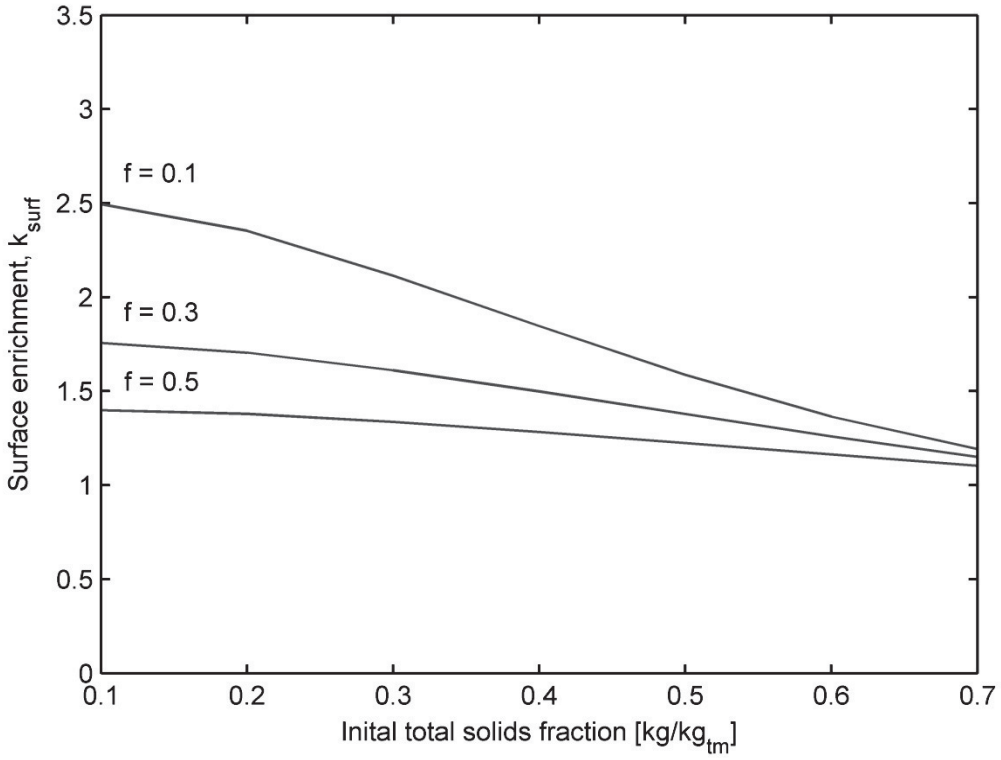

Figure 4.5 Influence of the initial total solid content and solid based mass fraction of slowly diffusing component B in the bulk (f) on the surface enrichment of particles, $r_0 = 50$ μm, u = 1 m/s, T_{air} = 65°C, $Y_g = 0.05$ kg/kg$_{dry\ air}$.

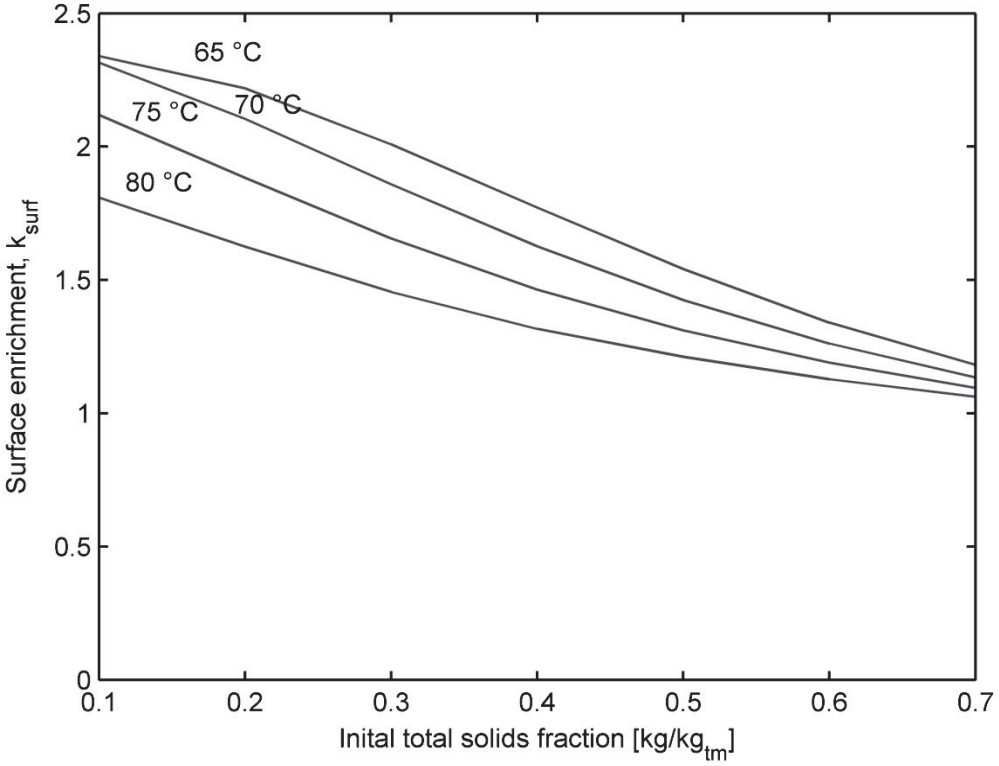

Figure 4.6 Influence of the initial total solid content and the drying air temperature on the surface enrichment of the slowly diffusing component B, r_0 = 50 µm, u = 1 m/s, f = 0.1, Y_g = 0.05 kg/kg$_{dry\ air}$.

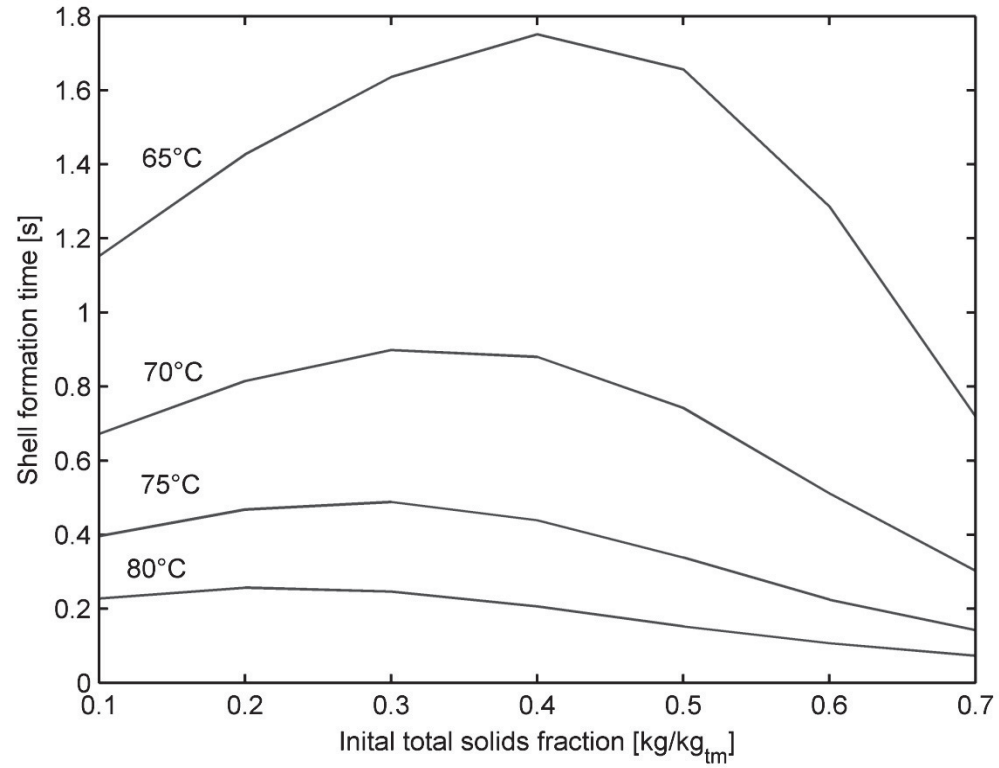

Figure 4.7 Influence of the initial total solid content and the drying air temperature on the shell formation time, r_0 = 50 µm, u = 1 m/s, f = 0.1, Y_g = 0.05 kg/kg$_{dry\ air}$.

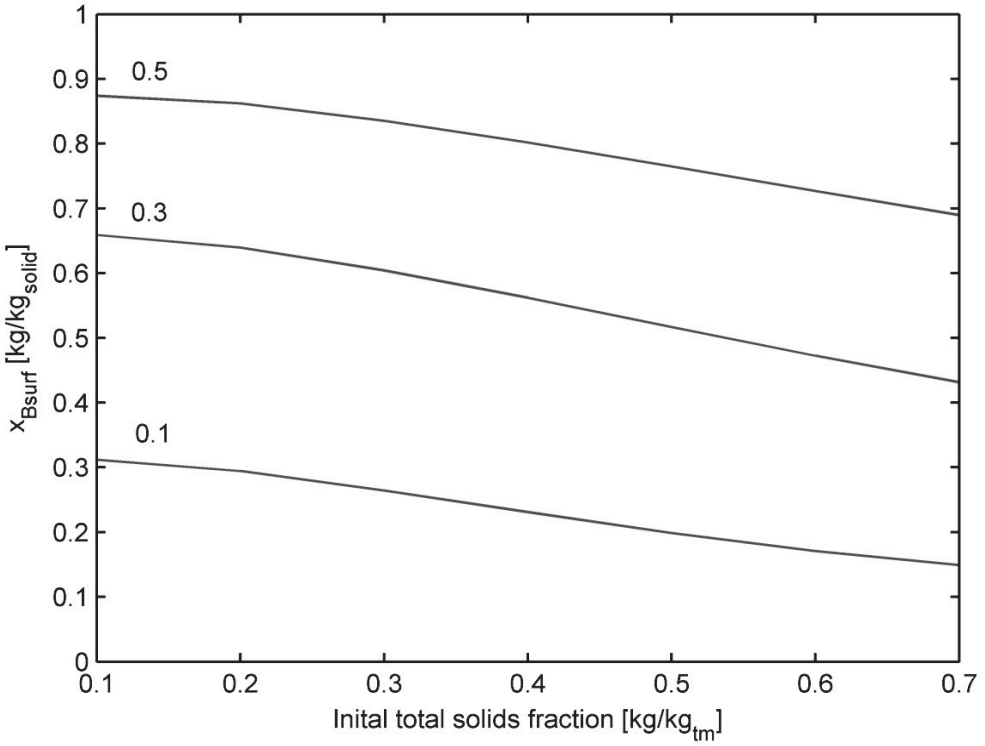

Figure 4.8 Influence of the initial total solid content and the bulk solid based mass fraction of slowly diffusing component B (f) on the dry mass based mass fraction of component B on the surface of a particle, r_0 = 50 µm, u = 1 m/s, T_{air} = 65°C, Y_g = 0.05 kg/kg$_{dry\ air}$.

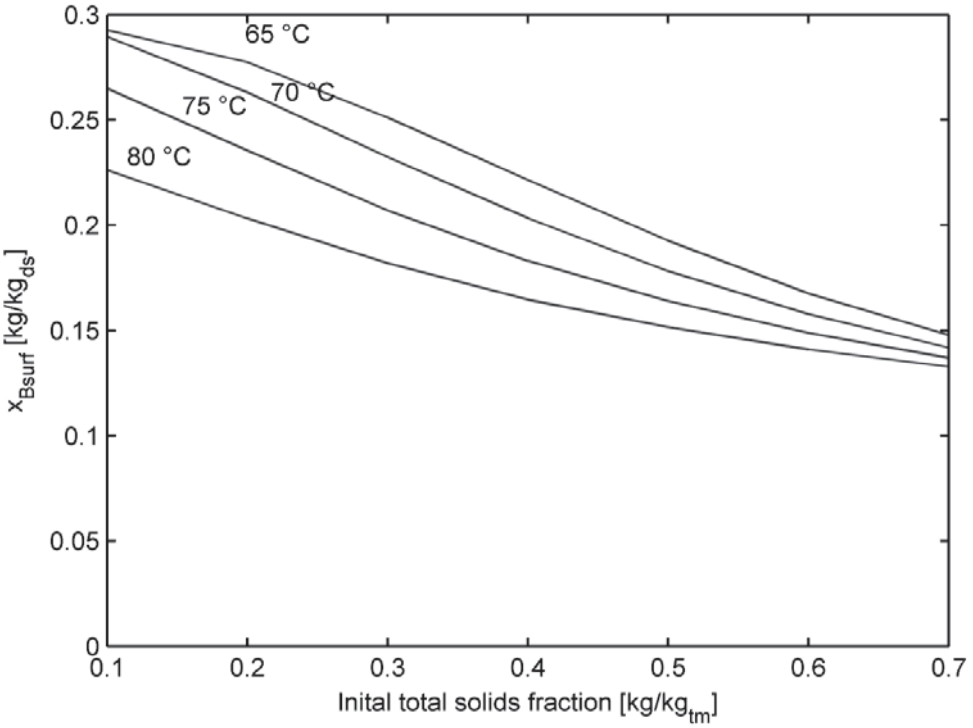

Figure 4.9 Influence of the initial total solid content and the drying air temperature on the dry mass based mass fraction of component B on the surface of a particle, r_0 = 50 µm, u = 1 m/s, f = 0.1, Y_g = 0.05 kg/kg$_{dry\ air}$.

5 Experimental investigation of powder properties

Drying rate influences morphology of powder, which plays an important role in surface related properties. Therefore, at first the primary properties of the powders produced under conditions defined in chapter 3 are characterized in order to identify possible sources of differences in powder properties. Further, surface composition of two powders with 1 wt. % and 10 wt. % of protein in the bulk are compared. The analysis of the wetting and flowability of the powders in relationship to other powder properties and process conditions leads to conclusions on the origin of differences in properties of powders.

5.1 Density of crystalline lactose and whey protein isolate

Density of crystalline lactose measured by helium pycnometry is 1357 kg/m^3. As can be seen in Table 5.1 this value is lower than the most reported in literature. This can be due to the presence of some fraction of amorphous material. The apparent density of the WPI powder measured by helium pycnometry is 998 kg/m^3.

Table 5.1 Density of lactose.

Type	Density [kg/m^3]	Temperature [°C]	Reference
Lactose (crystalline)	1357	20	Own measurement
α-lactose monohydrate	1540	20	(McDonald and Turcotte, 1948)
β-lactose	1589	20	(McDonald and Turcotte, 1948)
Lactose (not specified)	1525	50	(Chen et al., 2011)
Lactose (amorphous)	1520	n.a.	(Chen and Mujumdar, 2008)
Lactose (not specified)	1525	n.a.	(Lewis and Hawley, 2007)
Lactose (not specified)	1780	20	(Fox, 2003)

5.2 Characterization of primary properties of the powders

Before the effects of drying conditions and feed compositions on the surface wetting and powder flowability are discussed, in this section the primary properties of the powders obtained by spray drying are characterized.

5.2.1 Moisture and glass transition temperature of spray dried powders

In Figure 5.1 moisture of the spray dried powders is plotted against the outlet drying gas humidity, the data can be reviewed in Table 5.2 and 5.3. Powders dried at the higher temperatures are characterized by lower moisture. No clear effect of the composition on

powder moisture can be observed. The moisture content of the powders dried at the lower temperature correspond well to the desorption isotherm given by Lin et al. (2005) (Figure 1.5).

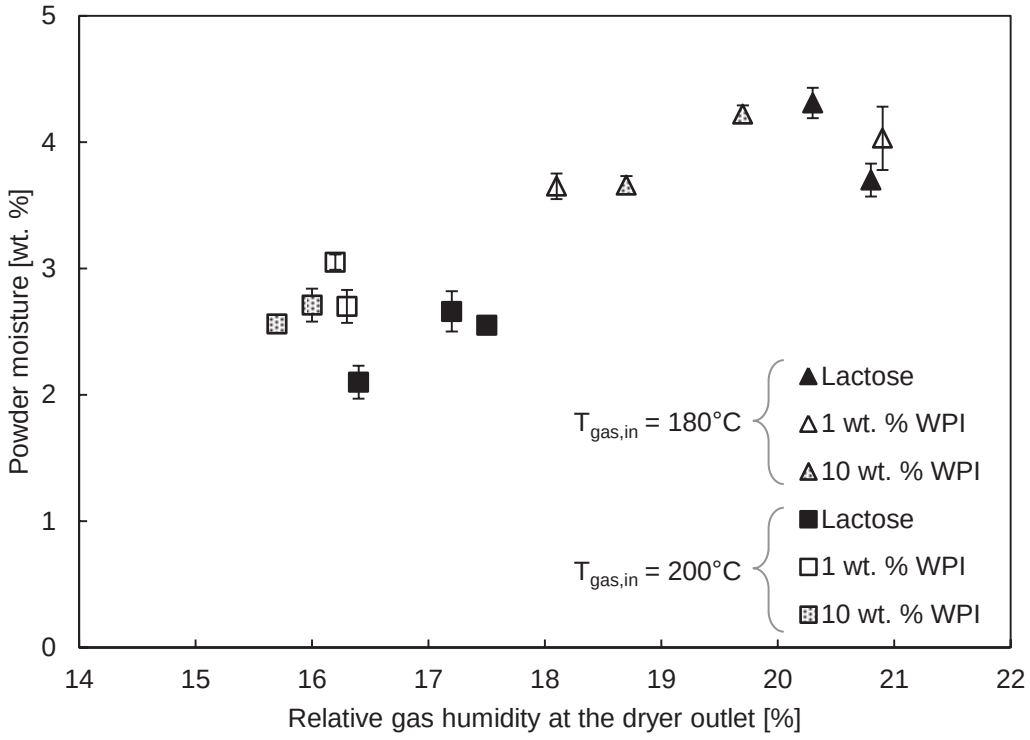

Figure 5.1 Dry solid based moisture of spray dried powders vs. relative gas humidity at the outlet of the dryer.

Table 5.2 Moisture and glass transition temperature of powders dried at drying gas inlet temperature of T_{inlet} = 180°C.

Composition	Batch No.	Moisture [g/ds]		T_g [°C]	T_{out}-T_g [°C]
		Mean	St. Dev.		
Lactose	1	4.31%	0.12%	58.79	28.4
	2	3.70%	0.13%	61.86	23.7
Lactose + WPI (99:1)	3	4.03%	0.25%	58.39	27.5
	4	3.65%	0.10%	65.54	28.4
Lactose + WPI (90:10)	5	3.66%	0.07%	64.97	27.1
	6	4.22%	0.07%	59.93	29.9

In Figure 5.2, the measured glass transition temperatures of the powders are plotted against wet solid based powder moisture. In the diagram also a theoretical glass transition curve and experimental data available in the literature (Vuataz, 2002) are plotted. The dashed lines indicate the gas temperature at the outlet of the spray dryer, which corresponds to the indicated gas inlet temperatures. It can be seen that the glass transition tem-

peratures of the powders, also these which contained WPI, correspond well to the theoretical glass transition curve of lactose. The values measured in this work are higher than predicted by a theoretical glass transition temperature curve. However, the difference is systematic and can originate from differences in the determination of the onset temperature.

Table 5.3 Moisture and glass transition temperature of powders dried at drying gas inlet temperature of T_{inlet} = 200°C.

Composition	Batch No.	Moisture [g/ds]		T_g [°C]	T_{out}-Tg [°C]
		Mean	St. Dev.		
Lactose	7	2.66%	0.16%	69.98	35.7
	8	2.55%	0.06%	70.48	33.8
	13	2.10%	0.13%	n.a.	n.a
Lactose + WPI (99:1)	9	3.05%	0.06%	69.38	36.4
	10	2.70%	0.13%	74.73	30.1
Lactose + WPI (90:10)	11	2.71%	0.13%	72.57	32.4
	12	2.56%	0.02%	75.74	29.7

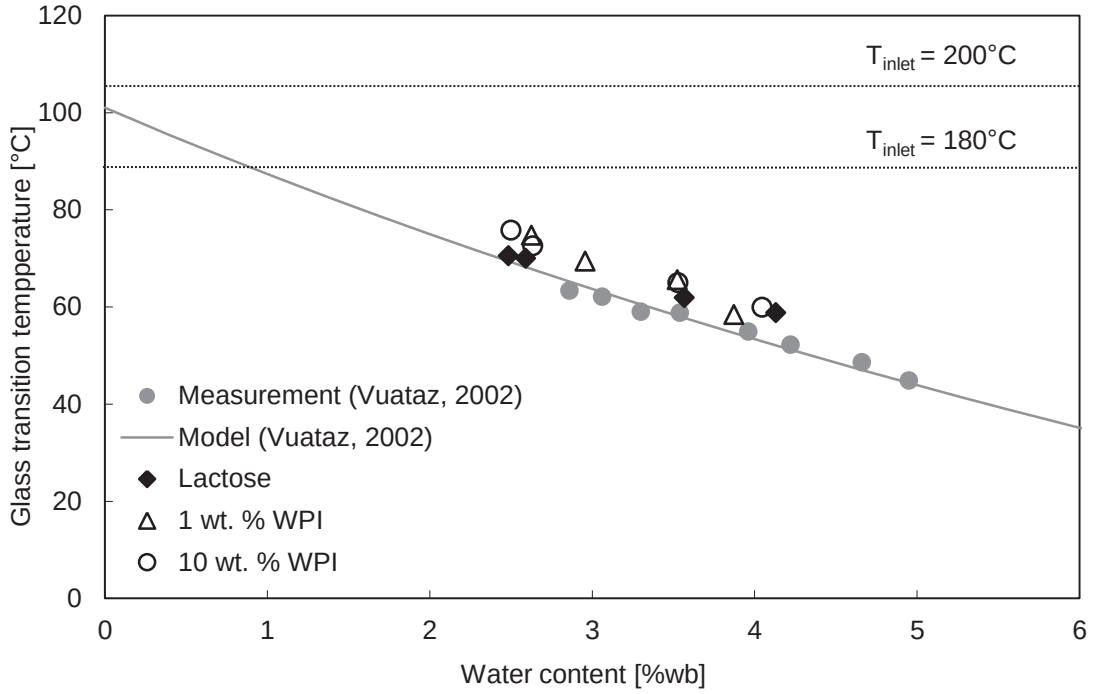

Figure 5.2 Comparison of the glass transition temperature with the literature data (Vuataz, 2002).

No effect of the WPI on the glass transition temperature of the lactose-WPI mixtures could be seen. This is in agreement with the observations of Wang and Langrish (2010), who studied lactose-WPI and lactose-sodium caseinate systems, as well as of Adhikari et

al. (2009a), who did not observe an increase in glass transition temperature of sucrose-WPI powders. Li et al. (2016) argue that this is due to phase separation in a particle and the fact that only the glass transition temperature of amorphous lactose phase is measured.

At moisture contents below 3.6 wt. % wet solid based, the glass transition temperature of powders with WPI are about 5°C above the lactose powders, which could indicate that at this low moisture contents the addition of WPI increases the glass transition temperatures of the composite. At higher moisture contents the glass transition temperatures of powders with protein are no different than that of lactose.

Moisture of the powders after conditioning is summarized in Tables 5.4 and 5.5. Due to exposure to air with 20 % r. h. powder moisture increased to about 5.1 wt. % and due to exposure to air with 30 % r. h. it increased to 7.5 wt. %. These values are close to the values predicted by Vuataz et al. (2002) (Figure 1.4) for skimmed milk and the differences can originate from the temperature difference. Therefore, it can be concluded, that the equilibrium moisture was reached in the stored powders. The differences in powder moisture between powders stored at the same humidity and temperature can be attributed mainly to local differences in exposure to the air of powder bulk and to the difference in the bulk composition.

Table 5.4 Moisture of powder dried at drying gas inlet temperature of T_{inlet} = 180°C after storage at 20 % r.h. and 30 % r.h. at 20°C.

Composition	Batch No.	Moisture after storage at 20 % [g/ds]		Moisture after storage at 30 % [g/ds]	
		Mean	St. Dev.	Mean	St. Dev.
Lactose	1	5.69%	0.06%	7.30%	0.14%
	2	n.a.	n.a.	7.82%	0.27%
Lactose + WPI (99:1)	3	5.61%	0.26%	8.13%	0.45%
	4	5.51%	0.34%	7.42%	0.20%
Lactose + WPI (90:10)	5	5.01%	0.12%	6.99%	0.12%
	6	5.12%	0.07%	7.82%	0.31%

The moisture content of lactose powders dried at the higher temperature is systematically lower than that of other powders. One possible reason can be a difference in the amount of crystalline phase in these powders. The gas outlet temperature during drying of this powder was 36°C above its glass transition temperature (Figure 5.2). According to the

WLF equation (Eq. 1.8) at this temperature difference, the crystallization rate is nine times faster than in the powder dried at the lower temperature. Chiou et al. (2008) have also observed different degrees of crystallinity of the spray dried powders.

Table 5.5 Moisture of powder dried at drying gas inlet temperature of T_{inlet} = 200°C after storage at 20 % r.h. and 30 % r.h. at 20°C.

Composition	Batch No.	Moisture after storage at 20 % [g/ds]		Moisture after storage at 30 % [g/ds]	
		Mean	St. Dev.	Mean	St. Dev.
Lactose	7	n.a	n.a	n.a	n.a
	8	4.45%	0.08%	n.a	n.a
	13	3.94%	0.20%	6.31%	0.91%
Lactose + WPI (99:1)	9	5.15%	0.09%	7.77%	0.11%
	10	5.22%	0.10%	7.82%	0.03%
Lactose + WPI (90:10)	11	4.94%	0.06%	7.45%	0.15%
	12	5.11%	0.02%	8.01%	0.67%

5.2.2 Particle size distribution of powders

The characteristic values of the particle size distributions of the powders and the average for all powders are collected in Table 5.6. All powders have similar particle size distributions, as can be seen in Figure 5.3 and 5.4. The variation in the values originates probably from small variations in the setting of the pump or atomizing gas pressure in each experiment. The similarity in the particle size distribution means that the effect of the particle size of the bulk on water penetration into the powder bulk or on the strength of adhesive forces between the particles is minimized.

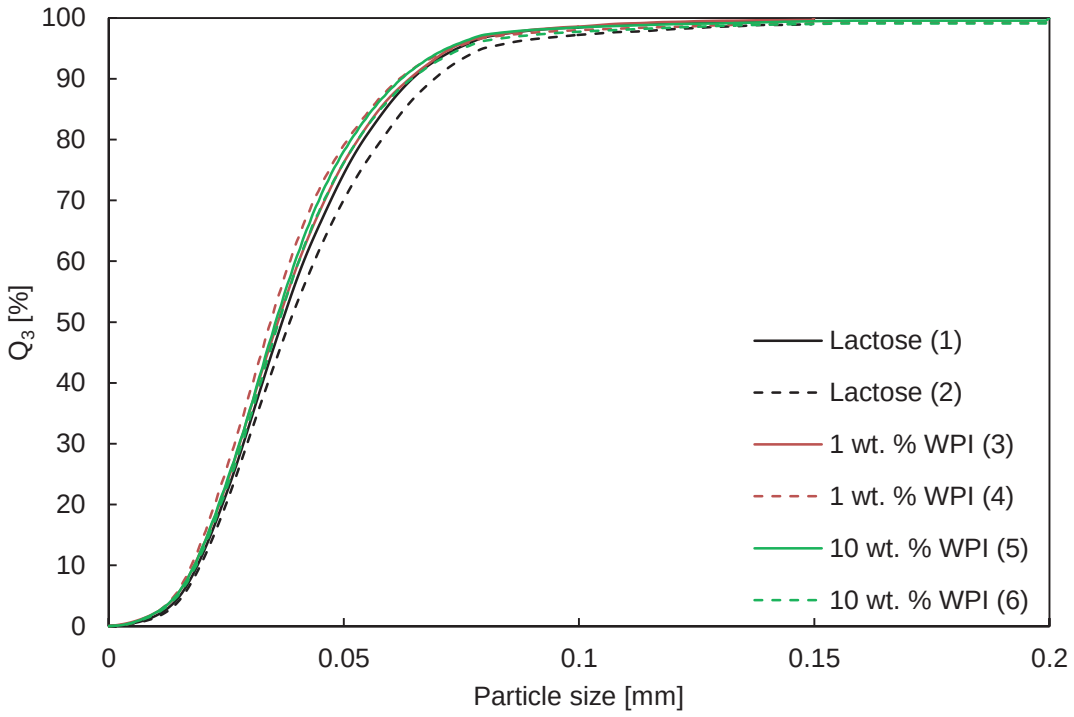

Figure 5.3 Cumulative particle size distribution of lactose and lactose with addition of 1 wt. % and 10 wt. % of WPI powders dried at T_{inlet} = 180°C. Numbers in brackets indicate the number of a batch.

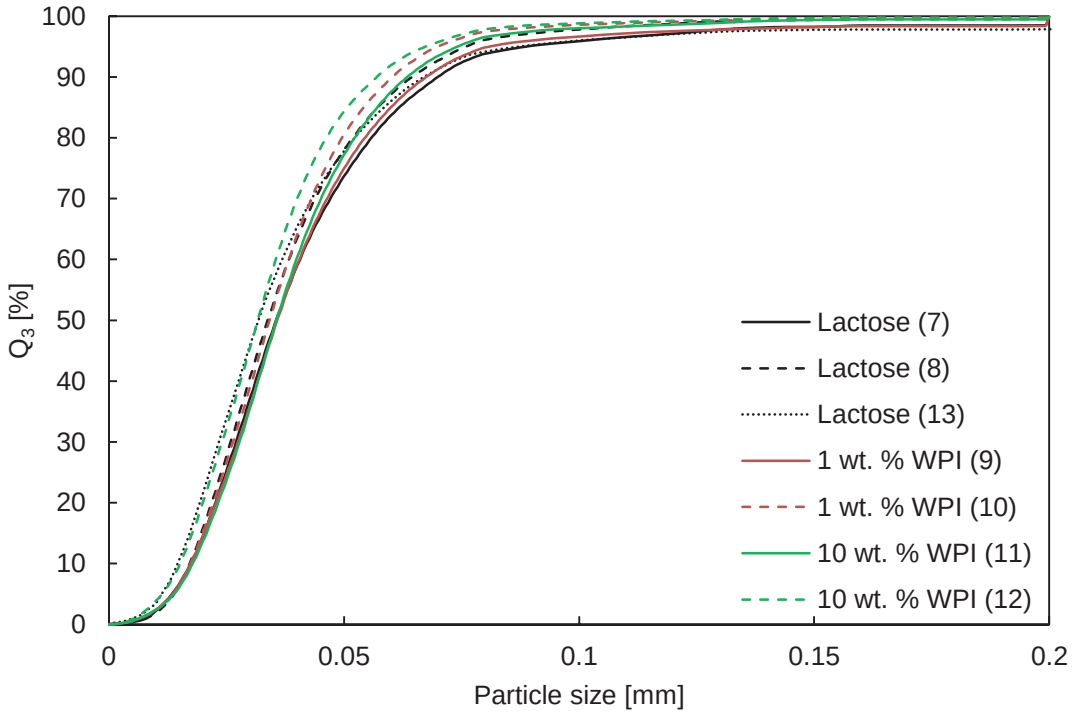

Figure 5.4 Cumulative particle size distribution of lactose and lactose with addition of 1 wt. % and 10 wt. % of WPI powders dried at T_{inlet} = 200°C. Numbers in brackets indicate the number of a batch.

Table 5.6 Particle size at 10, 50 and 90 % of the cumulative particle size distribution of the powders and the average size for each characteristic value.

Batch No.	Composition	d [µm] at Q_3 = 10 %		d [µm] at Q_3 = 50 %		d [µm] at Q_3 = 90 %	
		$d_{3.10}$	St. Dev.	$d_{3.50}$	St. Dev.	$d_{3.90}$	St. Dev.
1	Lactose	19.5	0.2	37.9	0.3	66.0	0.1
2	Lactose	20.0	0.2	39.0	0.4	69.8	0.2
3	Lactose + WPI (99:1)	18.7	0.0	36.5	0.2	64.5	0.6
4	Lactose + WPI (99:1)	18.3	0.1	35.1	0.1	62.5	0.5
5	Lactose + WPI (90:10)	18.9	0.0	36.2	0.1	62.9	0.6
6	Lactose + WPI (90:10)	19.2	0.1	36.9	0.1	65.1	0.7
7	Lactose	18.3	0.1	36.4	0.2	71.2	0.7
8	Lactose	17.8	0.1	34.4	0.3	65.2	1.2
9	Lactose + WPI (90:1)	18.0	0.0	36.5	0.1	68.2	0.3
10	Lactose + WPI (90:1)	17.5	0.1	34.0	0.2	59.2	0.2
11	Lactose + WPI (90:10)	18.5	0.1	36.3	0.3	68.2	0.3
12	Lactose + WPI (90:10)	15.8	0.0	32.3	0.0	57.6	0.8
13	Lactose	17.6	0.1	35.2	0.2	72.5	1.6
	Average	**18.3**	**1.0**	**35.9**	**1.7**	**65.6**	**4.2**

5.2.3 Morphology of powders obtained by spray drying

In the scanning electron microscopy (SEM) images of the lactose powders (Figure 5.5) morphological differences can be seen between lactose powders dried at different temperatures. The particles of lactose powder dried at lower temperature are shrivelled and partially wrinkled, whereas these dried at higher temperature are predominantly spherical. In both powders some extend of agglomeration can be seen.

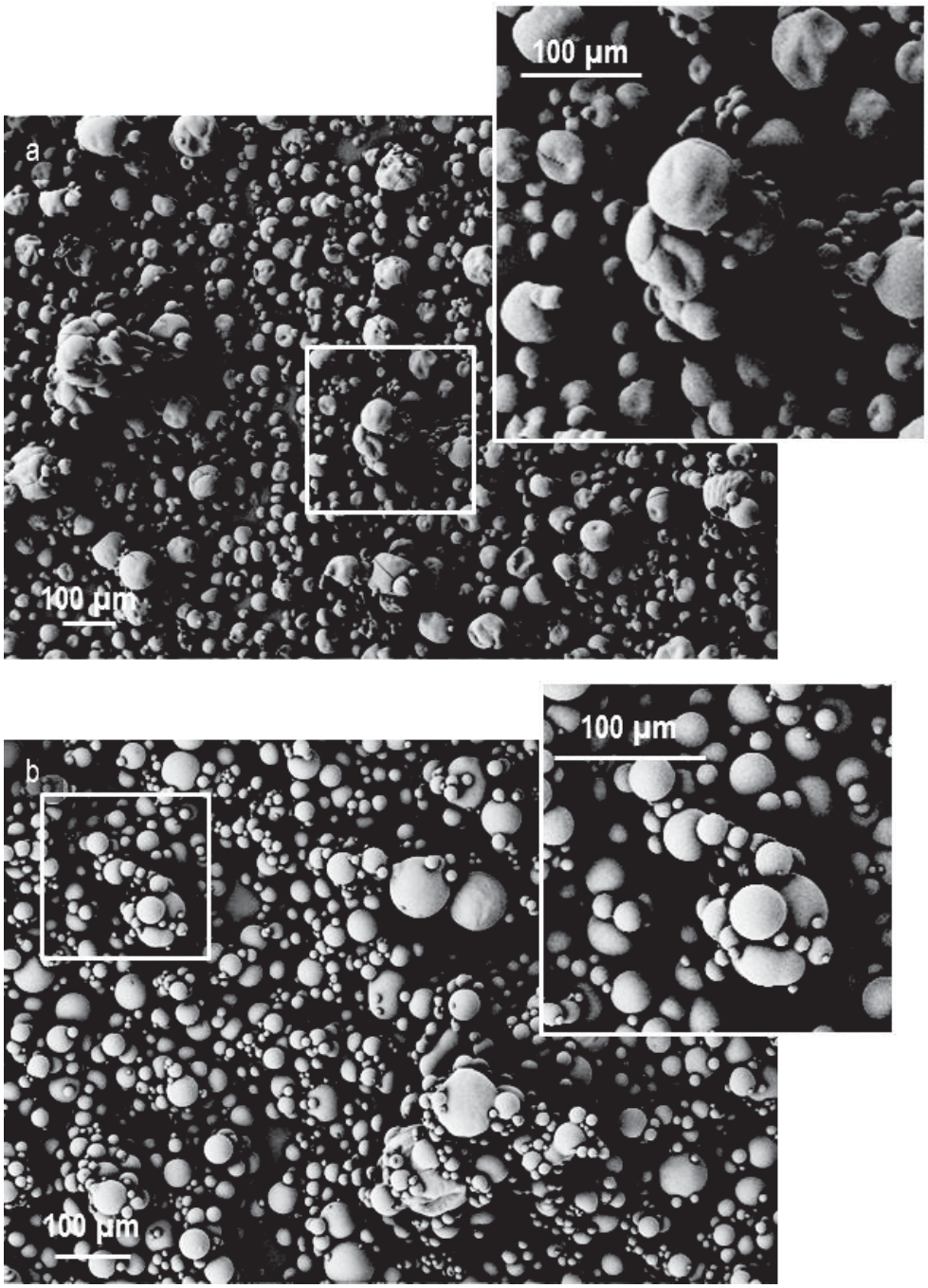

Figure 5.5 a: SEM image of a lactose powder dried at T_{inlet} = 180°C, b: SEM image of a lactose powder dried at T_{inlet} = 200°C.

Wrinkles and shrivels on the lactose particles dried at the lower temperature indicate that the material must have been sufficiently plastic and have sufficiently low viscosity to allow the deformation when the vapour pressure in the particle decreased, i.e. when the particle cooled off. The outlet temperature during spray drying experiments was above the measured glass transition temperatures of respective powders (Table 5.2), which suggest that the material of the particles was in a rubbery state when leaving the dryer and could deform.

In that regard, since the difference between the outlet temperature of the spray dryer and the measured glass transition temperatures of the lactose powders dried at the higher

temperature is even higher than for powders dried at lower temperature, it is expected that these particles will be also shrivelled. However, these particles are predominantly spherical. This is probably caused by high water removal rate which is followed by rapid viscosity decrease and formation of a rigid crust.

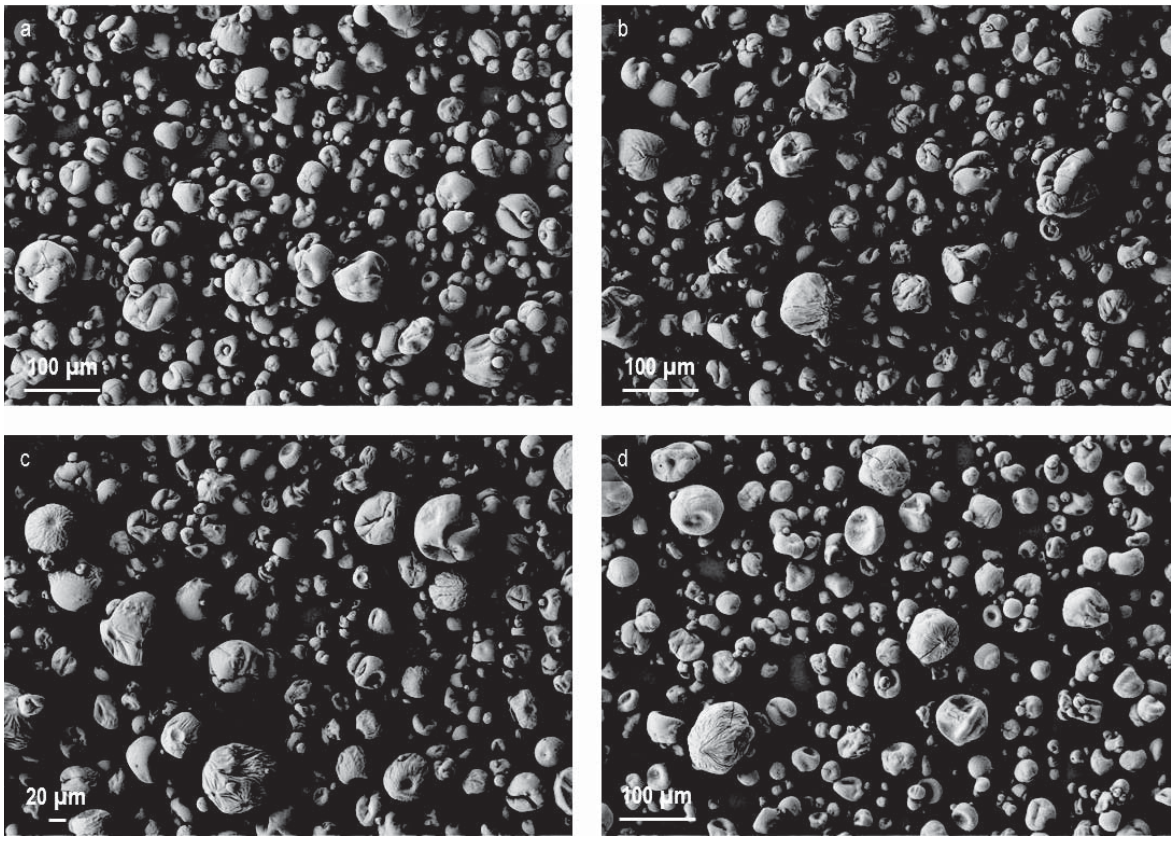

Figure 5.6 Morphologies of the spray dried powders a. lactose + WPI (99:1), T_{inlet} = 180°C; b. lactose + WPI (90:10), T_{inlet} = 180°C, c. lactose + WPI (99:1) T_{inlet} = 200°C; d. lactose + WPI (90:10) T_{inlet} = 200°C.

Such differences between powders dried at lower and higher temperature are not visible in the powders containing an addition of the WPI (Figure 5.6). Lactose powders with addition of WPI are less agglomerated and most of the particles are strongly shrivelled and wrinkled. It is also interesting to note that no differences in the morphology can be told between powders with 1 wt. % and 10 wt. % of WPI at any temperature. This observation suggests that due to addition of WPI the material becomes more plastic and that already 1 wt. % of WPI is sufficient to achieve this modification. Further addition of WPI does not change the morphology of the particles, indicating that the mechanical properties of the material remain unchanged in that regard. The large particles are shrivelled the most. This is reflected in the cumulative size distribution curves of the powders in Figure 5.3 and 5.4, which for powders with addition of the WPI fall slightly above that of lactose powders.

5.2.4 Bulk density and apparent density of particles

In Figure 5.7 bulk densities of the powders and apparent densities of the particles are plotted against the amount of the protein. The detailed data is presented in Tables 5.7 and 5.8. The variation in bulk density of powders with the same composition and dried at the same conditions, can be attributed to variation in the process parameters.

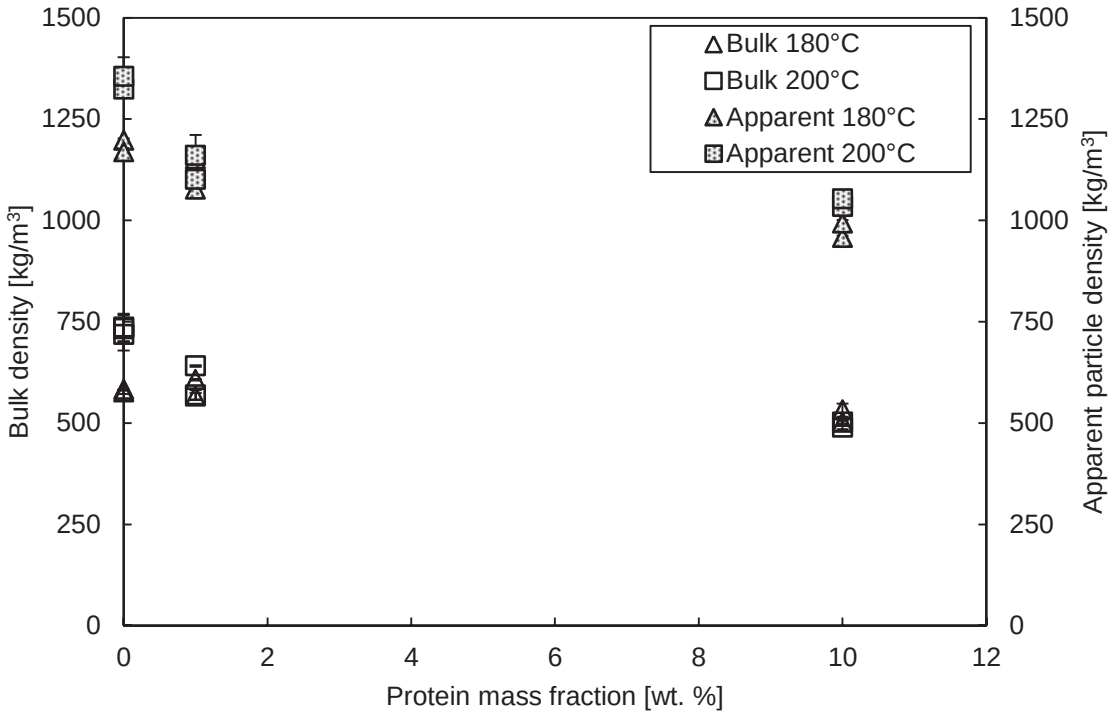

Figure 5.7 Bulk densities and apparent particle densities of powders.

Table 5.7 Bulk density and apparent particle density of powders dried at T_{inlet} = 180°C.

Composition	Batch No.	Bulk density [kg/m^3]		Apparent particle density [kg/m^3]	
		Mean	St. Dev.	Mean	St. Dev.
Lactose	1	576	4	1197	5
	2	582	1	1169	14
Lactose + WPI (99:1)	3	566	8	1076	21
	4	607	2	1151	60
Lactose + WPI (90:10)	5	502	8	957	5
	6	532	16	993	8

The bulk density of lactose powder dried at the lower temperature is about 580 kg/m^3 and is similar to the densities of the powder with 1 wt. % of WPI. The bulk density of pow-

ders with 10 wt. % of WPI is lower than that of the other powders. The difference in the bulk density between the lactose powder with the highest density and the powder with addition of 10 wt. % of the WPI with the lowest bulk density is 13 %.

In powders dried at the higher temperature the bulk density of lactose powder is about 730 kg/m^3 and is the highest of all powders. The density decreases with increasing protein content and already addition of 1 wt. % of WPI has a strong effect on reduction of the bulk density. It can be noted that for powders with addition of the same amount of WPI drying temperature does not have an influence on bulk density.

Table 5.8 Bulk density and apparent particle density of powders dried at T_{inlet} = 200°C.

Composition	Batch No.	Bulk density [kg/m^3]		Apparent particle density [kg/m^3]	
		Mean	St. Dev.	Mean	St. Dev.
Lactose	7	733	33	n.a.	-
	8	718	39	1323	5
	13	736	34	1355	48
Lactose + WPI (99:1)	9	641	2	1160	7
	10	569	12	1101	41
Lactose + WPI (90:10)	11	502	3	1034	5
	12	489	4	1053	10

In Figure 5.7 as filled symbols the experimentally determined apparent particle densities measured by helium pycnometry are plotted against the amount of protein in the powders. The theoretical density of the lactose-WPI powders, calculated as a weight based average of lactose (Chen and Mujumdar, 2008) and typical protein is 1518 kg/m^3 and 1502 kg/m^3 for powders with 1 wt. % and 10 wt. % of protein, respectively. Conducting the same calculation using the experimentally measured density values of crystalline lactose and WPI powder, the densities of the powders are 1353 kg/m^3 for the powder with 1 wt. % of WPI and 1321 kg/m^3 for the powder with 10 wt. % of WPI. These values are close to the density of lactose, since lactose is the main component by weight and has the higher density of the two components. As can be seen in Figure 5.7 the experimentally measured apparent particle densities are lower than the theoretical values. Since powders have similar particle size distributions, the different apparent densities must originate from different accessibility of the pores by the test gas.

The largest differences in apparent particle densities can be observed between the lactose powders dried at the different temperatures. The apparent density of lactose particles dried at low temperature is lower than the densities of lactose given in the literature (Table 5.1) and the density of crystalline lactose measured in this work. However, the measured apparent density of the lactose powder dried at high temperature is close to the density of crystalline lactose. The higher apparent density of the lactose powder dried at the higher temperature means that more pores are accessible to helium than in the powders dried at the lower temperature. Further on, a difference in the apparent densities of the powders can indicate different supramolecular structures. The lower apparent density of the lactose dried at the lower temperature can also be related to the presence of lactose in amorphous state.

Apparent densities of the lactose-WPI-mixture powders are lower than the theoretical values calculated as mass weighted density. This indicates that the particles have internal pores or are hollow. In Figure 5.7 can be seen that powders with the same amount of protein have similar apparent densities irrespectively of the drying temperature. The apparent density decreases with the increasing amount of the WPI, however, these changes are not larger than the variation within two replicates of the same powder. Powders with the highest amount of WPI must have the highest volume of closed pores, as their apparent densities are about 20 % lower than the apparent densities of lactose particles and up to about 10 % lower than that of the particles with 1wt. % of WPI. Some tendency can be observed, that powders dried at the higher temperature have higher apparent density. The density of the powders with addition of WPI is close to the density of pure WPI powder.

One reason for different apparent densities of the powders can be a difference in the amount of crystalline lactose phase in the particles, which has a higher density than amorphous lactose. Another reason can be a difference in the number of closed pores in the particles. Opened pores could be formed during particle formation or as a result of fracture of a dried powder. Blow holes were found on one of each pair of powders with addition of the WPI and on the lactose powder dried at higher temperature. Furthermore, some cracks could be observed on all powders. In case of lactose powder the difference can be attributed to different moisture contents, since water works as a plasticizer on glassy lactose. However, in case of the powders with addition of the protein also powders with low moisture content have few opened pores. This means that due to addition of the WPI particles become viscoelastic and can absorb more energy also at lower moisture contents.

5.2.5 Conclusion

Due to constant drying conditions the obtained powders were very similar in their primary properties, like moisture content and particle size distribution. Nevertheless, the different bulk compositions led to differences in morphologies of the powders. These differences are taken into consideration in the discussion of the resulting surface properties of the powders.

5.3 Characterization of surface composition

In Table 5.9 the atom percentages on the surfaces of the measured powder samples, which were obtained by XPS measurement are summarized. The measured spectra are presented in Figures 5.8 to 5.11.

Table 5.9 Measured atom-based surface compositions of powders.

Batch No.	Sample composition	Atom %		
		O 1s	C 1s	N 1s
2	Lactose	33.94	60.56	5.5
n. a.	Protein WPI	15.66	69.57	14.77
3	Lactose + WPI (99:1)	29.04	63.52	7.44
5	Lactose + WPI (90:10)	28.54	62.99	8.47

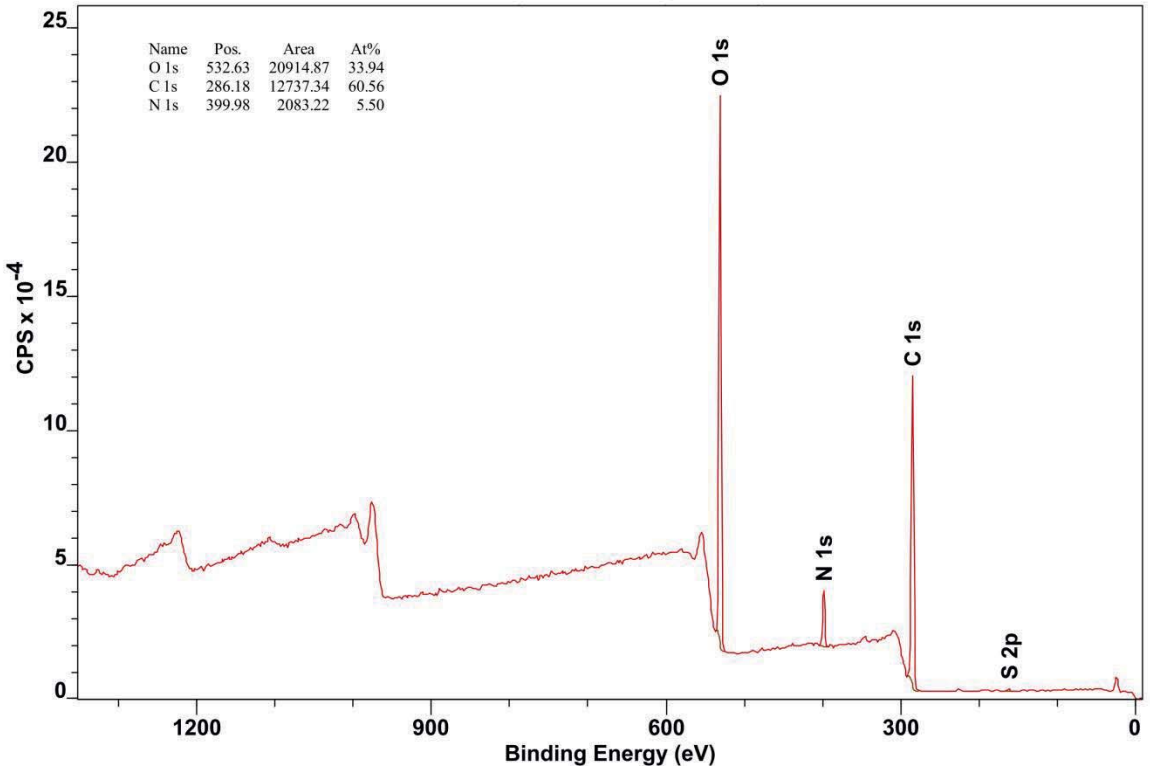

Figure 5.8 XPS spectrum of lactose powder.

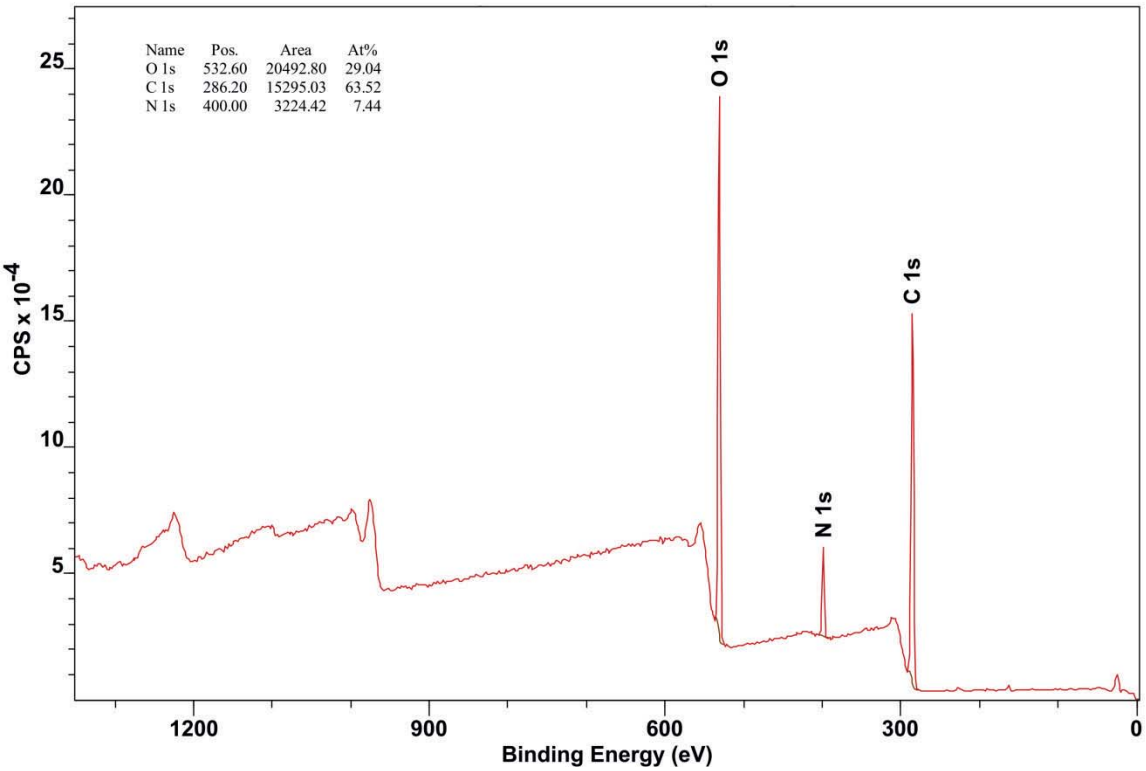

Figure 5.9 XPS spectrum of lactose powder with 1 wt. % of WPI.

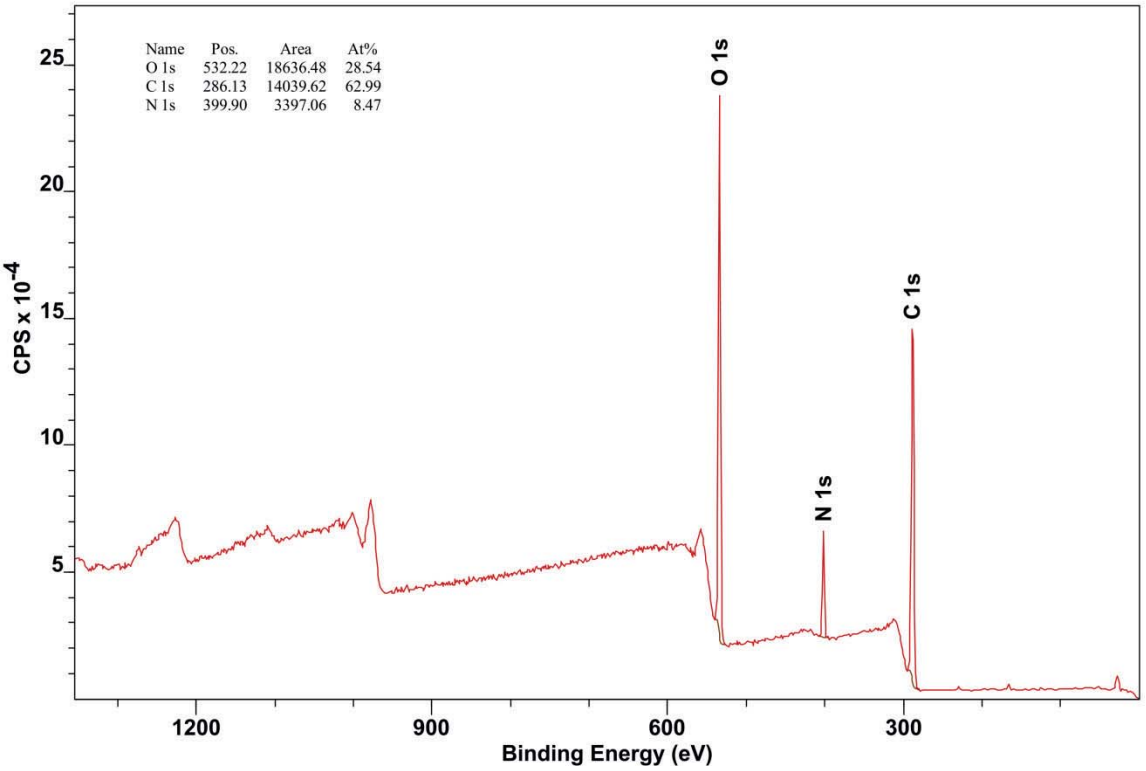

Figure 5.10 XPS spectrum of lactose powder with 10 wt. % of WPI.

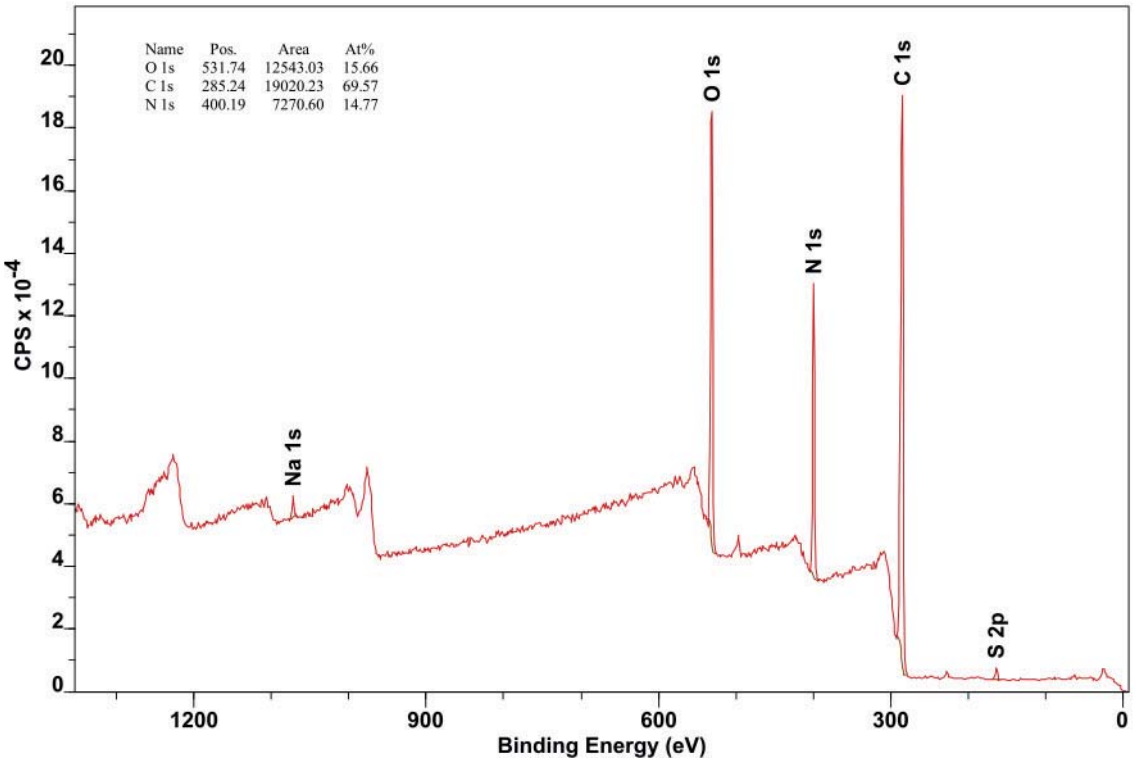

Figure 5.11 XPS spectrum of whey protein isolate powder.

Table 5.10 Theoretical and measured mass-based bulk compositions of the spray dried powder samples and crystalline lactose.

Composition	Theoretical composition [wt. %]			Measured [wt. %]	
	O 1s	C 1s	N 1s	C 1s	N 1s
Lactose spray dried	53.3	40.0	0.0	41.6	0.037[1]
Lactose crystalline	53.3	40.0	0.0	41.3	0.006[1]
WPI	22.3%	53.6%	16.3%	51.8%	15.2%
Lactose + WPI (99:1)	53.0%	40.1%	0.2%	42.0%	0.2%
Lactose + WPI (90:10)	50.2%	41.4%	1.6%	43.1%	1.6%

Surface composition of lactose and WPI powders, should be similar to respective bulk compositions, since they contain only one type of component. However, on the surface of lactose powder nitrogen was measured. In Table 5.10 the measured mass-based bulk compositions of the spray dried powder samples and crystalline lactose are compared with theoretical values, which were obtained from chemical formulas of the powders.

[1] Measured by Kjeldahl method

Analysis by elemental analysis and Kjeldahl method of the bulk composition of the spray dried lactose powder which was used in the XPS measurement revealed that it contained 0.37 g/kg of nitrogen (Table 5.10), whereas the bulk composition of crystalline lactose contained only 0.06 g/kg. Small amounts of nitrogen like in the crystalline sample can originate from the traces of proteins. However, the fact that more nitrogen was present in the spray dried lactose sample indicates a contamination with another material containing nitrogen.

Comparison of the theoretical and measured bulk compositions of other analysed samples revealed no increase in the amount of nitrogen. Therefore, it is concluded that only the lactose powder sample was contaminated and in the calculation of the surface coverage the theoretical atom-based composition of lactose was used, which was calculated from the elemental compositions (Table 5.11).

The atomic composition of the WPI powder measured by XPS also deviates from the theoretical composition shown in Table 5.10. However, the results lie in similar range as results of other authors (Nikolova et al., 2015). The differences with the theoretical composition are small and can be due to the fact that a food grade WPI was used, which contained small amounts of lactose and fat. Especially the higher carbon value might indicate a presence of a fat contamination. Moreover calculation of the elemental compositions from the chemical formula assumes a strict composition of WPI, as given in literature (de Wit, 1998). However, it is possible that the amounts of specific proteins were different.
Surface coverage with lactose and WPI of the two analysed lactose-WPI powders are shown in Table 5.12. The amount of protein on the surface in both powders is higher than in the powder bulk. It corresponds to a fifty-fold enrichment compared to the bulk composition on the surface of the powder with 1 wt. % of WPI and to almost a six-fold enrichment compared to the bulk composition on the surface of the powder with 10 wt. % of WPI. The powder with a higher bulk protein composition has also a higher surface coverage. However, the differences are not large, if related to the difference in bulk composition.

Table 5.11 Theoretical atom-based compositions of lactose and WPI calculated form the chemical formulas.

Sample composition	Atom %		
	O 1s	C 1s	N 1s
Lactose	44.0	56.0	-
WPI	19.9	63.6	16.6

Table 5.12 Mass based surface coverage of spray dried powders.

Batch No.	Composition	% coverage with lactose	% coverage with WPI
3	Lactose + WPI (99:1)	49.6	50.4
5	Lactose + WPI (90:10)	42.7	57.3

The increase in the protein amount on the surface with the increasing bulk concentration corresponds well to the observations of other authors [(Fäldt and Bergenståhl, 1994), (Millqvist-Fureby et al., 1999), (Landström et al., 1999)]. Surface coverage values are lower than in case of Fäldt and Bergenståhl (1994). Also protein coverage on the surface of spray dried saccharose powder with 1 wt. % of WPI measured by Adhikari et al. (2009a) is higher than the value obtained here. Protein coverage, which was measured on the surface of skimmed milk powder with 8.5 wt. % of protein in the bulk by Shrestha et al. (2007) is as well higher than the value measured on the powder with 10 wt. % of WPI. This lower coverage can be attributed to the differences in the measured atomic compositions of reference powders.

The six-fold enrichment on the surface of the powder with 10 wt. % of protein is of the same order of magnitude as surface enrichment obtained in the simulation. However, the absolute value obtained in the simulation is below the measured surface coverage. The differences can originate from an enhanced accumulation of the protein on the surface due to the surface activity of the protein and the difference in the definition of the depth of a particle surface.

5.4 Characterization of powder wetting

5.4.1 Static wetting of fresh and stored powder

In Figure 5.12 wetting time of fresh spray dried powders is shown. Lactose powder dried at higher temperature was wetted immediately and the undissolved powder sedimented to the bottom of the beaker. The wetting times of all remaining powders are above 20 minutes and no difference in wetting time can be observed. The protein does not influence wetting of the powder.

The slow wetting times can be attributed to amorphous structure of these powders. In such material water penetration and dissolution is rapid (Forny et al., 2011). Further on, due to small size of the particles and small density difference between particles and water (section 1.2) the dispersion of particles is slow. This leads to local increase in liquid viscosity, which hinders further solvent penetration in the powder bulk.

The fast wetting of the lactose powder dried at higher temperature can be related to the possibly crystalline supramolecular structure of this powder. According to observations of Fitzpatrick et al. (2016) powders with crystalline structure had shorter wetting times than amorphous powders.

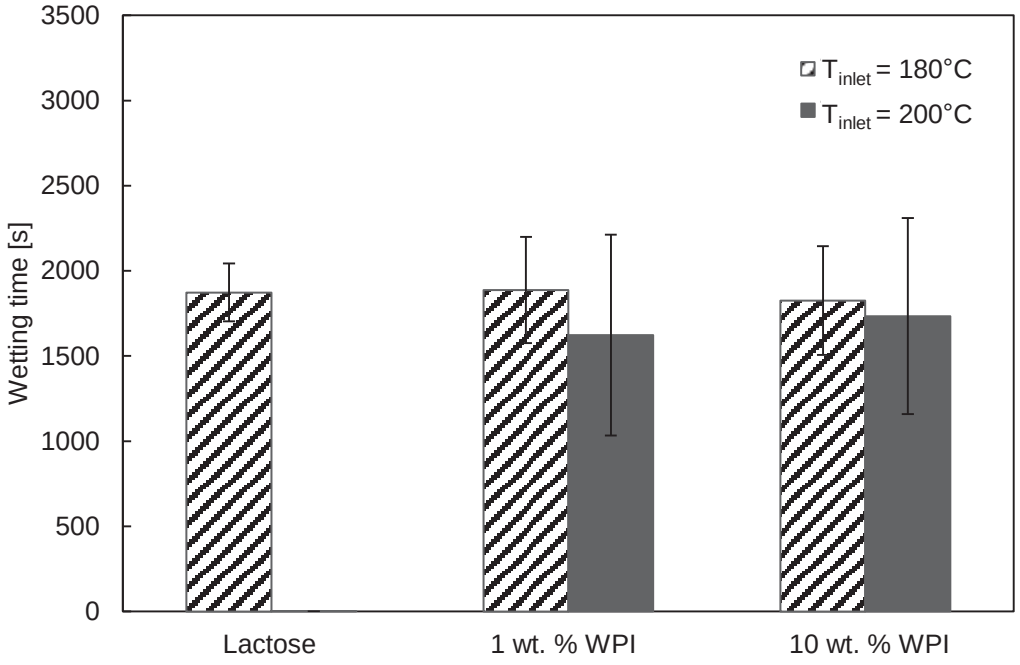

Figure 5.12 Wetting time of fresh powders, without storage and moisture adjustment.

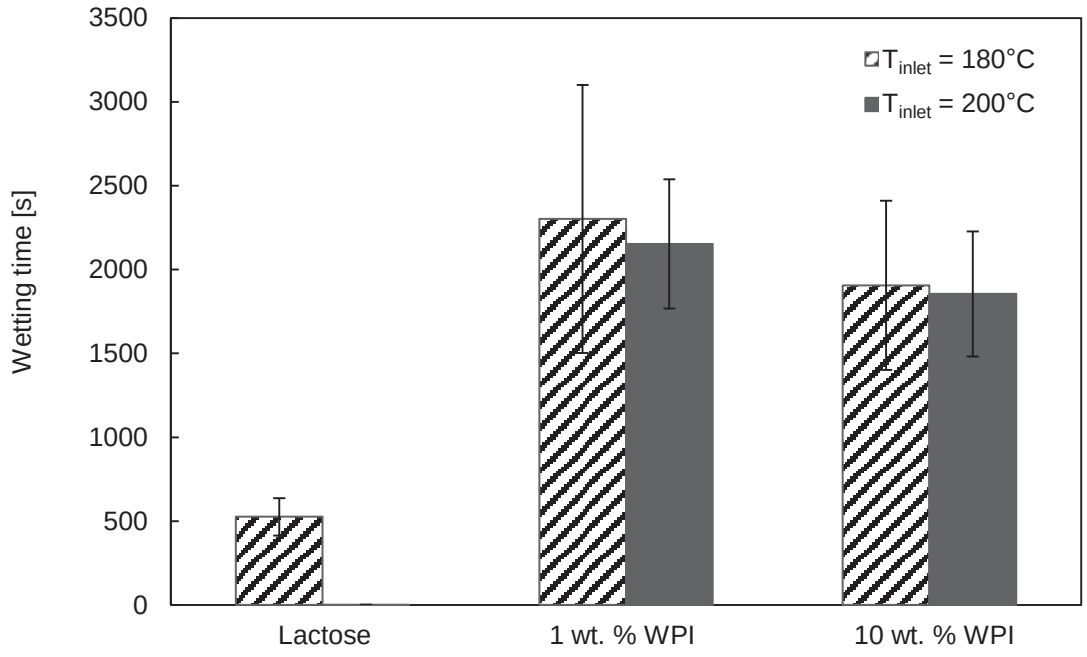

Figure 5.13 Wetting time of powders stored for two weeks at 30 % r.h.

In Figure 5.13 wetting times of powders, which were stored for two weeks at 30 % r.h. can be seen. The most apparent difference to Figure 5.12 is the decreased wetting time of lactose powder produced at lower temperature. This can be attributed to crystallization of

the powder, which was induced by storage at 30 % r.h. The wetting time of lactose produced at higher temperature remains instantaneous after storage. Between the powders with addition of the WPI no systematic difference can be told. However, it can be seen that the wetting times of powders with addition of WPI are higher than before storage. This can be caused by modification of the test procedure (section 3.5).

The fact that wetting times of lactose powders with addition of the protein remained high suggests, that despite storage and exposure to humidity, these powders remained more amorphous. Faster wetting of lactose than lactose with addition of protein is in accordance with the previous observations (Gianfrancesco et al., 2011). One reason for the slow wetting can be the high amount of the WPI on the surface of the particles, which was measured by the XPS for the powders dried at the lower temperature.

5.4.2 Characterization of apparent water contact angle on compacted powder

The average wetting time is characterized by large standard deviation of the sample. The results obtained in the static wetting test are compared to the apparent water contact angle measured on the surface of compacted powder tablets. In Figure 5.14 the decrease in the apparent water contact angle is caused by wetting of the tablet surface and penetration of the drop into the powder bed. The faster the decrease in the apparent contact angle the stronger the interaction between the solvent and the powder substrate.

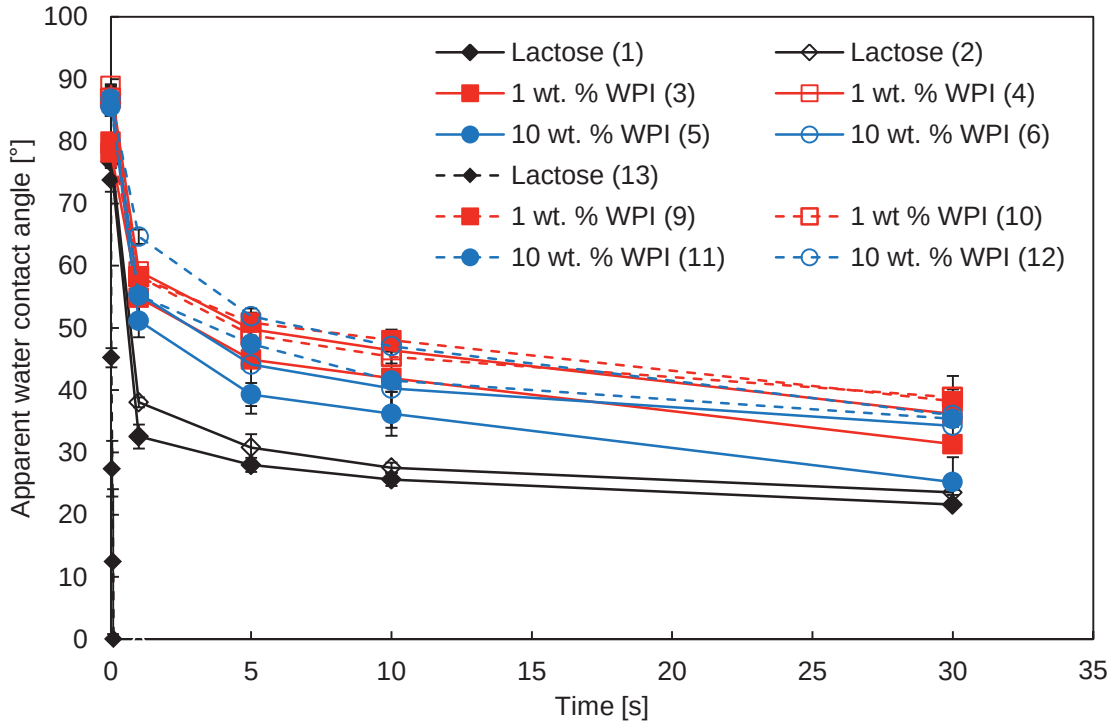

Figure 5.14 Apparent water contact angle on spray dried powders. Solid lines – powders dried at the lower temperature, T_{inlet} = 180°C, dashed lines – powders dried at the higher temperature, T_{inlet} = 200°C. Numbers in brackets indicate the number of a batch.

As expected, due to the roughness of the powder-disc surface, the apparent contact angle of a water drop measured at the initial contact with lactose is higher than values reported in the literature [(Lerk et al., 1976), (Hapgood et al., 2002), (Charles-Williams et al., 2013), (Kiesvaara and Yliruusi, 1993)]. It decreases then rapidly, below 60°, due to capillary action.

The results confirm the results obtained by the static wetting test, similar relationship was observed by Fitzpatrick et al. (2016) for other food powders The apparent water contact angle on the lactose dried at the higher temperature decreases to zero within milliseconds. This means that this powder interacts much stronger with water than the lactose dried at the lower temperature. One second after water drop deposition, the apparent water contact angle on the surface of the powders containing WPI is more than 15° higher than that on lactose dried at lower temperature. This can be attributed to the high amount of WPI on powder surface and its poor wettability (Ji et al., 2016).

The apparent water contact angle curves measured on powders containing different amounts of WPI in the bulk overlap. The higher contact angle on the powder with WPI might also be affected by protein swelling (Forny et al., 2011). The same is true for powders with the same amount of protein produced at different temperatures. However, the curves for two powders with the same composition, which were obtained in two separate spray drying runs, lie up to 10° apart. The results confirm, that no difference in the interaction of the powders containing an addition of WPI with water can be seen in relation to the bulk protein composition. This can be due to the similar surface composition and similar particle morphology.

5.4.3 Characterization of material wetting by contact angle on thin layers

In Figure 5.15 a water contact angle measured on thin solid layers of the lactose-WPI mixtures is shown. The water contact angle measured directly on a glass slide, on which a thin layers were spin coated, is different from the values measured on the coated layer. This means that the glass background was fully coated with the sample material and did not influence the measurement. The measured contact angle increases with the increasing amount of protein in the sample layer and is the highest for the layer consisting of WPI only. As the morphology of the surfaces is the same, the increasing contact angle is related to an increasing amount of the WPI.

Interesting to note is also the rate of the water contact angle decrease. It can be seen that it is the highest for the lactose layer and decreases with the increasing protein amount. This can be related to the solvent uptake (Tay et al., 2010) by the substrate. As the interaction between water and lactose is the strongest water is transported within the layer enhancing hydrophilicity of the layer. On the WPI surface the shape of the water contact

angle curve reminds that one of a drop on a glass slide, except that the measured values are higher. This indicates that the surface consisting of WPI only is the most hydrophobic. Therefore, the layer is wetted poorly and water is transported slowly through the layer matrix.

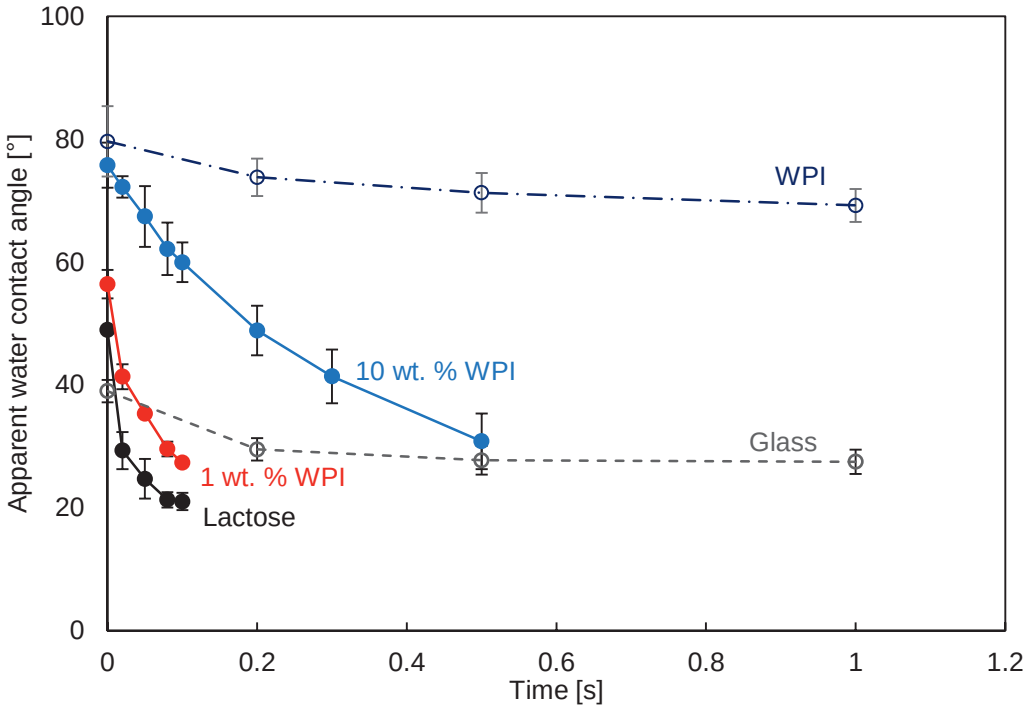

Figure 5.15 Apparent water contact angle on spin coated thin layers.

5.4.4 Conclusion

Comparing the apparent water contact angle measured on compacted powder tablets with that measured on the thin layers and the results of the static wetting test, it can be seen that the lactose powders with no addition of WPI are always wetted the fastest. The difference in wetting properties of lactose powders produced at different temperatures originates from a degree of crystallinity which is influenced by the drying conditions.

The results of the contact angle measurement on thin layers showed that an increase in the amount of WPI in the thin layers results in poorer wettability. However, in both tests, the static wetting and the apparent water contact angle measurement on powder tablets, no difference in the wetting properties of powders with different amount of WPI could be shown. This indicates, that the difference in the protein surface coverage of the powders with 1 and 10 wt. % of WPI is not sufficient to impact powder wettability in such a degree which is measurable. It is not clear, whether it is due to small differences in the surface composition as measured by XPS or whether also the wrinkled surface of the powders with WPI affects the wettability. Nevertheless, this suggests that also no differences in powder performance will be visible.

Finally, it should be stressed at this point that the lack of differences in powder wetting between the powders is influenced by the measurement method, which depends on powder dissolution. Nevertheless, this test method mimics the actual behaviour of powder in typical processes.

5.5 Characterization of powder flowability

5.5.1 Characterization of flow properties by uniaxial compression test

In the following two figures (Figure 5.16 and 5.17) the compressive strength of the powders compacted into pellets can be seen. In the diagrams the lines of constant flow factors which qualitatively characterize the flow properties of the powder are also indicated. The compressive strength of the powders produced at the lower drying temperature fall into the range of free flowing (ff_c>10) and easy flowing (4<ff_c<10) powders. These powders have, in general, higher compressive strengths than the powders produced at the higher temperature, what can be attributed to their higher moisture content. All powders produced at the higher drying temperature can be classified as free flowing.

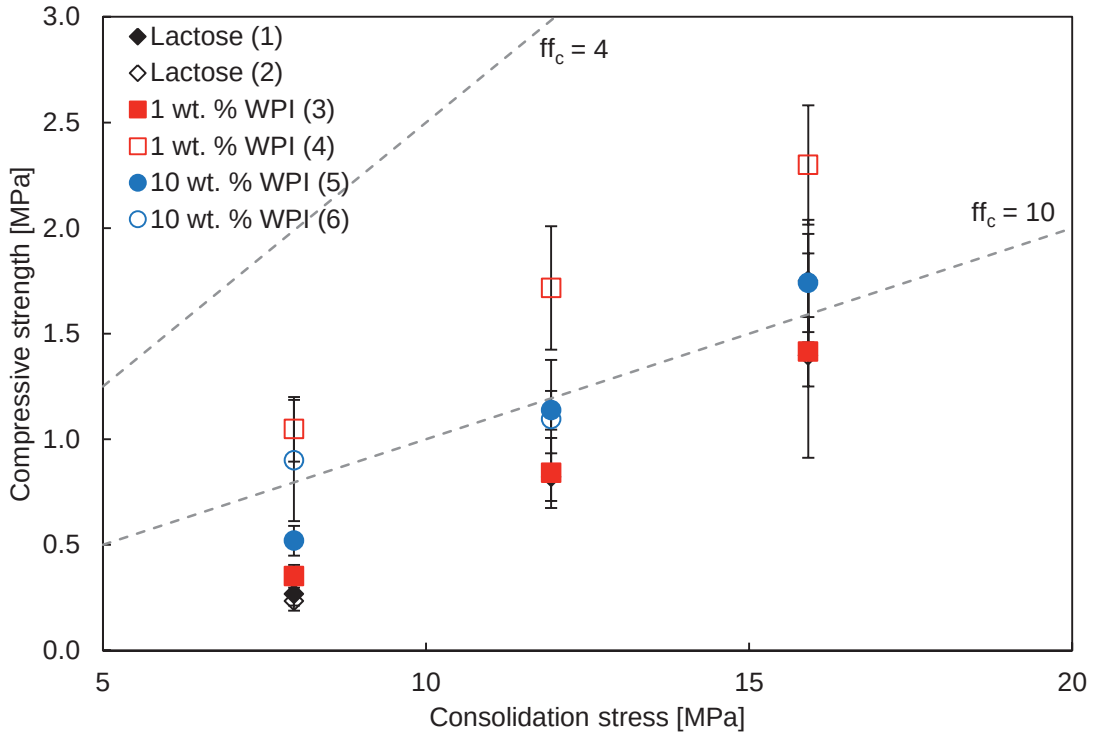

Figure 5.16 Compressive strength of the pellets made of the powders dried at the lower temperature, T_{inlet} = 180°C. Numbers in brackets indicate the number of a batch.

All powders produced at the lower temperature have similar compressive strengths in the investigated range of consolidation stresses, and can be classified as free flowing. The only data set, for which higher compressive strengths were measured are the pellets with 1 wt. % of WPI (batch 4). A possible reason why this measurement stands out can be a variation in the temperature or humidity of the room in which the measurements were

conducted. This indicates that the difference in surface composition between lactose and powder with WPI does not influence adhesion forces between the particles.

Pellets obtained by compacting the lactose powders dried at the higher temperature have compressive strengths at the level of about 200 kPa. They are much weaker than the pellets of powders with addition of WPI dried at the same conditions, despite similar powder moisture. Their compressive strength is also lower than compressive strength of the lactose powders produced at the lower temperature.

Despite the different amount of WPI in the powders, no significant differences can be told between the strength of the pellets of other powders produced at the higher temperature. It can be observed that with increasing WPI content the compressive strength increases. However, the differences are minor and the increase is very small in relation to the increase in the protein amount.

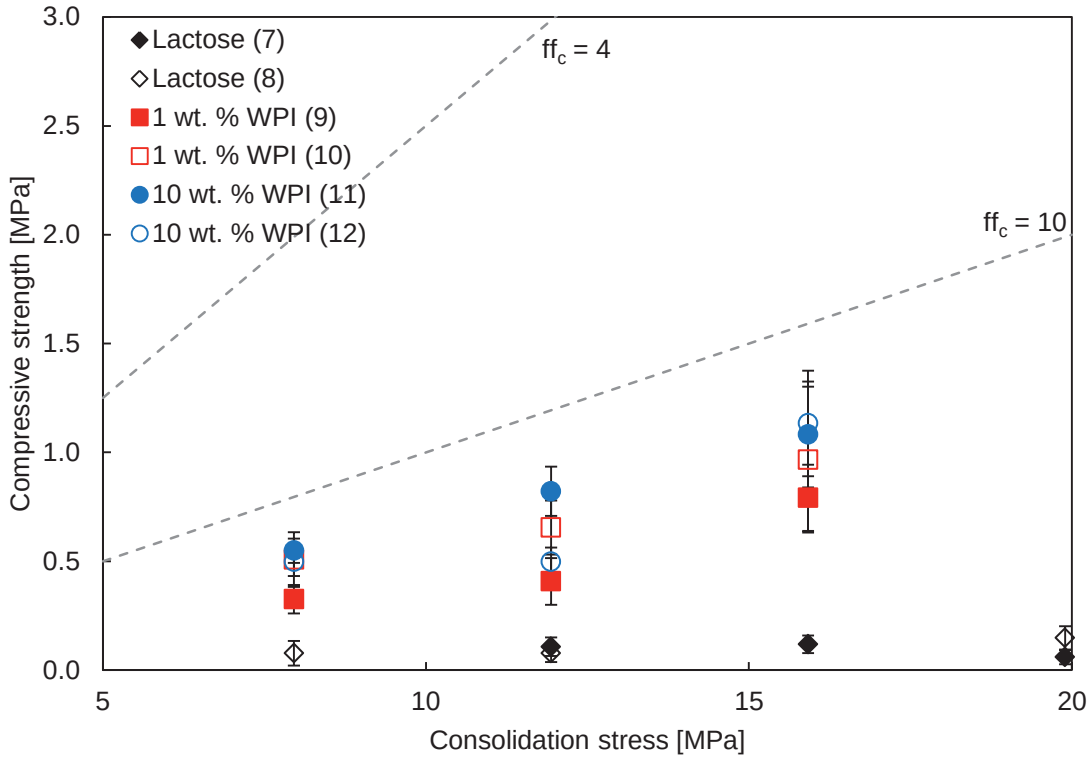

Figure 5.17 Compressive strength of the pellets made of the powders dried at the higher temperature, T_{inlet} = 200°C. Numbers in brackets indicate the number of a batch.

According to equations 1.3 – 1.6 differences in adhesion force can originate either from different surface energy or from different contact area between the particles, which depends on the degree of particle's deformation upon application of a normal load. Powders with WPI have different surface composition than lactose. Similar compressive strengths of all powders produced at the lower temperature suggest, that the deformation of the particles must have been sufficient to assure sufficiently small distance between the particles and sufficiently large contact area.

The compressive strength of lactose produced at the higher temperature is much lower than that of respective powders containing addition of the WPI. This difference in com-

pressive strength of the powders can be attributed to a poor degree of deformation of the lactose particles. As all powders dried at the higher temperature have similar moisture content, the lower deformation of lactose can be explained by a higher degree of crystallinity of this powders compared to lactose dried at the lower temperature.

According to the results of the simulation presented in this work and experimental observations of Nijdam and Langrish (2006), in powders produced at higher temperature the surface coverage of the particles with WPI is expected to be the same or smaller than in the powder dried at the lower temperature. Therefore, the differences in adhesive forces between lactose powder and powders with addition of WPI cannot be attributed to the different surface composition.

5.5.2 Characterization of flow properties by a ring shear tester

In Figure 5.18 and 5.19 the flow properties of the powders which were tempered for two weeks at 20 % r.h. at 20°C measured by a ring shear cell tester are presented. No differences in the flow properties can be observed between powders with different bulk compositions, which confirm results of the uniaxial compression tests. The compressive strengths of powders produced at different temperatures are also the same, which can be explained by the same moisture content of the powders.

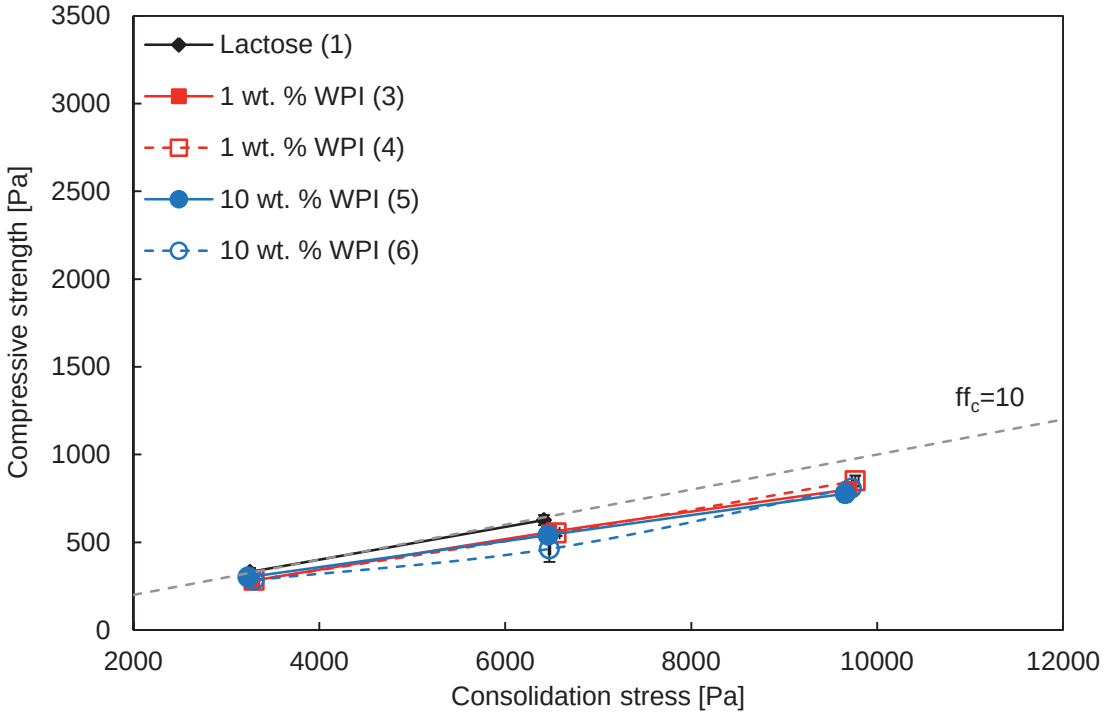

Figure 5.18 Compressive strength of powders dried at the lower temperature, T_{inlet} = 180°C. Numbers in brackets indicate the number of a batch.

The only exceptions are the flow properties of lactose powder produced at the higher drying temperature. On contrary to results obtained under high consolidation stress in the uniaxial compression test, under low consolidation stress this powder can be classified as cohesive. This can be related to the morphology of this powder as discussed in section

5.2. Due to the smooth surface, the particles can approach each other very closely what leads to higher van der Waals force. The roughness of the surfaces of other powders prevents the particles from approaching each other so close at these lower normal loads.

Flow properties under these condition of the powder confirm the results of Amagliani et al. (2016), although at low consolidation stress the values measured in this work are lower, which can be attributed to the lower powder moisture. Fitzpatrick et al. (2007) obtained under the same consolidation stresses similar results, with crystalline lactose classified as the powder with the lowest flow function among the investigated powders, whereas whey permeate powder and skimmed milk powder were classified as easy flowing. These authors also suggested that poor flowability of lactose could be assigned to higher frictional resistance.

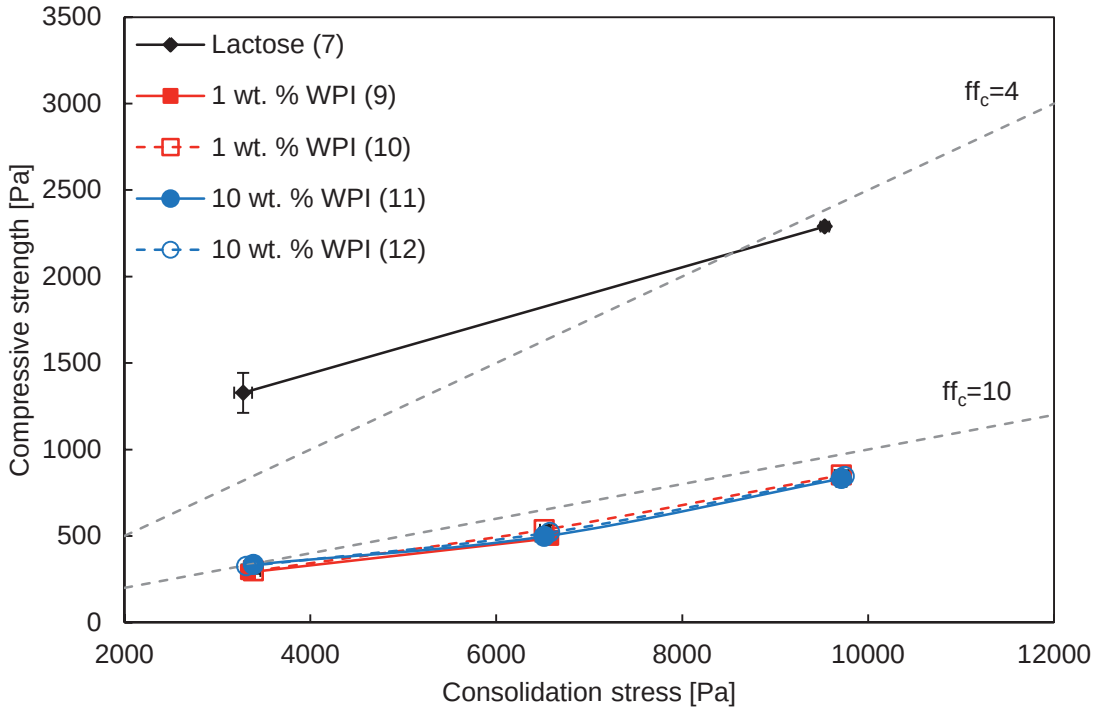

Figure 5.19 Compressive strength of powders dried at the lower temperature, T_{inlet} = 200°C. Numbers in brackets indicate the number of a batch.

5.5.3 Conclusion

In both tests it was confirmed that the powders do not differ in their mechanical properties despite different bulk and surface composition. The only powders, which stand out in the measurements are the lactose powders dried at the higher temperature. The different behaviour of these powders can be attributed to the higher level of crystallinity and to the spherical shape of the particles. These results underline the role of morphology and supramolecular structure on the flowability of powder.

6 Conclusions

In order to be able to tailor properties of a multicomponent spray dried powders to product requirements it is important to identify the primary powder properties, which lead to the modification of powder bulk properties, and to understand, how these primary properties are modified by the feed composition and drying conditions. This work focused on the fact, that many natural materials, which are produced by spray drying, like foods, are multicomponent systems and that the surface composition of spray dried particles of such materials can differ from its bulk composition.

In this work a modelling approach was used to consider the influence of drying conditions and feed composition on the final surface composition of a spray dried multicomponent drop. Based on a literature review the drivers of component reorganization in a drop during solvent evaporation were analysed. The formulated model presents a case of a system with two solute components characterized by different diffusivities.

Simulations of mass transport of protein and lactose within a drop during drying showed, that, within the investigated range of process parameters, the initial total solids content has the strongest influence on the extend of relative surface enrichment by the slowly diffusing component. The effect of different drying temperatures is the most pronounced at low initial total solids contents. This effect was investigated in detail by comparing mass fraction profiles of the components in a drop over drying time until the moment of surface solidification. Due to faster solvent removal at higher temperature the steep mass fraction gradient extends only in a thin surface layer resulting in lower surface enrichment. The effect of the solute composition in a drop is visible at low initial total solids content. The relative enrichment decreases with increasing mass fraction of the slowly diffusing component.

The experimental work showed how the drying rate can impact the surface composition of a powder and how these differences in the surface composition of particles affect bulk properties of the powder. Different drying gas inlet temperatures and a constant feed flow rate provided different times for particle surface formation and spatial component accumulation. In the analysis of the relationship between the surface composition and the powder properties further bulk properties, such as moisture content, glass transition temperature, particles size and morphology were considered as well, since these properties also influence the mechanical and physico-chemical properties of powders.

The obtained powders had two different levels of moisture content, which depended on drying temperature. In some measurements powder moistures were brought to a constant level by storage of the powder at specified atmosphere. The powders were characterized

by different glass transition temperatures between 58 and 76°C, which were related to the moisture of the particular powder according to the Gordon-Taylor equation given by the model of Vuataz (Vuataz, 2002). Due to constant feed flow rate and nozzle pressure all powders had very similar particle size distributions. The median of the particle size varied by less than 2 μm. This minimized the differences between the powders in packing or van der Waals forces. The particles of lactose powders dried at the higher temperature were spherical. All remaining powders had shrivelled and wrinkled particles. The differences in the apparent particle densities and the powder bulk densities were related to the different degrees of crystallinity of the powders. The apparent particle density of powders with addition of protein depended on the amount of protein, but not on the drying temperature. The density of lactose powders differed depending on the drying temperature.

The measurement of the surface composition by XPS showed that the amount of the protein on the powder surface clearly increased in relation to the bulk composition. For the powder with 1 wt. % of WPI it was a fifty-fold increase and for the powder with 10 wt. % this increase was almost six-fold related to the bulk composition. Powder with higher bulk protein composition has also a higher surface coverage, however, the differences are not large relative to the difference in bulk composition. These levels of surface enrichment are higher in absolute values than the results of the simulations. The differences can be attributed to the differences in the considered depth of the particle, which was defined as the surface. However, also other driving forces of component migration, like the surface activity of the protein, can have an influence on the accumulation on the powder surface.

For the investigated powders, wetting was dominated by the supramolecular structure of the powder and no differences in powder wetting could be attributed to the differences in surface compositions of the powders. Powders with a higher fraction of amorphous material on the surface had longer wetting times due to instant dissolution of the powder and resulting rapid increase in viscosity of the solvent between the particles. The differences in wetting of lactose powders dried at different temperatures stress the large impact of the supramolecular structure on powder-wetting. The differences in powder stickiness were as well more related to the supramolecular structure of the powder and its moisture than to the surface composition. Whereas the flowability measured at low loadings was affected by the morphology of the particles.

The practical conclusion for spray drying process obtained from simulations of a single drop drying is, that the initial solid content of the concentrate to be sprayed has a major impact on the surface composition. The drying temperature can influence the surface composition of a powder, if feeds with low amount of solutes are dried. Finally, within

the regarded range of protein fraction, initial total solids content and drying temperatures, a variation in the solute composition will not affect the surface composition.

Based on the experimental observations, it can be concluded that the different surface coverage with protein of powders did not impact in a visible manner the properties of powder. Further properties of the particles, like the supramolecular structure and the particle morphology, which were influenced by the drying conditions and bulk composition demonstrated a dominating influence on powder properties. In that regard the investigated system showed different behaviour as powders containing a lipid component, which presence on powder surface correlates with poorer wetting and flowability.

In the investigated systems the bulk composition had an influence on the final properties of the powder, through the effect on the powder morphology and supramolecular structure. Whereas an addition of the protein had a damping effect on the change in morphology and supramolecular structure of the lactose particles at extended process temperatures.

References

Adhikari, B., Howes, T., Bhandari, B., Troung, V., 2004. Effect of addition of maltodextrin on drying kinetics and stickiness of sugar and acid-rich foods during convective drying: experiments and modelling. Journal of Food Engineering 62 (1), 53–68. 10.1016/S0260-8774(03)00171-7.

Adhikari, B., Howes, T., Bhandari, B.R., Langrish, T.A.G., 2009 a. Effect of addition of proteins on the production of amorphous sucrose powder through spray drying. Journal of Food Engineering 94 (2), 144–154.

Adhikari, B., Howes, T., Bhandari, B.R., Troung, V., 2003. Surface stickiness of drops of carbohydrate and organic acid solutions during convective drying: Experiments and modeling. Drying Technology 21 (5), 839–873. 10.1081/DRT-120021689.

Adhikari, B., Howes, T., Wood, B.J., Bhandari, B.R., 2009 b. The effect of low molecular weight surfactants and proteins on surface stickiness of sucrose during powder formation through spray drying. Journal of Food Engineering 94 (2), 135–143. 10.1016/j.jfoodeng.2009.01.022.

Ahfat, N., Buckton, G., Burrows, R., Ticehurst, M.D., 2000. An exploration of interrelationships between contact angle, inverse phase gas chromatography and triboelectric charging data. European Journal of Pharmaceutical Sciences 9 (3), 271–276. 10.1016/S0928-0987(99)00063-9.

Alexander, K., Judson King, C., 1985. Factors governing surface morphology of spray-dried amorphous substances. Drying Technology 3 (3), 321–348. 10.1080/07373938508916275.

Al-Muhtaseb, A.H., McMinn, W., Magee, T., 2002. Moisture sorption isotherm characteristics of food products: A review. Food and Bioproducts Processing 80 (2), 118–128. 10.1205/09603080252938753.

Amagliani, L., O'Regan, J., Kelly, A.L., O'Mahony, J.A., 2016. Physical and flow properties of rice protein powders. Journal of Food Engineering 190, 1–9. 10.1016/j.jfoodeng.2016.05.022.

Bhandari, B.R., Datta, N., Howes, T., 1997. Problems associated with spray drying of sugar-rich foods. Drying Technology: An International Journal 15 (2), 671–684.

Blei, S., 2006. On the interaction of non-uniform particles during the spray drying process: Experiments and modelling with the Euler-Lagrange approach. Shaker, Aachen.

Bück, A., Peglow, M., Naumann, M., Tsotsas, E., 2012. Population balance model for drying of drops containing aggregating nanoparticles. AIChE J. 58 (11), 3318–3328. 10.1002/aic.13726.

Buckton, G., 1993. Assessment of the wettability of pharmaceutical powders. Journal of Adhesion Science and Technology 7 (3), 205–219. 10.1163/156856193X00664.

Charles-Williams, H., Wengeler, R., Flore, K., Feise, H., Hounslow, M.J., Salman, A.D., 2013. Granulation behaviour of increasingly hydrophobic mixtures. Powder Technology 238, 64–76. 10.1016/j.powtec.2012.06.009.

Chen, X.D., Lin, S.X.Q., 2005. Air drying of milk drop under constant and time-dependent conditions. AIChE J. 51 (6), 1790–1799. 10.1002/aic.10449.

Chen, X.D., Mujumdar, A.S., 2008. Drying Technologies in Food Processing. Blackwell Publishing, Singapore.

Chen, X.D., Sidhu, H., Nelson, M., 2011. Theoretical probing of the phenomenon of the formation of the outermost surface layer of a multi-component particle, and the surface chemical composition after the rapid removal of water in spray drying. Chemical Engineering Science 66 (24), 6375–6384. 10.1016/j.ces.2011.08.035.

Chen, X.D., Sidhu, H., Nelson, M., 2013. On the addition of protein (Casein) to aqueous lactose as a drying aid in spray drying - Theoretical surface composition. Drying Technology 31 (13-14), 1504–1512. 10.1080/07373937.2013.780247.

Chiou, D., Langrish, T., Braham, R., 2008. The effect of temperature on the crystallinity of lactose powders produced by spray drying. Journal of Food Engineering 86 (2), 288–293. 10.1016/j.jfoodeng.2007.10.005.

Choi, Y., Okos, M.R., 1986. Effects of temperature and composition on the thermal properties of foods. Food Engineering and Process Applications, 1 Transport Phenomena. Elsevier, London.

Cussler, E.L., 1984. Diffusion, mass transfer in fluid systems. Cambridge University Press, Cambridge [Cambridgeshire], New York.

Decker, E.L., Frank, B., Suo, Y., Garoff, S., 1999. Physics of contact angle measurement. Colloids and Surfaces A: Physicochemical and Engineering Aspects 156 (1-3), 177–189. 10.1016/S0927-7757(99)00069-2.

Dopfer, D., Palzer, S., Heinrich, S., Fries, L., Antonyuk, S., Haider, C., Salman, A.D., 2013. Adhesion mechanisms between water soluble particles. Powder Technology 238, 35–49. 10.1016/j.powtec.2012.06.029.

de Wit, J.N., 1998. Nutritional and functional characteristics of whey proteins in food products. Journal of Dairy Science 81, 597–608.

Fäldt, P., Bergenståhl, B., 1994. The surface composition of spray-dried protein-lactose powders. Colloids and Surfaces A: Physicochemical and Engineering Aspects 90 (2-3), 183–190. 10.1016/0927-7757(94)02914-8.

Fäldt, P., Bergenståhl, B., Carlsson, G., 1993. The surface coverage of fat on food powders analyzed by esca (Electron Spectroscopy for Chemical Analysis). Food Structure 12, 225–234.

Fischer, H., Polikarpov, I., Craievich, A.F., 2004. Average protein density is a molecular-weight-dependent function. Protein science : a publication of the Protein Society 13 (10), 2825–2828. 10.1110/ps.04688204.

Fitzpatrick, J., Iqbal, T., Delaney, C., Twomey, T., Keogh, M., 2004. Effect of powder properties and storage conditions on the flowability of milk powders with different fat contents. Journal of Food Engineering 64 (4), 435–444. 10.1016/j.jfoodeng.2003.11.011.

Fitzpatrick, J.J., Hodnett, M., Twomey, M., Cerqueira, P., O'Flynn, J., Roos, Y.H., 2007. Glass transition and the flowability and caking of powders containing amorphous lactose. Powder Technology 178 (2), 119–128. 10.1016/j.powtec.2007.04.017.

Fitzpatrick, J.J., van Lauwe, A., Coursol, M., O'Brien, A., Fitzpatrick, K.L., Ji, J., Miao, S., 2016. Investigation of the rehydration behaviour of food powders by comparing the behaviour of twelve powders with different properties. Powder Technology 297, 340–348. 10.1016/j.powtec.2016.04.036.

Forny, L., Marabi, A., Palzer, S., 2011. Wetting, disintegration and dissolution of agglomerated water soluble powders. Powder Technology 206 (1-2), 72–78. 10.1016/j.powtec.2010.07.022.

Fox, P.F., 2003. Advanced dairy chemistry, 3rd ed. Kluwer Academic/Plenum, New York.

Freudig, B., Hogekamp, S., Schubert, H., 1999. Dispersion of powders in liquids in a stirred vessel. Chemical Engineering and Processing: Process Intensification 38 (4-6), 525–532. 10.1016/S0255-2701(99)00049-5.

Frohn, A., Roth, N., 2000. Dynamics of drops. Springer, Berlin, New York.

Fu, N., Woo, M.W., Chen, X.D., 2011. Colloidal transport phenomena of milk components during convective drop drying. Colloids and surfaces. B, Biointerfaces 87 (2), 255–266. 10.1016/j.colsurfb.2011.05.026.

Furuta, T., Tsujimoto, S., Oazaki, M., Toei, R., 2007. Effect of drying on retention of ethanol in maltodextrin solution during drying of a single drop. Drying Technology 2 (3), 311–327. 10.1080/07373938308959834.

Gac, J.M., Gradoń, L., 2013. A distributed parameter model for the spray drying of multicomponent drops with a crust formation. Advanced Powder Technology 24 (1), 324–330. 10.1016/j.apt.2012.08.004.

Gaiani, C., Ehrhardt, J.J., Scher, J., Hardy, J., Desobry, S., Banon, S., 2006. Surface composition of dairy powders observed by X-ray photoelectron spectroscopy and ef-

fects on their rehydration properties. Colloids and surfaces. B, Biointerfaces 49 (1), 71–78. 10.1016/j.colsurfb.2006.02.015.

Gaiani, C., Morand, M., Sanchez, C., Tehrany, E.A., Jacquot, M., Schuck, P., Jeantet, R., Scher, J., 2010. How surface composition of high milk proteins powders is influenced by spray-drying temperature. Colloids and surfaces. B, Biointerfaces 75 (1), 377–384. 10.1016/j.colsurfb.2009.09.016.

Galen E. Downton, J.L.F.-L.C.J.K., 1982. Mechanism of stickiness in hygroscopic, amorphous powders. Ind. Eng. Chem. Fundamen. 21 (4), 447–451.

Gianfrancesco, A., Casteran, C., Andrieux, J.-C., Giardiello, M.-I., Vuataz, G., 2011. Assessment of physical characteristics and dissolution behaviour of protein based powders. Procedia Food Science 1, 601–607. 10.1016/j.profoo.2011.09.091.

Gianfrancesco, A., Turchiuli, C., Flick, D., Dumoulin, E., 2010. CFD Modeling and simulation of maltodextrin solutions spray drying to control stickiness. Food Bioprocess Technology 3 (6), 946–955. 10.1007/s11947-010-0352-2.

Glück, B., 1991. Zustands- und Stoffwerte: Wasser, Dampf, Luft ; Verbrennungsrechnung, 2nd ed. Verl. für Bauwesen, Berlin.

Good, R.J., 1992. Contact angle, wetting, and adhesion: A critical review. Journal of Adhesion Science and Technology 6 (12), 1269–1302. 10.1163/156856192X00629.

Gordon, M., Taylor, J.S., 1952. Ideal copolymers and the second-order transitions of synthetic rubbers. i. non-crystalline copolymers. Journal of Applied Chemistry 2 (9), 493–500. 10.1002/jctb.5010020901.

Gouin, S., 2004. Microencapsulation. Trends in Food Science & Technology 15 (7-8), 330–347. 10.1016/j.tifs.2003.10.005.

Griffith, J.D., Bayly, A.E., Johns, M.L., 2008. Magnetic resonance studies of detergent drop drying. Chemical Engineering Science 63 (13), 3449–3456. 10.1016/j.ces.2008.03.043.

Groenewold, C., Möser, C., Groenewold, H., Tsotsas, E., 2002. Determination of single-particle drying kinetics in an acoustic levitator. Chemical Engineering Journal 86 (1-2), 217–222. 10.1016/S1385-8947(01)00292-3.

Hamaker, H.C., 1937. The London-van der Waals attraction between spherical particles. Physica 4 (10), 1058–1072. 10.1016/S0031-8914(37)80203-7.

Handscomb, C., Kraft, M., Bayly, A., 2009 a. A new model for the drying of drops containing suspended solids. Chemical Engineering Science 64 (4), 628–637. 10.1016/j.ces.2008.04.051.

Handscomb, C., Kraft, M., Bayly, A., 2009b. A new model for the drying of drops containing suspended solids after shell formation. Chemical Engineering Science 64 (2), 228–246. 10.1016/j.ces.2008.10.019.

Hapgood, K.P., Litster, J.D., Biggs, S.R., Howes, T., 2002. Drop penetration into porous powder beds. Journal of colloid and interface science 253 (2), 353–366. 10.1006/jcis.2002.8527.

Haque, M.K., Roos, Y.H., 2005. Crystallization and X-ray diffraction of crystals formed in water-plasticized amorphous spray-dried and freeze-dried lactose/protein mixtures. Journal of Food Science 70 (5), 347–350. 10.1021/bp980010s.

Hartmann, M., Palzer, S., 2011. Caking of amorphous powders - material aspects, modelling and applications. Powder Technology 206 (1-2), 112–121. 10.1016/j.powtec.2010.04.014.

Hecht, J.P., King, J.C., 2000. Multicomponent diffusion and vapor-liquid equilibria of dilute organic components in aqueous sugar solutions. Ind. Eng. Chem. Res. 39 (6), 1766–1774.

Hoang Thi, T.H., Lemdani, M., Flament, M.-P., 2013. Optimizing the taste-masked formulation of acetaminophen using sodium caseinate and lecithin by experimental design. International Journal of Pharmaceutics 453 (2), 408–415. 10.1016/j.ijpharm.2013.05.026.

Hogekamp, S., Schubert, H., 2003. Rehydration of Food Powders. Food Science and Technology International 9 (3), 223–235. 10.1177/1082013203034938.

Jayasundera, M., Adhikari, B., Adhikari, R., Aldred, P., 2011. The effect of protein types and low molecular weight surfactants on spray drying of sugar-rich foods. Food Hydrocolloids 25 (3), 459–469. 10.1016/j.foodhyd.2010.07.021.

Ji, J., Fitzpatrick, J., Cronin, K., Maguire, P., Zhang, H., Miao, S., 2016. Rehydration behaviours of high protein dairy powders: The influence of agglomeration on wettability, dispersibility and solubility. Food Hydrocolloids 58, 194–203. 10.1016/j.foodhyd.2016.02.030.

Kiesvaara, J., Yliruusi, J., 1993. The use of the Washburn method in determining the contact angles of lactose powder. International Journal of Pharmaceutics 92 (1 - 3), 81–88.

Kim, E.H.-J., Chen, X., Pearce, D., 2002. Surface characterization of four industrial spray-dried dairy powders in relation to chemical composition, structure and wetting property. Colloids and Surfaces B: Biointerfaces 26 (3), 197–212. 10.1016/S0927-7765(01)00334-4.

Kim, E.H.-J., Chen, X.D., Pearce, D., 2005 a. Effect of surface composition on the flowability of industrial spray-dried dairy powders. Colloids and surfaces. B, Biointerfaces 46 (3), 182–187. 10.1016/j.colsurfb.2005.11.005.

Kim, E.H.-J., Chen, X.D., Pearce, D., 2005 b. Melting characteristics of fat present on the surface of industrial spray-dried dairy powders. Colloids and surfaces. B, Biointerfaces 42 (1), 1–8. 10.1016/j.colsurfb.2005.01.004.

Kim, E.H.-J., Chen, X.D., Pearce, D., 2009 a. Surface composition of industrial spray-dried milk powders. 1. Development of surface composition during manufacture. Journal of Food Engineering 94 (2), 163–168. 10.1016/j.jfoodeng.2008.09.021.

Kim, E.H.-J., Chen, X.D., Pearce, D., 2009b. Surface composition of industrial spray-dried milk powders. 2. Effects of spray drying conditions on the surface composition. Journal of Food Engineering 94 (2), 169–181. 10.1016/j.jfoodeng.2008.10.020.

Kim, E.H.-J., Dong Chen, X., Pearce, D., 2003. On the Mechanisms of Surface Formation and the Surface Compositions of Industrial Milk Powders. Drying Technology 21 (2), 265–278. 10.1081/DRT-120017747.

Landström, K., Bergenståhl, B., Alsins, J., Mats, A., 1999. A fluorescence method for quantitative measurements of specific protein at powder surfaces. Colloids and Surfaces B: Biointerfaces (12), 429–440.

Langrish, T., Kockel, T.K., 2001. The assessment of a characteristic drying curve for milk powder for use in computational fluid dynamics modelling. Chemical Engineering Journal 84 (1), 69–74. 10.1016/S1385-8947(00)00384-3.

Lazghab, M., Saleh, K., Pezron, I., Guigon, P., Komunjer, L., 2005. Wettability assessment of finely divided solids. Powder Technology 157 (1-3), 79–91. 10.1016/j.powtec.2005.05.014.

Lerk, C.F., Schoonen, A.J.M., Fell, J.T, 1976. Contact angles and wetting of pharmaceutical powders. J. Pharm. Sci. 65 (6), 843–847.

Lewis, R.J., Hawley, G.G., 2007. Hawley's condensed chemical dictionary, 15th ed. Wiley, Chichester.

Li, R., Roos, Y.H., Miao, S., 2016. Physical and mechanical properties of lactose/WPI mixtures: Effect of pre-crystallisation. International Dairy Journal 56, 55–63. 10.1016/j.idairyj.2015.12.014.

Lide, D.R., 2008. CRC handbook of chemistry and physics: A ready-reference book of chemical and physical data, 89th ed. CRC Press, Boca Raton.

Lifshitz, E., 1956. The theory of molecular attractive forces between solids 73 (2), 94–110.

Lin, S.X., Chen, X.D., Pearce, D.L., 2005. Desorption isotherm of milk powders at elevated temperatures and over a wide range of relative humidity. Journal of Food Engineering 68 (2), 257–264. 10.1016/j.jfoodeng.2004.05.036.

Lloyd, R.J., Dong Chen, X., Hargreaves, J.B., 1996. Glass transition and caking of spray-dried lactose. International Journal of Food Science Tech 31 (4), 305–311. 10.1046/j.1365-2621.1996.00352.x.

Loch, J., Polit, A., Górecki, A., Bonarek, P., Kurpiewska, K., Dziedzicka-Wasylewska, M., Lewiński, K., 2011. Two modes of fatty acid binding to bovine β-lactoglobulin--crystallographic and spectroscopic studies. Journal of molecular recognition : JMR 24 (2), 341–349. 10.1002/jmr.1084.

Masters, K., 1985. Spray drying handbook, 4th ed. Godwin, London.

McDonald, E.J., Turcotte, A.L., 1948. Density and refractive indices of lactose solutions. J. Res. Natl. Bur. Stan. 41 (1), 63. 10.6028/jres.041.009.

Meerdink, G., van't Riet, K., 2004. Modeling segregation of solute material during drying of liquid foods. AIChE Journal 41 (3).

Mezhericher, M., Levy, A., Borde, I., 2010a. Spray drying modelling based on advanced drop drying kinetics. Chemical Engineering and Processing: Process Intensification 49 (11), 1205–1213. 10.1016/j.cep.2010.09.002.

Mezhericher, M., Levy, A., Borde, I., 2010b. Theoretical models of single drop drying kinetics: A review. Drying Technology: An International Journal 28 (2), 278–293.

Mezhericher, M., Levy, A., Borde, I., 2012. Three-dimensional spray-drying model based on comprehensive formulation of drying kinetics. Drying Technology 30 (11-12), 1256–1273. 10.1080/07373937.2012.686136.

Millqvist-Fureby, A., Malmsten, M., Bergenståhl, B., 1999. Spray-drying of trypsin-surface characterisation and activity preservation. International Journal of Pharmaceutics (188), 243–253.

Mujumdar, A.S., 1995. Handbook of industrial drying, 2nd ed. Dekker, New York.

Müller, M., Scharfer, P., Kind, M., Schabel, W., 2010. Determination of diffusion coefficients of non-volatile additives in polymeric coatings by means of inverse micro Raman spectroscopy. Chemie Ingenieur Technik 82 (12), 2097–2102. 10.1002/cite.201000085.

Murrieta-Pazos, I., Gaiani, C., Galet, L., Scher, J., 2012. Composition gradient from surface to core in dairy powders: Agglomeration effect. Food Hydrocolloids 26 (1), 149–158. 10.1016/j.foodhyd.2011.05.003.

Nijdam, J.J., Langrish, T., 2006. The effect of surface composition on the functional properties of milk powders. Journal of Food Engineering 77 (4), 919–925. 10.1016/j.jfoodeng.2005.08.020.

Nikolova, Y., Petit, J., Sanders, C., Gianfrancesco, A., Scher, J., Gaiani, C., 2015. Toward a better determination of dairy powders surface composition through XPS matri-

ces development. Colloids and Surfaces B: Biointerfaces 125, 12–20. 10.1016/j.colsurfb.2014.11.009.

Palzer, S., 2001. Einfluss der Rauhigkeit einer Feststoffoberfläche auf den Kontaktwinkel. Chemie Ingenieur Technik 73 (8), 1032–1038.

Palzer, S., 2009. Influence of material properties on the agglomeration of water-soluble amorphous particles. Powder Technology 189 (2), 318–326. 10.1016/j.powtec.2008.04.034.

Palzer, S., Dubois, C., Gianfrancesco, A., 2012. Generation of product structures during drying of food products. Drying Technology 30 (1), 97–105. 10.1080/07373937.2011.622060.

Pawar, S.K., Padding, J.T., Deen, N.G., Jongsma, A., Innings, F., Kuipers, J., 2014. Lagrangian modelling of dilute granular flow-modified stochastic DSMC versus deterministic DPM. Chemical Engineering Science 105, 132–142. 10.1016/j.ces.2013.11.004.

Puri, V., Dantuluri, A.K., Kumar, M., Karar, N., Bansal, A.K., 2010. Wettability and surface chemistry of crystalline and amorphous forms of a poorly water soluble drug. European Journal of Pharmaceutical Sciences : Official Journal of the European Federation for Pharmaceutical Sciences 40 (2), 84–93. 10.1016/j.ejps.2010.03.003.

Räderer, M., 2001. Drying of viscous, shrinking products: Modelling and experimental validation. VDI-Verl., Düsseldorf.

Ranz, W.E., Marshall, (None), W.R., 1952. Evaporation from drops. Chem. Eng. Progress 48, 141–146, 173–178.

Ribeiro, A.C.F., Ortona, O., Simões, S.M.N., Santos, Cecília I. A. V., Prazeres, Pedro M. R. A., Valente, A.J.M., Lobo, V.M.M., Burrows, H.D., 2006. Binary mutual diffusion coefficients of aqueous solutions of sucrose, lactose, glucose, and fructose in the temperature range from (298.15 to 328.15) K. J. Chem. Eng. Data 51 (5), 1836–1840. 10.1021/je0602061.

Roos, Y., Karel, M., 1990. Differential scanning calorimetry study of phase transitions affecting the quality of dehydrated materials. Biotechnol. Prog. 6 (2), 159–163. 10.1021/bp00002a011.

Roos, Y.H., Karel, M., 1991. Plasticizing effect of water on thermal behavior and crystallization of amorphous food models. Journal of Food Science 56 (1), 38–43. 10.1111/j.1365-2621.1991.tb07970.x.

Sano, Y., Keey, R., 1982. The drying of a spherical particle containing colloidal material into a hollow sphere. Chemical Engineering Science 37 (6), 881–889.

Schabel, W., Scharfer, P., Kind, M., Mamaliga, I., 2007. Sorption and diffusion measurements in ternary polymer-solvent-solvent systems by means of a magnetic suspen-

sion balance - experimental methods and correlations with a modified Flory-Huggins and free-volume theory. Chemical Engineering Science 62 (8), 2254–2266. 10.1016/j.ces.2006.12.062.

Schiffter, H., Lee, G., 2007. Single-drop evaporation kinetics and particle formation in an acoustic levitator. Part 2: Drying kinetics and particle formation from microdrops of aqueous mannitol, trehalose, or catalase. J. Pharm. Sci. 96 (9), 2284–2295. 10.1002/jps.20858.

Schmelzer, J.W.P., Gutzow, I.S., 2011. Glasses and the Glass Transition. Wiley-VCH Verlag GmbH & Co. KGaA, Weinheim, Germany.

Schmitz-Schug, I., Kulozik, U., Foerst, P., 2016. Modeling spray drying of dairy products - impact of drying kinetics, reaction kinetics and spray drying conditions on lysine loss. Chemical Engineering Science 141, 315–329. 10.1016/j.ces.2015.11.008.

Schulze, D., 2008. Powders and bulk solids: Behavior, characterization, storage and flow. Springer, Berlin, New York.

Seydel, P., 2006. Modellierung der Feststoffbildung in Einzeltropfen bei der Sprühtrocknung. Bochum.

Shrestha, A., Howes, T., Adhikari, B., Wood D, B., Bhandari, B.R., 2007. Effect of protein concentration on the surface composition, water sorption and glass transition temperature of spray-dried skim milk powders. Food Chemistry 104 (4), 1436–1444. 10.1016/j.foodchem.2007.02.015.

Palzer, S., 2011. Agglomeration of pharmaceutical, detergent, chemical and food powders - similarities and differences of materials and processes. Powder Technology 206 (1-2), 2–17. 10.1016/j.powtec.2010.05.006.

Stalder, A.F., Melchior, T., Müller, M., Sage, D., Blu, T., Unser, M., 2010. Low-bond axisymmetric drop shape analysis for surface tension and contact angle measurements of sessile drops. Colloids and Surfaces A: Physicochemical and Engineering Aspects 364 (1-3), 72–81. 10.1016/j.colsurfa.2010.04.040.

Susana, L., Campaci, F., Santomaso, A.C., 2012. Wettability of mineral and metallic powders: Applicability and limitations of sessile drop method and Washburn's technique. Powder Technology 226, 68–77. 10.1016/j.powtec.2012.04.016.

Tay, A., Monteux, C., Bendejacq, D., Lequeux, F., 2010. How a coating is hydrated ahead of the advancing contact line of a volatile solvent drop. The European Physical Journal. E, Soft matter 33 (3), 203–210. 10.1140/epje/i2010-10662-7.

Tsotsas, E., Metzger, T., Gnielinski, V., Schlünder, E.-U., 2000. Drying of Solid Materials, in: , Ullmann’s Encyclopedia of Industrial Chemistry. WILEY-VCH Verlag GmbH & Co. KGaA.

Tsotsas, E., 2012. Influence of drying kinetics on particle formation: A personal perspective. Drying Technology 30 (11-12), 1167–1175. 10.1080/07373937.2012.685139.

Vehring, R., 2008. Pharmaceutical particle engineering via spray drying. Pharmaceutical research 25 (5), 999–1022. 10.1007/s11095-007-9475-1.

Vehring, R., Foss, W.R., Lechuga-Ballesteros, D., 2007. Particle formation in spray drying. Journal of Aerosol Science 38 (7), 728–746. 10.1016/j.jaerosci.2007.04.005.

Vuataz, G., 2002. The phase diagram of milk: a new tool for optimising the drying process. Lait 82 (4), 485–500. 10.1051/lait:2002026.

Walton, D.E., Mumford, C.J., 1999. Spray dried products - characterization of particle morphology. Chemical Engineering Research and Design 77 (1), 21–38. 10.1205/026387699525846.

Wang, S., Langrish, T., 2010. The use of surface active compounds as additives in spray drying. Drying Technology: An International Journal 28 (3), 341–348.

Wang, S., Langrish, T., Adhikari, B., 2013. A multicomponent distributed parameter model for spray drying: Model development and validation with experiments. Drying Technology 31 (13-14), 1513–1524. 10.1080/07373937.2013.813533.

Wawrzyniak, P., Podyma, M., Zbicinski, I., Bartczak, Z., Rabaeva, J., 2012. Modeling of air flow in an industrial countercurrent spray-drying tower. Drying Technology 30 (2), 217–224. 10.1080/07373937.2011.618282.

White, G.W., Cakebread, S.H., 1966. The glassy state in certain sugar-containing food products. International Journal of Food Science & Technology 1 (1), 73–82.

Williams, M.L., Landel, R.F., Ferry, J.D., 1955. The temperature dependence of relaxation mechanisms in amorphous polymers and other glass-forming liquids. Journal of the American Chemical Society 77 (14), 3701–3707.

Xiao, J., Chen, X.D., 2014. Multiscale modeling for surface composition of spray-dried two-component powders. AIChE J. 60 (7), 2416–2427. 10.1002/aic.14452.

Xiao, J., Zhang, H., Wu, W.D., Chen, X.D., 2015. An improved calculation procedure on surface composition of spray-dried protein-sugar two-component systems. Drying Technology 33 (7), 817–821. 10.1080/07373937.2014.990978.

Young, M.E., Carroad, P.A., 1980. Estimation of diffusion coefficients of proteins. Biotechnology and Bioengineering 23, 947–955.

Zbicinski, I., Strumillo, C., Delag, A., 2002. Drying kinetics and particle residence time in spray drying. Drying Technology 20 (9), 1751–1768. 10.1081/DRT-120015412.

Appendix

A.1 Correlations used in calculation of material properties

- Latent heat of evaporation of water (Glück, 1991):

$$\Delta h_v = 2.501488 \cdot 10^3 - 2.404164 \cdot T_{air} + 1.326154 \cdot 10^{-3} \cdot T_{air}^2 - 1.680282 \cdot 10^{-5} \cdot T_{air}^3 \quad (8.1)$$

- Prandtl number (Glück, 1991) [-]:

$$Pr = 0.702 - (2.629487 \cdot 10^{-4} \cdot T_{air}) + (1.55288 \cdot 10^{-6} \cdot T_{air}^2) - (1.522436 \cdot 10^{-9} \cdot T_{air}^3) \quad (8.2)$$

- Specific heat capacities of water (W), carbohydrate (C) and protein (P) (Choi and Okos, 1986):

$$c_{pW} = 4176.2 + 0.909 \cdot T_d - 5.4731 \cdot 10^{-3} \cdot T_d^2 \quad (8.3)$$

$$c_{pC} = 1548.8 + 1.9625 \cdot T_d - 5.9399 \cdot 10^{-3} \cdot T_d^2 \quad (8.4)$$

$$c_{pP} = 2008.2 + 1.2089 \cdot T_d - 1.3129 \cdot 10^{-3} \cdot T_d^2 \quad (8.5)$$

A.2 Numerical implementation of the model of drying of a single drop

Model input

The values are summarized in Table A.1.

Table A.1 Input values of the model.

Name, symbol	Value	Unit
Initial total amount of solids, TS_0	0.1 – 0.7	[-]
Mass fraction of slowly diffusing component, f	0.1 – 0.5	[-]
Initial radius of a drop, r_0	$50 \cdot 10^{-6}$	m
Initial temperature of a drop, T_{d0}	20	°C
Humidity of drying air at room temperature, φ	50	%
Velocity of drying air, u	1	$m \cdot s^{-1}$
Temperature of drying air, T_{air}	65 – 80	°C
Initial gradient of the temperature of the drop, dT_d/dt	0	[-]
Initial enthalpy flow, H_v	0	$J \cdot s^{-1}$
Initial heat flow to a drop, Q_d	0	$J \cdot s^{-1}$

Initial vapour mass, $m_{vap,0}$	0	kg
Initial vapour mass flow, $\dot{m}_{vap,0}$	0	kg
Density of component A, ρ_A	(Table 4.1)	$kg \cdot m^{-3}$
Density of component B, ρ_B	(Table 4.1)	$kg \cdot m^{-3}$
Density of water, ρ_W	(Table 4.1)	$kg \cdot m^{-3}$
Hydrodynamic radius of component A, r_A	(Table 4.1)	m
Hydrodynamic radius of component B, r_B	(Table 4.1)	m
Sorption isotherm (approximated), $x_{Wisotherm}$	0.5	[-]
Mass fraction of water in the outer shells at which solid shell forms, x_{Wshell}	0.03	$kg \cdot kg^{-1}$
Gas constant, R	8.314	$J \cdot mol^{-1} \cdot K^{-1}$
Number of classes in which a radius of a drop is discretized, $n_{Classes}$	300 – 1200	[-]
Molecular mass of water, M_{water}	0.018	$g \cdot mol^{-1}$
Molecular mass of air, M_{air}	0.028	$kg \cdot mol^{-1}$
Diffusion coefficient of water, $D_{W,0}$	$5.7 \cdot 10^{-10}$	$m^2 s^{-1}$
room temperature, T_{room}	20	°C
Pressure, P	$1.01325 \cdot 10^5$	Pa

The remaining input parameters are calculated accordingly to the drying conditions:

- Initial mass fractions of component A, x_{A0}, and B, x_{B0}, and water, x_{W0}, in a drop:

$$x_{A0} = f \cdot TS \tag{8.6}$$

$$x_{B0} = TS - x_{B0} \tag{8.7}$$

$$x_{W0} = 1 - TS \tag{8.8}$$

- Initial mass of a drop:

$$m_{d0} = 4/3 \cdot \pi \cdot r^3 \cdot (\rho_W \cdot x_{W0} + \rho_A \cdot x_{A0} + \rho_B \cdot x_{B0}) \tag{8.9}$$

- Initial diffusion coefficient:

$$D_0 = D_{o303} \cdot \exp(-16/(1 + 16 \cdot X_{W0})) \cdot \exp(-(100 + 195 \cdot X_{W0})/(1 + 10 \cdot X_{W0}) \cdot (1/T_d - 1/303)/R)) \quad (8.10)$$

The initial mass fraction of water on the surface of a drop is equal the initial mass fraction of water in the system, $x_{Wsurf,t} = x_{W0}$.

Discretization of space

The volume of a drop is discretized into hole-spheres-volumes with a thickness Δr (Figure 8.1, Eq. 8.11). To each such a cell an index *i* is ascribed. The index i_b is the boundary index, with initial value ascribed as $i_b = n_{Classes}$. The initial index of the inner radius of a forming shell is $i_{Shell} = i_b$.

$$\Delta r = \frac{r_0}{n_{Classes}} \quad (8.11)$$

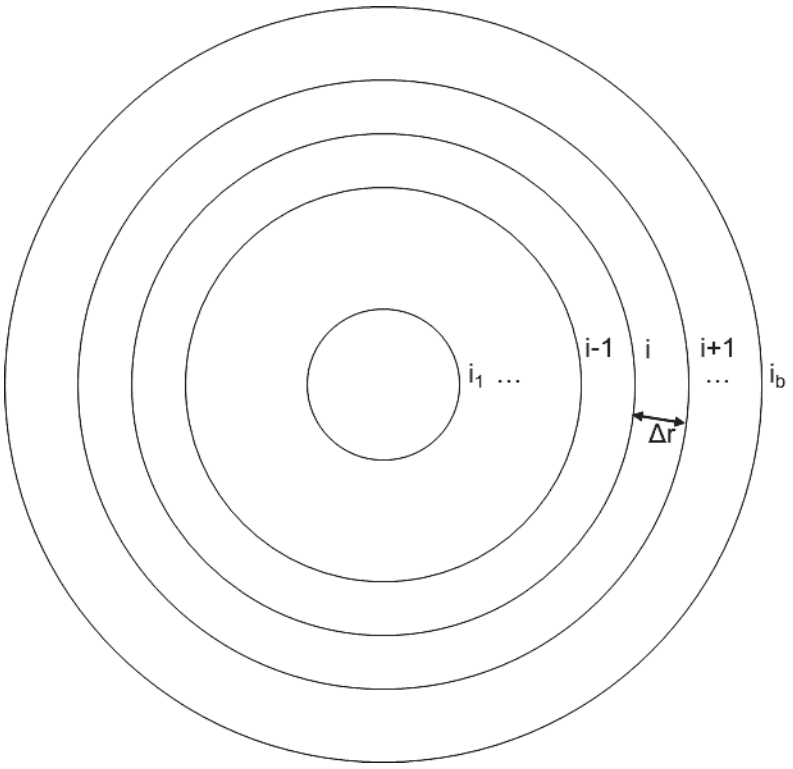

Figure A.1 Schematic of a discretization of a drop volume.

The number of outer classes of a drop, in which solute is accumulated, and which are considered as a shell, were assumed as 10 % of initial radius r_0, $n_{Shell} = 0.1 \cdot n_{Classes}$ and the number of outer classes defined as a surface of a forming particle were assumed as 0.36 % of initial radius r_0, $n_{Surf} = 0.0036 \cdot n_{Classes}$.

Initially in all classes from $i = 1$ to $n_{Classes}$ the properties are the same as in the bulk of a drop. The volume of a hole-sphere with an index *i* is

$$V_i = \frac{4}{3} \cdot \pi \cdot (r_i^3 - r_{i-1}^3) \tag{8.12}$$

- The surface of such a sphere:

$$S_i = 4 \cdot \pi \cdot r_i^2 \tag{8.13}$$

- Initial solid mass in each discrete volume of a drop:

$$k_1 = \frac{x_{Wi}}{(1 - x_{Wi})} \tag{8.14}$$

$$k_2 = x_{Bi} \cdot (1 + k_1) \tag{8.15}$$

$$k_3 = \frac{k_2}{(1 - k_2)} \tag{8.16}$$

$$m_{Ai} = \frac{V_i}{\frac{1}{\rho_A} + \frac{k_3}{\rho_B} + \frac{k_1 + k_1 \cdot k_3}{\rho_W}} \tag{8.17}$$

$$m_{Bi} = k_3 \cdot m_{Ai} \tag{8.18}$$

$$m_{Wi} = k_1 \cdot m_{Ai} + m_{Bi} \tag{8.19}$$

Calculation of input properties dependent on the drying conditions

- Saturated vapour pressure at a given temperature [Pa] (Bück et al., 2012):

$$P_{sat} = \exp\left(A - \frac{B}{C + T_{air}[°C]}\right) \tag{8.20}$$

with A = 23.4588; B = 3977.3782; C = 233.172.

- Absolute humidity of air Y_g and of saturated air Y_{sat} at a given temperature (Eq. 8.1 and 8.2):

$$Y_{sat} = 0.622 \cdot \frac{\varphi \cdot P_{sat}}{P - \varphi \cdot P_{sat}} \tag{8.21}$$

$$Y_g = 0.622 \cdot \frac{P_{sat}}{P - P_{sat}} \tag{8.22}$$

- Density of saturated water vapour:

$$\rho_V = P_{sat} \cdot \frac{M_W}{(R \cdot T_{Air})} \tag{8.23}$$

- Diffusion coefficient of water vapour in air at given temperature:

$$D_{vap} = 2.6 \cdot 10^{-5} \cdot T_{air}^{1.15} \tag{8.24}$$

- Dynamic viscosity of air (Glück, 1991):

$$\eta_{air} = 1.72436 \cdot 10^{-5} + 5.04587 \cdot 10^{-8} \cdot T_{air} - 3.923361 \cdot 10^{-11} \cdot T_{air}^{2} - 4.046118 \cdot 10^{-14} \cdot T_{air}^{3} \tag{8.25}$$

- Density of air at given temperature:

$$\rho_{air} = P \cdot \frac{M_{air}}{R \cdot T_{air}} \tag{8.26}$$

Mass transport in a drop

At each time step water evaporation and mass transport in a drop caused by water removal from a drop are calculated by the following method:

a) in each volume from *i = 1* to *i = i_{b-1}* the diffusion coefficient of water is calculated (Eq. 2.10):

$$D_{Wi} = D_{W,0} \cdot \exp\left(\frac{-16}{1 + 16 \cdot X_{Wi}}\right) \cdot \exp\left(\left(-\frac{100 + 195 \cdot X_{Wi}}{1 + 10 \cdot X_{Wi}}\right) \cdot \frac{1}{R}\left(\frac{1}{T_d} - \frac{1}{303}\right)\right) \tag{2.27}$$

b) the mass flux and mass flow for each discretized volume *i* to *i=i_{b-1}*:

$$J_{fWi} = -\rho_W \cdot D_{Wi} \cdot \frac{x_{W(i+1)} - x_{Wi}}{\Delta r} \tag{8.28}$$

c) for each discretized volume *i* to *i = i_{b-1}* the corresponding mass flow i. e. mass, which flows between two neighbouring volumes at a given time step, is calculated:

$$M_{fWi} = J_{fWi} \cdot \Delta t \cdot S_i \tag{8.29}$$

d) for each discretized volume *i = 2* to *i = i_{b-1}* the following is calculated:

- the water mass transported from the inside of a drop towards the surface

$$M_{fWi} = m_{W(i-1)} \tag{8.30}$$

- if in the volume *i+1* there is no component B, only component A is transported towards the centre of a drop

$$M_{fAi} = \rho_A \cdot \frac{M_{fWi}}{\rho_W} \tag{8.31}$$

- if in the volume *i+1* there is no component A, only component B is transported towards the centre of a drop

$$M_{fBi} = \rho_B \cdot \frac{M_{fWi}}{\rho_W} \tag{8.32}$$

If both components are available in volume *i+1*, the proportion of the components transported to the next discrete volume *i* from volume *i+1* is calculated according to Eq. 2.14 – 2.17, whereas only that much component can be transported as available in the volume *i+1*:

$$s_i = \frac{r_B \cdot (x_{Ai} - x_{A(i+1)})}{r_A \cdot (x_{Bi} - x_{B(i+1)})} \tag{8.33}$$

- mass flow of component B

$$M_{fBi} = \frac{\rho_A \cdot \rho_B \cdot M_{fWi}}{\rho_W \cdot (s_i \rho_B + \rho_A)} \tag{8.34}$$

- mass flow of component A

$$M_{fAi} = s_i \cdot M_{fBi} \tag{8.35}$$

In case the mass of a component in the neighbouring cell is lower than the calculated mass, only the available mass is transported to the next cell. The change of the mass of each component in each discretized volume *i* to $i=i_{b-1}$ is calculated under consideration of the boundary conditions for *i=1*.

$$m_{W1} = m_{W1} - M_{fW1} \tag{8.36}$$

$$m_{A1} = m_{A1} + M_{fA1} \tag{8.37}$$

$$m_{B1} = m_{B1} + M_{fB1} \tag{8.38}$$

- for volumes *i* to $i=i_b$

$$m_{Wi} = m_{Wi} - M_{fWi} + M_{fW(i-1)} \tag{8.39}$$

$$m_{Ai} = m_{Ai} + M_{fAi} - M_{fA(i-1)} \tag{8.40}$$

$$m_{Bi} = m_{Bi} + M_{fBi} - M_{fB(i-1)} \quad (8.41)$$

- water is only transported towards and solutes removed from the boundary volume i_b

$$m_{Wi_b} = m_{Wi_b} + M_{fW(i_b-1)} \quad (8.42)$$

$$m_{Ai_b} = m_{Ai_b} - M_{fA(i_b-1)} \quad (8.43)$$

$$m_{Bi_b} = m_{Bi_b} - M_{fB(i_b-1)} \quad (8.44)$$

Evaporation

a) Calculation of mass transfer coefficient at a given time step until the maximal time, t_{end}

- current drop radius

$$r_L = i_b \cdot \Delta r \quad (8.45)$$

The corresponding Re, Sc and Sh Numbers and mass transfer coefficient are calculated like equations 2.2 – 2.5.

b) Calculation of the absolute humidity at the surface of a drop according to equations 2.21 and 2.22

a) Mass of vapour at a given time step *t*, which evaporates from a drop during a time increment (Eq. 2.1)

$$m_{vap,t} = \Delta t \cdot \rho_V \cdot \beta \cdot (Y_{surf} - Y_g) \cdot 4 \cdot \pi \cdot r_L^3 \quad (8.46)$$

In one time step the amount of water removed from a drop can be larger than the mass of water present in a single discrete volume. To calculate the drop shrinkage due to removal of water and shift of solids into the more central cells in the place of the removed water the following approached is used:

a) From the consecutive volumes from V_{ib} to V_{ib-n} the mass of water is removed until the discrete volume is reached in which the mass of water is larger than the remaining mass of vapour, that is to be removed in the given time step *t*.

b) In that last volume with the index i_{b-n-1} only the amount of water equal to the remaining water vapour is removed and the mass of water in this volume is:

$$m_{Wi_{b-n-1},t} = m_{Wi_{b-n-1},t} - m_{vap,i_{b-n-1},t} \tag{8.47}$$

c) The voids in the discrete volumes generated by water removal are filled with solid, which is shifted from most outer cells from which water was removed. For that purpose a second special coordinate, $j = i+1$, is introduced. From the cell in which water is present ($i = i_{b-n-1}$) towards the surface of the drop, $j = i+1$ the solids are shifted towards the centre of a drop by removing it from a cell j and adding it to the cell i.

If the volume of the solids in a cell j is larger than the void left by removal of water from a cell with an index i, than the solids are shifted from cell j to cell i proportionally to the volume of these solids in cell j.

$$g = \frac{m_{Aj}\rho_B}{m_{Bj}\rho_A} \tag{8.48}$$

The masses of component A and B in the cells change then:

$$m_{Ai} = m_{Ai} + \frac{g \cdot V_i}{(1+g)} \cdot \rho_A \tag{8.49}$$

$$m_{Aj} = m_{Ai} - \frac{g \cdot V_i}{(1+g)} \cdot \rho_A \tag{8.50}$$

$$m_{Bi} = m_{Bi} + \frac{V_i}{(1+g)} \cdot \rho_B \tag{8.51}$$

$$m_{Bj} = m_{Bi} - \frac{V_i}{(1+g)} \cdot \rho_B \tag{8.52}$$

If only one of the components is present in the cell j, only this component is transported as shown for component A.

$$m_{Ai} = m_{Ai} + V_i \cdot \rho_A \tag{8.53}$$

$$m_{Aj} = m_{Aj} - V_i \cdot \rho_A \tag{8.54}$$

If the void in the cell i is larger than the volume of the solids available in cell j, then also the solids from next cells are shifted to the cell with the index i until the void is completely filled with solids.

Calculation of drop shrinkage

If no material is present in a volume this volume is removed and the index i_b is ascribed to that most outer volume, which is not void. The radius of the liquid core of a drying drop is calculated by assigning an index $i=i_{shell}$ to the most outer discrete volume of the drop which contains more water than the specified value of shell formation, x_{Wshell}.

Calculation of mass fractions of components

The mass fractions of solutes A and B and water in each discretized volume increment from *i=1* to $i=i_b$ are calculated based on the masses of each component in each volume in this time step.

$$x_{Ai} = \frac{m_{Ai}}{m_{Ai} + m_{Bi} + m_{Wi}} \tag{8.55a}$$

$$x_{Bi} = \frac{m_{Bi}}{m_{Ai} + m_{Bi} + m_{Wi}} \tag{8.55b}$$

$$x_{Wi} = 1 - x_{Ai} - x_{Bi} \tag{8.55c}$$

The mass fraction of water in the shell region of the forming particle is the average mass fraction of water in the volumes designated as the boundary of the drop and the surface region.

$$x_{Wsurf,t} = \frac{\sum_{i=i_b-i_{shell}}^{i=i_b} m_{Wi}}{\sum_{i=i_b-i_{shell}}^{i=i_b} (m_{Wi} + m_{Ai} + m_{Bi})} \tag{8.56}$$

Mass of a forming particle,

$$m_d = \sum_{i}^{i=i_b} (m_{Wi} + m_{Ai} + m_{Bi}). \tag{8.57}$$

If the mass fraction of water in the region, designated as the maximal possible shell thickness, reaches the mass fraction, designated as the mass fraction, at which the shell reached its mechanical stability $x_{Wshell,t} < x_{Wshell}$, the calculation is terminated because no component movement can takes place in the shell region any more. The mass fraction of component B and the solid based mass fraction of component B in the surface are calculated as the average of the mass fractions in the region of a drop designated as the surface, i.e. from the i_b to i_{surf}. The mass fraction of the component B on the surface and the surface enrichment *f* is then calculated according to Eq. 4.2 as:

$$x_{Bsurf} = \sum_{i=i_b-i_{surf}}^{i=i_b} x_{Bi} \tag{8.58}$$

$$f = \frac{\sum_{i=i_b-i_{surf}}^{i=i_b} m_{Bi}}{\sum_{i=i_b-i_{surf}}^{i=i_b} m_{Ai} + m_{Bi} + m_{Wi}} \tag{8.59}$$

Temperature of a drop

The temperature of a drop at each time step during drying was calculated as:

$$T_d = T_d \cdot \Delta t \cdot \frac{dT_d}{dt}. \tag{8.60}$$

A.3 Powder flowability

Table A.2 Compressive strength in MPa of the powders measured by uniaxial compression test, standard deviations of the sample are given in brackets.

	Consolidation stress [MPa]	8	12	16	20	24
Batch No.	Composition					
1	Lactose	0.27 (0.05)	0.82 (0.11)	1.75 (0.29)		
2	Lactose	0.23 (0.05)		1.40 (0.48)		
3	Lactose + WPI (99:1)	0.35 (0.05)	0.84 (0.17)	1.41 (0.16)		
4	Lactose + WPI (99:1)	1.05 (0.12)	1.72 (0.29)	2.30 (0.28)		
5	Lactose + WPI (90:10)	0.52 (0.07)	1.14 (0.09)	1.74 (0.23)		
6	Lactose + WPI (90:10)	0.52 (0.07)	1.14 (0.09)	1.74 (0.23)		
7	Lactose	0.11 (0.04)	0.12 (0.04)	0.06 (0.03)	0.64 (0.20)	
8	Lactose	0.08 (0.06)	0.08 (0.04)	0.15 (0.05)	0.17 (0.06)	0.16 (0.08)
9	Lactose + WPI (90:1)	0.33 (0.07)	0.41 (0.11)	0.79 (0.15)		
10	Lactose + WPI (90:1)	0.51 (0.13)	0.65 (0.12)	0.97 (0.33)		
11	Lactose + WPI (90:10)	0.55 (0.06)	0.82 (0.11)	1.08 (0.24)		
12	Lactose + WPI (90:10)	0.50 (0.07)	0.50 (0.07)	1.13 (0.24)		

Table A.3 Compressive strength of the powders measured in a shear cell.

Batch No.	Composition	Compressive strength [MPa]	Consolidation stress [MPa]
1	Lactose	3254	331
		6417	627
3	Lactose + WPI (99:1)	3278	281
		6473	557
		9701	802
4	Lactose + WPI (99:1)	3300	284
		6549	552
		9765	849
5	Lactose + WPI (90:10)	3235	301
		6461	541
		9659	777
6	Lactose + WPI (90:10)	3298	284
		6475	462
		9723	809
8	Lactose	3277	1328
		9535	2289
9	Lactose + WPI (90:1)	3330	289
		6591	487
10	Lactose + WPI (90:1)	3390	297
		6518	536
		9714	852
11	Lactose + WPI (90:10)	3299	335
		6394	497
		9800	832
12	Lactose + WPI (90:10)	3313	325
		6579	520
		9749	845